British Geological Survey
NATURAL ENVIRONMENT RESEARCH COUNCIL

Site Survey for a T-Phase Station (HA-09) At Tristan Da Cuhna, United Kingdom.

Earthquake Seismology and Geomagnetism Programme
Commissioned Report CR/02/322N

BRITISH GEOLOGICAL SURVEY

COMMISSIONED REPORT CR/02/322N

Site Survey for a T-Phase Station (HA-09) At Tristan Da Cuhna, United Kingdom.

B.J. Baptie, D.L. Petrie and C.W.A. Browitt

Key words

T-phase.

Front cover

View of Tristan Da Cuhna from the sea.

Bibliographical reference

BAPTIE, B., PETRIE, D.L. AND BROWITT, C.W.A.. 2002. Site Survey for a T-Phase Station (HA-09) At Tristan Da Cuhna, United Kingdom.. *British Geological Survey Commissioned Report*,CR/02/322N. 44pp.

Keyworth, Nottingham British Geological Survey 2002

BRITISH GEOLOGICAL SURVEY

The full range of Survey publications is available from the BGS Sales Desks at Nottingham and Edinburgh; see contact details below or shop online at www.thebgs.co.uk

The London Information Office maintains a reference collection of BGS publications including maps for consultation.

The Survey publishes an annual catalogue of its maps and other publications; this catalogue is available from any of the BGS Sales Desks.

The British Geological Survey carries out the geological survey of Great Britain and Northern Ireland (the latter as an agency service for the government of Northern Ireland), and of the surrounding continental shelf, as well as its basic research projects. It also undertakes programmes of British technical aid in geology in developing countries as arranged by the Department for International Development and other agencies.

The British Geological Survey is a component body of the Natural Environment Research Council.

Keyworth, Nottingham NG12 5GG

☎ 0115-936 3241 Fax 0115-936 3488
e-mail: sales@bgs.ac.uk
www.bgs.ac.uk
Shop online at: www.thebgs.co.uk

Murchison House, West Mains Road, Edinburgh EH9 3LA

☎ 0131-667 1000 Fax 0131-668 2683
e-mail: scotsales@bgs.ac.uk

London Information Office at the Natural History Museum (Earth Galleries), Exhibition Road, South Kensington, London SW7 2DE

☎ 020-7589 4090 Fax 020-7584 8270
☎ 020-7942 5344/45 email: bgslondon@bgs.ac.uk

Forde House, Park Five Business Centre, Harrier Way, Sowton, Exeter, Devon EX2 7HU

☎ 01392-445271 Fax 01392-445371

Geological Survey of Northern Ireland, 20 College Gardens, Belfast BT9 6BS

☎ 028-9066 6595 Fax 028-9066 2835

Maclean Building, Crowmarsh Gifford, Wallingford, Oxfordshire OX10 8BB

☎ 01491-838800 Fax 01491-692345

Parent Body
Natural Environment Research Council, Polaris House, North Star Avenue, Swindon, Wiltshire SN2 1EU

☎ 01793-411500 Fax 01793-411501
www.nerc.ac.uk

Contents

List of Figures

List of Tables

Summary

The purpose of the site survey was to determine a suitable location and prepare for the establishment of a hydroacoustic T-phase station at Tristan Da Cuhna. Seismic measurements were made at 9 temporary sites at different geographical locations around the island for periods of continuous recording of at least 24 hours, with at least two stations operating simultaneously. Stations were found to be very noisy due to a combination of local geological conditions and proximity to natural noise sources. We used power spectra to compare noise levels at different sites and identify noise sources. Noise levels in the 2-7 Hz range are high and dominated by the surf noise due to waves crashing against the shore. Amplitudes of these signals are higher on the horizontal components than on the vertical. Almost all sites show very high noise levels in this band and we find that noise exceeds the commonly used high noise model. Thirteen seismo-acoustic events from earthquake sources in oceanic areas at a range of distances and azimuths deemed likely to generate T-phase arrivals occurred during the survey. However, no T-phase arrivals from any of these events could be positively identified. In addition, RMS amplitudes at coastal stations exhibit a strong correlation with tidal variations. Measurements from sites to the southwest of the settlement of Edinburgh were found to exhibit the lowest noise in the 1-10 Hz range. Therefore, in the absence of measured signal-to-noise ratio for T-phase arrivals at different stations, we suggest that this may be the most suitable area for the establishment of a permanent station. Such a station will require a radio telemetry link with a base station at the settlement, with at least one repeater station. A second sensor should be deployed in the area of the Settlement of Edinburgh, close to the central facility, with a direct cable link to provide power and data transmission. This station, though perhaps noisier, based on the measurements made over the survey period, will present less logistical complexity, which is an important consideration owing to the remoteness of the site. This additional station will also provide both an element of redundancy and slight improvement in azimuthal coverage of ocean areas to the north.

Introduction

Tristan Da Cuhna is a group of 4 small islands situated in the South Atlantic at approximately 37.2° S, 12.5°W. These islands form the most remote inhabited territory in the world and are only accessible by sea. The very remoteness of the islands, infrequent visits, and lack of major facilities adds significant complexity to any operations.

The purpose of the site survey was to determine a suitable location and prepare for the establishment of a hydroacoustic station, as specified in Annex 1 to the Protocol of the Comprehensive Nuclear-Test Ban Treaty. The purpose of the hydroacoustic station is to measure seismic T-phases (Okal, 2001) resulting from the conversion of the acoustic T-waves at the island shore. Acoustic energy from earthquakes, explosions and underwater volcanism propagates efficiently in the SOFAR channel, the layer of low acoustic velocity extending between depths of approximately 600-1800m in the world's oceans. This low velocity layer acts as a wave-guide for

acoustic waves at frequencies of greater than 2.5 Hz, and means that T-waves can be used to detect very small sources at very large distances.

Signal-to-noise ration is the main criteria for a T-phase station and it is important to have good coupling to the ocean T-phase signals. This coupling is believed to be a function of the island's bathymetry, with steep, smooth slopes maximizing this function (Okal, 2001). Factors such as overall noise conditions and local geology are less important. The site should also have an unobstructed view of distant oceans over as wide an azimuth as possible and avoid any local bathymetric features that might affect this. A significant noise source will be generated by surf as ocean waves strike the island shore. As a sensor is moved inland, away from the shore, the amplitude of the T-phase signal will fall-off at a different rate than that of the surf noise.

During the site survey continuous seismic measurements were conducted at a total of 9 sites around the island over periods of at least 24 hours with at least two stations recording simultaneously. Ambient noise levels were characterized using power spectra across a frequency band between at least 0.5 and 20 Hz to compare with low and high noise models (Petersen, 1983) and to determine diurnal variation in noise. Characteristics of different noise sources were identified at each site and relative noise levels determined to evaluate their effect on station performance. An estimate of the noise levels at varying distances from the shore was established using a profile of sensors. We examined the variation of the noise levels at each site, with time, by determining average signal amplitude in a moving window.

Over the duration of the survey we identified a number of seismo-acoustic events in oceanic areas at a wide variety of azimuths and distances. Data at different stations were examined for potential T-phase arrivals from these events to assess signal-to-noise ratios and azimuthal coverage at each site.

In addition, we made a thorough investigation of the logistical factors affecting installation and operation of a permanent station. These included land ownership issues, local infrastructure such as power supply and transport, intra-site communications, availability of local materials and labour, facilities for the transportation of goods and materials.

Geographic setting and bathymetry

The island group lies about 200 km to the east of the Mid Atlantic ridge crest, and consists of Tristan Da Cuhna, the largest of the group, with Nightingale Island lying to the southwest and south-southwest respectively at distances of 25 and 35 km (Figure 1). Gough Island, the fourth island in the archipelago, lies some 352km southeast. Nightingale and Inaccessible islands as well as the channel between them produce a bathymetric high in the area to the southwest (Figure 1). This raises the possibility of a blockage of T-waves propagating in the SOFAR channel from these azimuths. The SOFAR channel is thought to lie at a depth of approximately 800m at these locations.

The submarine extent of the volcanic complex that forms Inaccessible Island is far greater than that which breaks the surface. The multi coned complex trends east west,

with the centre lying to the west of Inaccessible (Ollier 1984). Surrounding the neighbouring Nightingale Island is a shallow plateau at about 50mbsl, elongate along a north-south axis. On the outside of this plateau is a ridge that extends a further 20m toward the surface after which the depth increases rapidly. The east-west trend of the shallows around Inaccessible meet with the north-south trend of the shallower submarine topography around Nightingale to form a 15km wide channel between them. The maximum depth of this channel along its median line is 631m and the minimum is 234m.

Tristan Da Cuhna itself is roughly circular in shape with a diameter of approximately 12 km (Figure 2). The highest point stands at over 2000m above sea level. The island rises sharply from the sea and is ringed by cliffs on all sides that rise to an initial height of between 700-800 m. Above the cliffs the plateau rises rather more gently to the central peak. The flanks of the peak consist extensively of relatively young lavas that are now heavily vegetated in most places.

A narrow strip of land 1-2 km wide to the Northwest of the island forms the settlement plain. The plain primarily consists of colluvium – coarse breccio-conglomerates and finer gravels produced by fluvial outwash from the streams issuing from the cliffs backing the coastal plain. These deposits overlie older lava flows such as those found around the harbour. The settlement of Edinburgh lies at the Northern end of this plain, flanked on the North and the West by sea and consisting of around 100 mainly low-lying buildings of stone and concrete construction with corrugated, galvanized iron roofs. Between the south edge of the settlement and the base of the cliffs there is a small area of pasture providing grazing for sheep and cattle. The southwestern edge of the settlement is marked by Hottentot Gulch, a steep canyon some 10 m deep in places.

Immediately to the East of the settlement are the remains of the 1961 volcanic eruption that resulted in the evacuation of the island. The report of the Royal Society expedition (1964) provides a detailed description of this event. Weak fumarolic activity around the 1961 lava dome is typical of that caused by the heating of percolating ground water by residual heat within the vent area (Dunkley, 2001). Beyond Hottentot Gulch, the plain extends to the southwest to the area locally known as the Patches. This area is of significant importance to the islanders as the principle area for cultivation of crops and grazing for sheep and cattle. The cultivated areas take the form of enclosed strips of land, whose primary crop is potatoes. Although all the land on the island is commonly owned, each family has an individual plot of land here. A narrow tarmac road links the settlement and the Patches.

A group of hills, almost 200 m high, called Hillpiece, and formed by an explosive basaltic eruption of lava flows and scoria cones, block the narrow neck of land between the Patches and the settlement. These effectively prevent direct line of sight for radio communications and the islanders are unable to use VHF radio between the Settlement and the Patches. Any permanent site to the Southwest of this will require a repeater site on the top to relay the data stream back to the central facility. However, this also forms a natural barrier against the prevailing winds making this area rather more sheltered and suitable for crops than the Settlement itself.

A number of tracks exist that allow the islanders access to the plateau above the cliffs to tend grazing sheep. These tracks are extremely steep and somewhat impermanent in nature.

There are smaller coastal plains at the southern end of the island at Seal Bay and at Stonyhill Point. The islanders use this land for cattle and there are some additional temporary dwelling houses in these areas. Access is made by sea, with landings at Cave Point and Stonybeach Bay. Theoretically it is possible to access the south of the island by foot from the settlement plain, either via Bluff Gulch and around the top of the cliffs or along the shoreline at the base of the cliffs. However, there are no roads and the tracks are only used occasionally, making the terrain highly demanding and presenting significant risk of injury from falling rocks for the latter option. Transportation of equipment is only practically possible by sea or air (in the rare event that air transport is available). Weather conditions dictate the possibility of visits.

Seismic data acquisition

The geographic location of each temporary seismic station deployed during the site survey is also shown in Figure 2. Details of the seismic data acquisition, including dates and times of operation of each station is summarized in Table 1. Further detailed station information can be found in Appendix 1.

Following arrival on 6 November 2001 we carried out an initial reconnaissance around the settlement and decided to deploy sensors at 4 locations in this area, TDC1, TDC2, TDC3 and TDC4 (Figure 3), giving good azimuthal coverage of the ocean area to the North and West, unobstructed by any local bathymetric features. In addition, the logistics of installing a permanent station in the vicinity of the settlement are relatively simple in comparison to other areas around the island, given the expected availability of direct power from and communications with any central facility in this area, thus increasing ease of operation and long-term reliability. To minimize cultural noise we positioned the stations outside the main settlement in areas to the south (TDC1 and TDC2) and to the west (TDC3 and TDC4). The 4 stations form a linear profile, approximately 1 km long running from the base of the cliffs beyond the Southeast edge of the settlement, to the shoreline in the Northwest, (Figure 3). Local geology consists of thick colluvial/alluvial deposits overlying older lava flows. It is clear that there is no possibility of finding solid bedrock at shallow depths.

Each of these four stations was constructed in the same way. An initial hole was excavated with a JCB and local assistance to a depth of at least 1m. The pit was further cleared by hand to establish a well-consolidated base of rock/gravel. A raft of concrete some 10-20cm thick was laid in the base of the pit with a slate set on top, to give a solid and level platform for the sensor. When the concrete had set the sensor was oriented according to true North, some 24° East of magnetic North and levelled precisely. The sensor was then covered with an insulated plastic box sitting on the concrete raft, then back-filled with soil and gravel and covered with turf, designed to minimize wind-noise and ensure some degree of thermal stability. The recording equipment was situated on the surface, a few meters from the pits.

At station TDC1 we deployed both a broadband Streckeisen STS-2 three component sensor, together with a Lennartz LE-3D short period, three-component sensor, with recording on Reftek 72A-08 and Reftek 72A-06 data acquisition systems, respectively. Station TDC2 used a CMG-40T broadband sensor with an Earth Data PR2400 recording unit. Stations TDC3 and TDC4 both used Lennartz LE-3D short period sensor and Reftek 72A-06 data acquisition units. Sensor sensitivity, pre-amplifier gain and recording media gain are shown in Table 2.

On 11 November we installed station TDC5 near the Patches (Figure 3). The station was installed some 400m southeast of the road on the opposite side from the actual potato patches, close to a small conical hill call 'Big Hill', at a distance of some 1500 m from the shoreline. The station operated from 15:48 on 11 November to 13:30 on 13 November. The sensor was set on a rocky base that was found immediately underlying the turf then covered with insulating box and turf. Instrumentation consisted of a LE-3D sensor and Reftek 72A-06 data acquisition unit, previously used at station TDC3.

Station TDC6 was installed on 12 November at Stonyhill Point in the south of the island. The sensor was placed on the hard rock outcrop of lava flow deposits that form Stony Hill, due West of Stony Beach Gulch (Figure 4), and again covered with an insulating box and turf to minimize wind noise. Instrumentation consisted of a LE-3D sensor and Reftek 72A-06 data acquisition unit, previously used at station TDC4. This station operated from 12 November 1328 to 14 November 1336.

Access to the site was made using a boat from the Settlement, a journey that took about 60 minutes. A landing is made at Stonybeach Bay but this is only possible in relatively calm seas. It is worth pointing out that we had attempted to reach this area on the previous three days, but it was impossible due to the sea conditions. From the landing spot it takes about 30 minutes on foot to the seismic station.

Any site in this area would need complete power self-sufficiency that would only practically be achievable using a large array of solar panels and batteries. In addition, data telemetry from this site to the central facility would be difficult. Radio telemetry using UHF radio will require at least two and more probably even three or four separate relay sites, making this link extremely vulnerable. Conventional satellite communications would require a prohibitively large power budget. A lower power Nanometrics Libra satellite VSAT link to the central facility is probably the only available solution. The elevation of the cliffs to the North was measured at 34-42° between azimuths of 300-350°. We believe that this would allow a sufficiently clear view of the sky to make satellite communications possible.

Also, on 12 November we installed station TDC7 at the top of the cliffs above the settlement (Figure 3). The sensor was positioned on a ledge excavated from a rock outcrop of a narrow gulch, then covered by an insulating box and turf strips. Instrumentation consisted of a LE-3D sensor and Reftek 72A-06 data acquisition unit, previously used at station TDC1. This station operated from 12 November 1446 to 15 November 0909.

Station TDC8 was installed in 14 November at the southern end of the Patches, beyond the end of the road in the area near Spring Ridge (Figure 3). The broadband Streckeisen STS-2 three component sensor, previously deployed at station TDC1, was placed on a flat rock outcrop of a large buried boulder, protected with an insulating box to provide thermal stability, then covered with rock and turf slabs to minimize wind noise. Data were recorded on a Reftek 72A-08 data acquisition system. The station operated from 11:10 on 14 November to 1205 on 15 November.

Finally, station TDC9 was installed on 13 November at a site very close to TDC1. In this case we placed the sensor on a small rock ledge chiselled from the cliff face, in order to make a comparison of a sensor placed on relatively hard rock and one in a pit with a concrete base. The sensor was covered with a protective case, and then surrounded by turf to minimize wind noise. Instrumentation consisted of a LE-3D sensor and Reftek 72A-06 data acquisition unit, previously used at station TDC5. This station operated from 13 November 1536 to 15 November 1436.

Logistics and available infrastructure

Land Ownership

Land on Tristan Da Cuhna is commonly owned. Arrangements for leasing land for a central facility and outstations can be arranged with the local administration. A typical lease agreement would last for a period of 5 years. However, given such a limited area of land, grazing for cattle and sheep is at a premium. Any station locations must have minimal impact on these areas. In addition, the islanders would resist any plans to situate the central facility or stations in an area that would encroach on the cultivated land around the Patches. For the seismic outstations this is less of a problem, since the equipment can be deployed on rocky areas not used for grazing or cultivation. We discussed with James Glass, the Chief Islander, some preliminary details of a typical outstation. This may consist of a small subsurface vault, perhaps 1-2 m in diameter and with minimal surface profile, containing the sensor, with a requirement for a second structure for solar panels, batteries and radio transmitters and a small radio mast at more distant stations. James agreed that none of these would be a problem at any of the sites tested throughout the survey.

Power

Mains electrical power on the island is supplied from the lobster processing plant operated by a South African company called Eurex. This is part of an agreement with the island in return for fishing rights in the island's waters. Power is supplied between the hours of 0600 and 0000 only. The diesel powered Caterpillar generators are capable of providing up to 400V at 500A giving 200 KW of three-phase power. In practice, the generator is run up to 400A, since the circuit breakers may trip beyond this level. The two generators are cycled, with one on standby at all times. The fuel consumption of the generators is approximately 600 litres per day and the total fuel storage capacity of the plant is 200,000 litres. Fuel levels are kept at as high a level as

possible, with refuelling from passing ships when available. Representatives of the islanders voiced no objections to an additional facility to provide power to the central facility on a 24-hour basis, as long as they did not produce an excessive amount of noise. Noise could be minimized with appropriate soundproofing insulation. To this end, we held discussions with a representative of Eurex in Capetown. They have appeared willing to be sub-contracted to install and operate an additional pair of generators that would provide power to the central facility.

Freight handling

Large ships cannot dock at the harbour, since it is too small. There is an anchorage about ½ a mile offshore. Freight is offloaded using the ship's crane into the islander's fishing boats. Larger freight is handled using inflatable pontoon rafts or a small barge. This places important limitations on the types and sizes of cargo that can be safely accommodated. The S.A. Agulhas has two main cranes on the forward deck. A travelling deck crane servicing all three cargo hatches, with an operational weight limit of 5 tonnes, and a luffing/slewing crane situated on foc'sle head with an operational weight limit of 25 tonne at 17m. Only the former of these is used for operations at Tristan Da Cuhna. The fixed pedestal hydraulic crane in the harbour has a safe working load of 8 tonnes. A crawler/jib crane with a safe maximum load of 37 tonnes is also available. In practice this is used for loads up to 20 tonnes. Previously, 16 tonne bulldozers were unloaded using this.

Local transport

Transportation for equipment on the island can be arranged locally and a variety of vehicles are available, from Land Rovers and 4WD to tractors with trailers and JCB's owned by the Public Works Department.

Construction

Equipment and manpower is available on island for construction of concrete foundations and structures and the laying of cabling ducts for power and data transmission. Equipment includes a number of JCBs that can be used for excavation of the vault and cement mixers for concrete. Sand, cement and gravel for concrete can also be purchased locally. It would be prudent to employ local labour during the installation phase, though guidance and supervision during the construction of the vault and central facility will be required. Arrangements for payment in cash (Pounds Sterling) can be made through the Tristan Treasury. Cabling ducts for power and communications can be excavated locally, but the ducting material would have to be imported.

Communications

The telecommunications building has an INMARSAT satellite telephone for international voice and fax communications that is available for public use. This also supports a facility for sending and receiving email. There is also a satellite communications system in the administrative offices, but this is for official use only and was not operational at the time of the site survey. There is no local telephone system. VHF radio transmission in the marine band is used for fisheries and the Public Works Department. The area of effective usage is severely affected by topography. For instance, the islanders are unable to use VHF radio between the Settlement and the Patches. To our knowledge, UHF is not used. Licensing may be required for the use of a fixed frequency and requests should be submitted to the local administration.

Local operator

Alan Swain, the Post and Telecommunications director and his assistant, Ian Lavarello, both have some of the technical expertise necessary for local station operations. In particular, Iain Lavarello was trained in the UK to operate the satellite communications equipment. The matter was discussed with Ian (with the approval of Alan) and he seemed enthusiastic about such a possibility. Supplementary training in all the operating technology would be required before installation. Arrangements for payment of a local operator should be made through the local administration.

Weather

Given the latitude and situation, weather conditions on Tristan can be severe and highly variable. Gale force winds to 60 mph are common, as are high seas with swells in excess of 5-6 m. Prevailing winds are typically from the northwest (though during the survey the wind was mostly from the south-southwest, Figure 37) and both the anchorage and the settlement are very exposed. This means that disembarkation of people and cargo is highly dependent on the weather, raising the possibility that landing from visiting ships will be impossible. The swell runs straight into the harbour and small boats can easily be broached by large waves. Similarly, access to the south and the adjacent islands can be difficult. For example, during the site survey it was only possible to land in the south on perhaps three of the ten days that we were present on island.

Accommodation

The "William Glass Guest House" provides accommodation for up to seven visitors. At the time of the survey the cost per person was £(??) per night, including meals. Extra accommodation is available with other islanders. All accommodation needs to be arranged in advance through the local administration.

Noise characteristics of each station

We characterize the variations in noise at each site using power spectral estimates determined from randomly selected segments of data. Power spectral density estimates were determined using Welch's (1967) modified periodogram method, which combines averaging periodograms and windowing, using overlapping 8192-point windows. The data record is sectioned and a window is applied to the data segments before computation of the periodograms. This method is widely used because it can be efficiently implemented using the fast Fourier transform algorithm. Ten data segments of length 10.5 minutes were used for both day (0600-1759) and night (1800-0559) to assess the variability of signal power. Median values for all segments were used to determine a composite noise model and median values for the day and night data to show the diurnal variation.

The noise models developed by Petersen (1983) represent the upper- and lower-bound envelopes of a cumulative compilation of representative ground acceleration power spectral densities determined for noisy and quiet periods at 75 digital stations world-wide. The models are commonly referred to as the New High Noise Model (NHNM) and New Low Noise Model (NLNM), respectively, and they represent a commonly accepted standard for expected limits of seismic noise.

Figure 5 to Figure 13 show the power spectral estimates for each of the twenty data segments (grey) and for each component of ground acceleration at stations TDC1 through to TDC9. Also shown in blue, red and green are the median values for each component. We see immediately that noise values are very high and exceed the high noise model at some stations, particularly in the 2-5 Hz band on the horizontal components. Also, there is considerable variation between individual estimates made at different times. Variability in power spectral density is strongest at high frequencies, approximately 20dB, but is also noticeable at lower frequencies and around the secondary microseismic peak at 3-6 seconds.

Composite noise curves, determined from the median value of all estimates for a given station component, are shown in Figure 14 to Figure 22 for each station. From these it is clear that of all the sites chosen during the site survey, stations TDC5 and TDC8 show the lowest noise in the 1-10 Hz range. All the other stations show significantly more noise in this range with a noise peak at around 2-4 Hz particularly on the horizontal components, that exceeds the high noise model. We suggest that this peak is due to the action of individual waves crashing on the shore, coupling energy into the ground

Of the stations around the settlement, TDC4 appears rather quieter than the others, which is surprising given its close proximity to the shore. The east-west component of station TDC2 show a number of integer harmonic peaks that we believe may be a result of a problem with the instruments self-centring mechanism.

The composite PSD plot from station TDC7 (Figure 20) shows high noise levels in the 0.5-2 Hz range that we believe is a result of wind action on the vegetation at this site. Wind action on the ground and vegetation typically results in seismic noise that is broadband in nature with typical frequencies of 0.5-15 Hz (Young et al 1996).

Cultural noise

At higher frequencies, say above 15 Hz, noise is more likely to be man-made resulting from traffic or machinery. Figure 23 shows a spectrogram for 30 minutes of data from station TDC3 starting at 1211 on 8 November. There are a number of discrete events that are essentially broadband in nature with a frequency content of between 10-30 Hz. These are caused by traffic travelling up and down the only road on the island. The road is at a distance of approximately 200 m from TDC3. Also clearly observed is a continuous noise peak at 24 Hz. This is thought to be due to the diesel generators that provide the island's electricity supply. This noise peak can also be observed on the composite noise plot for station TDC3.

Ocean microseism

Primary ocean microseisms are generated by wave energy converted into seismic energy either through vertical pressure variations, or by waves breaking on the shore, and have the same period as the water waves (Cessaro, 1994). The primary microseismic noise peak is usually observed at periods of around 14±2 seconds but was not observed on Tristan Da Cuhna.

Secondary ocean microseisms were explained by Longuet-Higgins (1950) as being generated by the superposition of ocean waves of equal period travelling in opposite directions, thus generating standing gravity waves of half the period. The secondary microseismic noise peak appears between periods of 3-6 seconds on Tristan Da Cuhna. Horizontal and vertical noise amplitudes are similar and the particle motion is of Rayleigh wave type.

Diurnal variation

Figure 24 to Figure 32 show the median power spectral density at each station and on each component for the day and night data. Diurnal variations are in general small and only appear significant at stations TDC1 and TDC2 at frequencies above 10 Hz. The 24 Hz noise peak due to the electrical generators is apparent in the day at stations TDC3 and TDC4.

Coherence of noise between stations

We used cross-spectral analysis to determine the coherence of the signals from pairs of stations and search for coherent noise sources across groups of stations in a given geographic area. Coherence was estimated using Welch's averaged periodogram method for a number of randomly selected noise segments from each site for both daytime and night-time, and gives the correlation of the two signals at each frequency. Figure 33 shows the results for station pairs from TDC1, TDC2, TDC3 and TDC4 over the period 8 to 10 November. Grey lines show the coherence function for individual noise segment pairs, while the red lines indicate the median value. The individual pairs are ordered by increasing distance. The most striking feature is the

strong coherence of signals between TDC3 and TDC4 in both the 0.1-1 Hz range, showing that the ocean microseism is coherent between these two stations. Given the close proximity of these stations to the sea this is perhaps unsurprising. Signals from TDC3 and TDC4 also exhibit reasonable coherence in the 2-4 Hz range. Aside from this there are a number of sharp peaks at discrete frequencies observed for given noise segments. The peak at approximately 25 Hz seems coherent between a numbers of station pairs and can be attributed to the diesel generators.

Figure 34 shows the median values of the coherence functions for daytime (magenta) and night-time (blue) noise segments. Overall, signals exhibit low coherence except between stations TDC3 and TDC4. The strong coherence at 25 Hz between these two stations is clearly a daytime phenomenon and can be linked to their proximity to the diesel generator.

To further examine the correlation of signal noise between different stations we calculated the cross correlation functions between noise segments from individual station pairs in six discrete frequency bands. The results are shown in Figure 35 as a function of distance. These show that the correlation in the background noise is low, except perhaps at lower frequencies, where correlation coefficients rise slightly.

Variation in noise levels with time and local dependency

To examine variations in the background noise at each station with time we calculated root mean square amplitudes in ten-minute windows over the duration of recording at each station. Two different filters were applied to the data, firstly a bandpass filter of 0.5-5 Hz and a highpass filter at 5 Hz. The results for the bandpass filter are shown in Figure 36 for each station. These show an approximately 12 hourly periodicity at all stations, although this is also modulated by some longer period variation. The highpass filtered data (not shown) also shows daytime noise peaks caused by cultural noise sources. These are particularly clear at stations TDC3 and TDC5, which are rather too close to the road.

We compared the RMS amplitude estimates with tidal predication calculated by the Proudman Oceanographic Laboratories, who previously operated a tide gauge on Tristan Da Cuhna. Figure 36 shows that the RMS data correlates very well with the tidal predictions (black line) and the peaks in noise level correspond with the high tide and the troughs with the low tide. This reinforces the supposition that the primary source of noise in the 1-10 Hz band is caused by the surf.

Environmental parameters

The following environmental parameters were logged as part of the site survey for the infrasound station: pressure, temperature, wind-speed and wind direction. These are shown in Figure 37. Barometric pressure dropped to a low in the middle of the survey period and rose towards the end of the survey. Temperatures varied between 10-16°. Wind directions were dominantly southwesterly with occasional easterly winds at times.

Signals recorded from natural sources

Over the duration of the survey a number of seismo-acoustic events occurred in oceanic areas that may have generated T-phase arrivals on Tristan Da Cuhna. Data recorded at different stations were carefully examined for the presence of detectable signals from these events. These events covered a wide range of azimuths and epicentral distances and varied in magnitude from 3.9-5.1 Mb. Epicenters for each event are shown in Figure 38 and the locations computed by the International Seismological Centre using all available phase data are listed in Table 3. Calculated epicentral distances, back azimuths, P- and T-phase arrival times and detection status for P- and T-phases are given in Table 4. Each event is analysed in turn below using a ten-minute window about the theoretical T-phase arrival time for both raw and filtered seismograms and spectrograms to assess the detection capability for different arrivals.

Figure 40 shows seismograms of the vertical component of ground velocity recorded at stations TDC1 and TDC2 in a ten minute window about the theoretical T-phase arrival for the magnitude 4.2 southern mid-Atlantic event on 8 November at 03:58 UTC. Figure 41 shows the same time window as Figure 1, but a 4th order Butterworth filter with a pass band of 3-7 Hz has been applied to the data. The event has an epicentral distance of 18.1° and backazimuth of 152.6°. No body waves were detected for this event in the 0.6-5.0 Hz band. There are a number of signal peaks throughout the time window of interest that appear well correlated between the two stations, however, it is difficult to attribute any of these to a possible T-phase arrival given the short duration and repetitive nature. Figure 42 shows the spectrogram calculated for the vertical component of ground velocity at stations TDC1 and TDC2. Both stations show near continuous noise peaks in the 3-5 Hz band that dominate the spectrograms. The theoretical T-phase arrival is expected at a time of 316 seconds from the start of the record. There is no suggestion of an increase in energy in the 3-7 Hz band that might be associated with the T-phase arrival.

Figure 43 shows the P-wave arrival recorded at stations TDC1, TDC2, TDC3 and TDC4 for the magnitude 4.4 South Sandwich island event on 8 November at 22:52 UTC, at an epicentral distance of 22.1° and backazimuth of 220.5° from North. No filters have been applied to the data. The observed P-wave arrival agrees well with the theoretical arrival time. Figure 44 shows the P-wave arrival recorded at stations TDC1, TDC2, TDC3 and TDC4 for the magnitude 5.1 South Sandwich islands earthquake on 8 November at 22:57 UTC. The P-waves have a slightly longer period than those for the previous smaller event, but again the signal-to-noise ratio is highest at station TDC1.

Figure 45 shows raw, unfiltered seismograms of the vertical component of ground velocity recorded at stations TDC1, TDC2, TDC3 and TDC4 at the time of the expected T-phase arrivals from the previous two events in the South Sandwich Islands. Figure 46 shows the seismograms in Figure 45 filtered with a 4th order Butterworth filter with a pass-band of 3-7 Hz. There are no obvious changes in signal character at the time of the theoretical arrivals on either the raw or filtered records and the seismograms are again dominated by a succession of short duration noise bursts. Figure 47 shows spectrograms calculated for the vertical component of ground

velocity at stations TDC1, TDC2, TDC3 and TDC4. The theoretical T-phase arrivals for each event are expected at 321 and 852 seconds from the start of the record, but again there is no indication of the T-phase arrival. Instead, signals are dominated by a broad continuous peak in the 2-8 Hz range.

Figure 48 shows raw, unfiltered seismograms of the vertical component of ground velocity recorded at stations TDC1, TDC2, TDC3 and TDC4 at the time of the expected T-phase arrivals for the magnitude 4.2 and 4.9 North Atlantic ocean events on 9 November at 05:28 and 05:36 UTC, at an epicentral distance of 91.9° and back-azimuth of 341.9°. Figure 49 shows the same signals filtered with a 4^{th} order Butterworth filter with a pass-band of 2-6 Hz. Signals are dominated by a series of short duration high amplitude signals, some of which appear well correlated across all channels, but are strongest at TDC3. These seismograms can be contrasted with the seismograms of the T-phase arrivals for the same two events recorded at IMS station HA05 on Guadeloupe in Figure 50. Examination of spectrograms (Figure 51) calculated for the same data show that the signals are broadband in nature and have a frequency content of between5-20 Hz. This may be in keeping with signals commonly associated with cars and other vehicles.

Figure 52 and Figure 53 show seismograms of the vertical component of ground velocity recorded at stations TDC1, TDC2 and TDC4 at the time of the expected T-phase arrivals for the magnitude 4.2 event South of Africa on 10 November at 21:25 UTC, at a distance of 30.9° and back-azimuth of 106.1°. There is no evidence of a T-phase arrival on any station on either the raw or the filtered seismograms or on the spectrogram in Figure 54.

The three northern mid-Atlantic events on 12 November, with magnitudes 3.9-4.0, did not result in clearly detectable T-phase signals at any of the stations TDC1, TDC2 or TDC5 (Figures 55-63). There is a gradual increase in signal amplitude at the time of the expected T-phase arrival from the 09:31 event on TDC5 (Figure 56) but this is not conclusive. The cigar shaped envelope and high frequency content of the arrival observed on TDC5 at the expected arrival time of the 10:11 event (Figures 58-60) suggest that this is likely to be due to a passing vehicle.

Figure 64 shows seismograms of the vertical component of ground velocity recorded at stations TDC2, TDC6, TDC7 and TDC9 at the time of the expected T-phase arrival for the magnitude 4.5 Mid-Indian ridge event on 14 November at 00:19 UTC. Figure 65 shows the same signals filtered with a 4^{th} order Butterworth filter with a pass-band of 2-6 Hz. Again there is no clearly detectable T-phase arrival on either the raw or filtered records. Instead signals consist of short duration bursts of noise. These noise bursts are most clear on station TDC6, the station on the south of the island and are likely to be caused by surf crashing on the shore. The spectrograms calculated for the vertical component of ground velocity (Figure 66) also show no indication of a T-phase arrival on any of the stations. Signals from TDC7 are dominated by rather broadband bursts of energy on the 1-20 Hz range that we believe result from high winds at this exposed site.

Figure 67 and 68 show raw and filtered seismograms, respectively, at the time of the expected T-phase arrivals from the magnitude 4.0 South Sandwich Islands event on 14 November at 16:38. There is no evidence of a change in character that might

suggest the T-phase arrival. Similarly the spectrograms shown in Figure 69 show no indication of the T-phase arrival. The broadband nature of the noise on station TDC7 is again clear.

Figure 70 shows seismograms recorded on stations TDC7, TDC8 and TDC9 of the magnitude 4.9 event, north of Ascension island on 15 November at 01:03 UTC. The high amplitude signals observed on TDC8 are long period surface waves and are only detected on the broadband sensor. However, the P-wave is not detected. The filtered data (Figure 71 and Figure 72) shows no indication of the T-phase arrival. Spectrograms for a 10-minute window about the theoretical T-phase arrival are shown in Figure 73.

Seismograms from the second Ascension Islands event on 15 November at 02:28 are shown in Figure 74 and Figure 75 along with spectrograms in Figure 76. Again the T-phase arrival is not detected.

Recommendations for sensor locations

Signal-to-noise ratio is the main criteria for a T-phase station as it is more important to have good coupling to the ocean T-phase signals rather than overall low noise conditions. However, the absence of detectable T-phase signals at any stations for any of the oceanic events examined makes it impossible to use this as a criteria to determine permanent station locations, beyond saying that signal-to-noise ratio is very low for these event. In addition, particularly in a remote location such as Tristan Da Cuhna, site selection compromise between the availability of infrastructure and the seismic conditions. The noise levels at any site depend on the local geology and the proximity of noise sources both man-made, as roads and infrastructure, and natural, such as surf and wind.

In general, the geological conditions on Tristan Da Cuhna are poor for seismograph installation. The absence of solid basement rock at shallow depths anywhere on the settlement plain means that any sensor will be situated in relatively soft sediments and likely to be rather noisy, whereas a seismograph installed on solid rock will be relatively insensitive to local disturbances.

Cultural noise is only a problem close to the settlement of Edinburgh and alongside the islands only road and seems to be restricted mainly to passing vehicles and other machinery and also to the diesel generator plant that provides power. Stations around the settlement display higher levels of natural noise due to the exposed position on the Northern coast of the island, whereas stations to the southwest of the settlement, TDC5 and TDC8, were found to exhibit the lower noise level in the 1-10 Hz range and are more sheltered from wind and sea noise. In the absence of measured signal-to-noise ratio, we suggest that this is the most suitable area for the establishment of a permanent station, provided that infrastructure issues can be resolved. The position of TDC5 is rather too close to the road linking the Patches and the Settlement, however TDC8 is reasonably far from any cultural noise sources and therefore, a more appropriate site. A station here will require a radio telemetry link to transmit data to the central facility at the settlement, with at least one repeater station.

Discussions with survey teams for both the infrasound and radionuclide technologies suggest that the most appropriate site for the central facility will be at the edge of the golf course, close to where TDC3 was deployed. We also recommend that a second sensor be deployed close to this site with a direct cable link to provide power and data transmission. This station, though perhaps noisier will provide both an element of redundancy and slight improvement in azimuthal coverage of ocean areas to the north.

Recommendations for vault construction

In general a seismic vault should satisfy the following general requirements

- Provide adequate environmental conditions for the equipment;
- Good contact of seismic sensors with bedrock;
- Minimize seismic noise generated by wind, people, animals, and by potential noise sources within the vault;
- Assure a suitable electric ground for sensitive electronic equipment;
- Provide sufficient space for easy access and maintenance of the instruments.

There are many designs available for seismic vaults. However, given the limited infrastructure on Tristan a simple design is the most practical. We recommend that all non-concrete parts be pre-fabricated before shipping. Ideally the depth to bedrock determines the depth of the vault, but in the present case this is uncertain. We estimate that it may be several meters to any form of bedrock, which in this case is likely to comprise lava flows underlying the colluvium. In general, a shallow vault will suffer seismic noise because of the near-surface installation. The surface wave nature of seismic noise results in the exponential decay of seismic noise amplitude with depth, so high frequency noise will attenuate relatively rapidly.

The vault itself should be made of large diameter metal or plastic pipe, at least 1.5m wide, to allow access, with a high quality watertight concrete base that will act as a seismic pier. A metal construction will provide additional lightning protection, whereas plastic will be easier to handle. Both are watertight. This should preferably have a ladder built into the side to allow easy access to the pier.

The sensor must be situated on a levelled pier, consisting of concrete only. Steel reinforcing (re-bar), wire mesh, and rock aggregates all have different coefficients of thermal expansion and should not be used in a seismic pier. A mixture of 50 percent cement and 50 percent sharp sand will produce a very hard, smooth pier. If the intention is to use a broadband sensor, then the pier should also be isolated from the walls of the vault.

The vault should include reasonable lightning protection that includes the following measures:

- Proper cabling that minimizes voltage induction during lightning.

- Protection of all cables entering the seismic vault from voltage surges by special electronic devices.
- A good grounding system

There must be a water-drainage ditch around the base of the pier, with an additional external drainage pipe. This must have a metal grill to prevent ingress of rodents and other animals.

The vault should be insulated with a tight thermal cover made of Styrofoam, foam rubber or other such insulation material that will minimize fluctuations in vault temperature due to external variations. The metal cover of the vault should slope slightly and overhang the top of the wall to minimize water entry during high winds.

Batteries charged by solar panels will provide power at the site. The solar panel array should be at a distance of at least 50 m from the vault. The number of batteries and panels will depend on the overall power consumption. A steel or glass-fibre structure will provide both a housing for the batteries and a frame for the panels. The panels must be oriented to ensure optimum charging. The radio transmitter should also be sited at the power source, together with either a whip or directional antennae.

A fence to minimize the noise from animals that graze in the nearby area should surround the vault. We recommend an enclosure of 10m by 10m, but this will depend on land availability.

Discussion and Conclusions

As expected for a small island, high levels of noise are observed due to the proximity of the primary natural noise source, the sea. In addition, local geological conditions on this volcanic island are not ideal for the deployment of seismic instrumentation. Noise levels in the 2-7 Hz range are particularly high and dominated by the surf noise due to waves crashing against the shore. Amplitudes of these signals are higher on the horizontal components than on the vertical. Sites around the settlement of Edinburgh showed particularly high noise levels in this band with the noise exceeding the Peterson high noise model. We attribute this to the exposure of this location to the prevailing winds and seas.

The natural seismic events that occurred during the survey did not result in any detectable T-phase signals on any stations. This suggests both that the signal-to-noise ratio for any T-phases generated by these events is very low, given that noise levels are high in the frequency band of interest and also that there may be a possibility of a blockage of oceanic T-waves from some azimuths.

Measurements from sites to the southwest of the settlement of Edinburgh were found to exhibit the lowest noise in the 1-10 Hz range. In the absence of measured signal-to-noise ratio, we suggest that this is the most suitable area for the establishment of a permanent station. This area offers considerably more shelter from winds and sea. However, maintenance of remote stations may prove relatively difficult on this small

island A second sensor should be deployed near the Settlement of Edinburgh with a direct cable link to the central facility to provide power and data transmission. This station, though perhaps noisier will provide both an element of redundancy and slight improvement in azimuthal coverage of ocean areas to the north.

RMS amplitudes measurements from all stations exhibit a strong correlation with tidal variations, with 12 hourly noise peaks the correlate with the high tide.

References

Cessaro, R.K. (1994). Sources of primary and secondary microseisms. Bull. Seism. Soc. Am., **84**, 1, 142-148.

Dunkley, P., 2001. Volcanic hazard assessment of Tristan Da Cuhna. British Geological Survey Report.

Longuet-Higgins, M.S., 1950. A theory of the origin of microseisms, *Phil. Trans. R. Soc. London*, **243**, 1-35.

Peterson, J., 1993. Observations and modelling of background seismic noise. Open File report 93-322, U.S. Geological Survey, Albuquerque, New Mexico.

Okal, E.A. 2001. T-phase stations for the International Monitoring System of the Comprehensive Nuclear-Test Ban Treaty: a global perspective. *Seis. Res. Lett.* **72**, 2, 186-196.

Ollier C D, 1984. Geomorphology of South Atlantic Volcanic Islands Part I: The Tristan da Cunha Group. Zeitschrift für Geomorphologie N F Vol. 28, Pt3, 367-382.

Welch, P.D., 1967. The Use of Fast Fourier Transform for the Estimation of Power Spectra: A Method Based on Time Averaging Over Short, Modified Periodograms. *IEEE Trans. Audio Electroacoust*., **AU-15**, 70-73.

Young, Ch.J., Chael, E.P., Withers, M.W. and Aster, R.C. (1996). A comparison of the high-frequency (>1Hz) surface and subsurface noise environment at three sites in the United States. Bull. Seism. Soc. Am. **86**, 5, 1516-1528.

Tables

Table 1: Station coordinates and times of operation for site survey HA09

Station	Latitude	Longitude	Height	Start	Stop
TDC1	37 04.298 S	12 18.577 W	X	7/11/2001 17:50	12/11/2001 0925
TDC2	37 04.248 S	12 18.633 W	X	7/11/2001 19:00	14/11/2001 1800
TDC3	37 04.062 S	12 18.912 W	X	8/11/2001 10:00	10/11/2001 19:30
TDC4	37 03.973 S	12 19.055 W	X	8/11/2001 12:05	11/11/2001 11:00
TDC5	37 05.447 S	12 19.492 W	X	11/11/2001 15:48	13/11/2001 13:30
TDC6	37 09.978 S	12 16.292 W	X	12/11/2001 13:28	14/11/2001 13:36
TDC7	37 04.580 S	12 18.166 W	710	12/11/2001 14:46	15/11/2001 09:09
TDC8	37 05.852 S	12 20.080 W	X	14/11/2001 11:10	15/11/2001 12:05
TDC9	37 04.298 S	12 18.573 W	X	13/11/2001 15:36	15/11/2001 14:36

Table 2: Acquistion parameters for site survey HA09

Station	Sensor	S/N	Sensitivity (V/m/s)	Acquisition	S/N	Gain	Recording
TDC1	STS2	89925	1500	Reftek 72A-08	1115	1	1.907μV/bit
TDC1	LE-3D	LE203	400	Reftek 72A-06	0274	32	3.576μV/bit
TDC2	CMG40T	T4C36	800	ED-PR2400	XXX	1	0.9537μV/bit
TDC3	LE-3D	LE215	400	Reftek 72A-06	0333	32	3.576μV/bit
TDC4	LE-3D	LE202	400	Reftek 72A-06	0331	32	3.576μV/bit
TDC5	LE-3D	LE215	400	Reftek 72A-06	0333	32	3.576μV/bit
TDC6	LE-3D	LE202	400	Reftek 72A-06	0331	32	3.576μV/bit
TDC7	LE-3D	LE203	400	Reftek 72A-06	0274	32	3.576μV/bit
TDC8	STS2	89925	1500	Reftek 72A-08	1115	1	1.907μV/bit
TDC9	LE-3D	LE215	400	Reftek 72A-06	0333	32	3.576μV/bit

Table 3. Seismo-acoustic events chosen for analysis, using locations computed by the ISC

Date	Time	Latitude	Longitude	Mb	Locality
2001/11/08	03:58:21.29	53.996S	02.366W	4.2	Southern Mid-Atlantic
2001/11/08	22:52:45.42	55.598S	30.121W	4.4	South Sandwich Island
2001/11/08	22:57:52.78	60.781S	25.644W	5.1	South Sandwich Island
2001/11/09	05:28:25.33	52.950N	35.100W	4.2	North Atlantic Ocean
2001/11/09	05:36:10.12	53.0970N	35.157W	4.9	North Atlantic Ocean
2001/11/10	21:25:00.60	53.216S	25.723E	4.2	South of Africa
2001/11/12	09:31:00.43	22.220N	45.087W	3.9	Northern Mid- Atlantic
2001/11/12	10:11:16.84	22.368N	45.153W	4.0	Northern Mid- Atlantic
2001/11/12	10:31:18.74	22.418N	45.038W	4.0	Northern Mid- Atlantic
2001/11/14	00:19:40.31	25.165S	69.982E	4.5	Mid-Indian Ridge
2001/11/14	16:38:19.56	55.992S	29.040W	4.0	South Sandwich Island
2001/11/15	01:03:06.53	1.542S	15.616W	4.9	North of Ascension Island
2001/11/15	02:28:03,72	1.323S	15.366W	4.0	North of Ascension Island

Table 4. Theoretical arrival times and detections for P- and T- phases for the 13 seismo-acoustic events listed in Table 3

Date	Origin Time	Δ	Back-azimuth	P-wave arrival time	P-wave Detected	T-phase arrival time	T-phase detected
2001/11/08	03:58:21.29	18.1	152.6	04:02:35.0	NO	04:21:16.1	NO
2001/11/08	22:52:45.42	22.1	220.5	22:57:39.3	YES	23:20:21.8	NO
2001/11/08	22:57:52.78	22.1	220.5	23:03:20.8	YES	23:29:12.1	NO
2001/11/09	05:28:25.33	91.8	341.9	05:41:33.42	NO	07:23:00.3	NO
2001/11/09	05:36:10.12	91.8	341.9	05:49:18.9	NO	07:30:56.4	NO
2001/11/10	21:25:00.60	30.9	106.1	21:31:16.46	NO	22:03:31.4	NO
2001/11/12	09:31:00.43	66.6	331.9	09:41:49.8	NO	10:54:06.3	NO
2001/11/12	10:11:16.84	66.6	331.9	10:22:08.7	NO	11:34:33.8	NO
2001/11/12	10:31:18.74	66.6	331.9	10:42:10.3	NO	11:54:36.7	NO
2001/11/14	00:19:40.31	69.4	133.8	00:30:48.7	NO	01:46:20.7	NO
2001/11/14	16:38:19.56	22.0	217.9	16:42:55.5	NO	17:05:43.1	NO
2001/11/15	01:03:06.53	35.5	355.5	01:10:03.3	NO	01:47:25.4	NO
2001/11/15	02:28:03,72	35.5	355.5	02:35:02.2	NO	03:12:37.95	NO

Appendix A: Details of Data Acquisition

Station	TDC1 (short period)
Sensor	LE-3D serial number L203
Channels	SHZ, SHN, SHE
Digitizers	Reftek 72A-02 serial number 0274
GPS Position	37 04 17.9 S 012 18 34.6 W
Start date	7/11/2001 1750 (311)
Stop date	12/11/2001 0925 (316)
Location	Pasture directly above settlement at base of cliffs
Notes	Sensor misaligned, 24° west of magnetic North instead of 24° east. In pit with concrete base, covered with insulated box, backfilled with rock and gravel and covered with turf.

Acquisition Log

Date	DOY	Time	Disk	Comment
7/11	311	1750	350	Acquisition started, event number 1
9/11	313	1500	350	Acquisition stopped for data download
9/11	313	1700	350	Acquisition restarted at event number ?
10/11	314	1710	350	Acquisition stopped for download.
10/11	314	1730	350	Acquisition restarted
12/11	316	0925	350	Acquisition stopped at event number 110

Station	TDC1 (broadband)
Sensor	STS-2 89925
Channels	BHZ, BHN, BHE
Digitizers	Reftek 72A-08 serial number 1115
GPS Position	37 04 17.9 S 012 18 34.6 W
Start date	7/11/2001 1750 (311)
Stop date	13/11/2001 (317)
Location	Pasture directly above settlement at base of cliffs
Notes	Sensor misaligned, 24° west of magnetic North instead of 24° east. In pit with concrete base, covered with insulated box, backfilled with rock and gravel and covered with turf.

Acquisition Log

Date	DOY	Time	Disk	Comment
7/11	311	1800	350	Acquisition started
13/11	317	0925	350	Acquisition stopped

Station	TDC2 (broadband)
Sensor	CMG-40T serial number T4C36
Digitizer	Earth Data PR2400
GPS position	37 04 14.9 S 012 18 38.0 W
Start date	7/11/2001 1900 (311)
Stop data	14/11/2001 1800 (318)
Location	Pasture above settlement about halfway between the cliffs and the edge of the settlement.
Notes	In pit with concrete base set on consolidated rock/soil. Covered with insulated box, backfilled with soil and covered with turf.

Acquisition Log

Date	DOY	Time	Disk	Comment
7/11	311	1900		Acquisition started
9/11	313	1510		Acquisition stopped for data download
9/11	313	1830		Acquisition restarted
11/11	315	1655		Acquisition stopped for data download.
11/11	315	1825		Acquisition restarted
13/11	317	0935		Interruption to acquisition
13/11	317	1010		End of interruption
14/11	318	1330		Acquisition stopped for data download
14/11	318	1430		Acquisition restarted
14/11	318	1800		Acquisition stopped

Station	TDC3
Sensor	LE-3D serial number 215
Digitizer	Reftek 72A-02 serial number 0333
GPS Position	37 04 03.7 S 012 18 54.7 W
Location	Golf course, near remains of sighting beacon.
Notes	In pit with concrete base set on consolidated rock/soil. Covered with box, then back-filled with soil and covered with turf.

Acquisition Log

Date	Time	Disk	Comment
8/11	1035	5136	Acquisition started at event number 1
9/11	1825	5136	Acquisition stopped for download, 32 events
9/11	1838	5136	DAS reset and acquisition restarted at event 33
10/11	1815	5136	Acquisition stopped for download, 57 events
10/11	1826	5136	DAS reset and acquisition restarted at event 58
10/11	2000	5136	Acquisition stopped, 59 events.

Station	TDC4
Sensor	LE-3D serial number 202
Digitizer	Reftek 72A-02 serial number 0331
GPS position	37 03 58.4 S 012 19 03.3 W
Location	Site of old wind generator on edge of the cliff.
Notes	In pit with concrete base set on consolidated rock/soil. Covered with box, then back-filled with soil and covered with turf.

Acquisition Log

Date	Time	Disk	Comment
8/11	1200	5789	Acquisition started event number 1.
9/11	1851	5789	Acquisition stopped for download, 31 events
9/11	1906	5789	Acquisition restarted event number 32
10/11	1836	5789	Acquisition stopped for download 55 events
10/11	1849	5789	Acquisition restarted event 56
12/11	0810	5789	DAS dead due to low voltage (5.7V). Last event 72.

Station	TDC5
Sensor	LE-3D serial number 215
Digitizer	Reftek 72A-02 serial number 0333
GPS Position	37 05 26.8 S 012 19 29.5 W
Location	Potato patches, 400m away from road towards the cliffs
Notes	Sensor placed on rock surface, just below turf.

Acquisition Log

Date	Time	Disk	Comment
11/11	1548	5136	Acquisition started event number 60
13/11	1330	5136	Acquisition stopped event number 105

Station	TDC6
Sensor	LE-3D serial number 202
Digitizer	Reftek 72A-02 serial number 0331
GPS position	37 09 58.7 S 012 16 17.5 W
Location	Stony Beach point
Notes	Sensor placed on rock outcrop on basalt lava flow covered with box and turf.

Acquisition Log

Date	Time	Disk	Comment
12/11	1328	5789	Acquisition started event number 74
14/11	1336	5789	Acquisition stopped event number 124

Station	TDC7
Sensor	LE-3D serial number L203
Digitizer	Reftek 72A-02 serial number 0274
GPS Position	37 04.580 S 012 18.166 W 710 m
Location	Top of cliffs above settlement
Notes	Sensor misaligned, 24° west of magnetic North instead of 24° east. On rock ledge in narrow gully, covered with box and turf.

Acquisition Log

Date	Time	Disk	Comment
7/11	1800	350	Acquisition started, event number 1
9/11	1500	350	Acquisition stopped for data download

Station	TDC8
Sensor	STS-2
Digitizer	Reftek 72A-08 serial number 1115
GPS Position	37 05 51.1 S 012 20 04.8 W
Location	Potato Patches, at end of road beyond sheep pens.
Notes	Sensor placed on flat rock surface, covered with insulated box and turf

Acquisition Log

Date	Time	Disk	Comment
14/11	1100		Acquisition started.
15/11	1200		Acquisition stopped.

Station	TDC9
Sensor	LE-3D serial number 215
Digitizer	Reftek 72A-02 serial number 0333
GPS Position	37 04 17.9 S 012 18 34.4 W
Location	On side of cliff in pasture above village
Notes	Sensor placed on rock ledge, covered with pot and turf.

Acquisition Log

Date	Time	Disk	Comment
13/11	1536	5136	Acquisition started event number 106
15/11	1436	5136	Acquisition stopped event number 152

Appendix B. Response Information

Format description for seismometer responses.
1st line: description, 5 fields

1. Source - theoretical|measured
2. Sequence nr - 1|2|...
3. Instrument name
4. Type paz|fir|fap
5. Information source

2nd line: normalisation factor and frequency
3rd line: number of poles
4th to 4+(number of poles)-1: poles (real and imaginary part)
4+(number of poles): number of zeros
4+(number of poles)+1 to 4+(number of poles)+(number of zeros): zeros (real and imaginary part)
Sensor Sensitivity.

Velocity response for GURALP CMG-40T - vertical channel
Theoretical 1 T4C36/vertical paz GURALP
-0.314159 1.0
3
-0.1480 0.1480
-0.1480 -0.1480
-314.159 0.0000
3
0.000000 0.000000
0.000000 0.000000
999.0264 0.000000
Sensor Sensitivity 824 V/m/s

Velocity response for GURALP CMG-40T – north channel
Theoretical 1 T4C36/north paz GURALP
-0.314159 1
3
-0.1480 0.1480
-0.1480 -0.1480
-314.159 0.0000
3
0.000000 0.000000
0.000000 0.000000
999.0264 0.000000
Sensor Sensitivity 806 V/m/s

Velocity response for Guralp CMG-40T - east channel
Theoretical 1 T4C36/east paz GURALP
-0.314159 1
3

-0.1480 0.1480
-0.1480 -0.1480
-314.159 0.0000
3
0.000000 0.000000
0.000000 0.000000
999.0264 0.000000
Sensor Sensitivity 798 V/m/s

Velocity response for STRECKEISEN STS-2 89225 - vertical channel
Theoretical 1 S89925/vertical paz STRECKEISEN
5.92e7 1
5
-0.03656 0.03688
-0.03656 -0.03688
-251.33 0.0
-131.04 467.29
-131.04 -467.29
2
0.000000 0.000000
0.000000 0.000000

Sensor Sensitivity 1500.0 V/m/s

Velocity response for STRECKEISEN STS-2 89225 - north channel
Theoretical 1 S89925/north paz STRECKEISEN
5.92e7 1
5
-0.03656 0.03688
-0.03656 -0.03688
-251.33 0.0
-131.04 467.29
-131.04 -467.29
2
0.000000 0.000000
0.000000 0.000000

Sensor Sensitivity 1500.0 V/m/s

Velocity response for STRECKEISEN STS-2 89225 - east channel
Theoretical 1 S89925/east paz STRECKEISEN
5.92e7 1
5
-0.03656 0.03688
-0.03656 -0.03688
-251.33 0.0
-131.04 467.29
-131.04 -467.29
2
0.000000 0.000000

0.000000 0.000000
Sensor Sensitivity 1500.0

Generic velocity response for LENNARTZ LE-3D LITE - vertical channel
Theoretical 1 LE-3D/vertical paz LENNARTZ
1.0 1
2
-4.44288 -4.44288
-4.44288 4.44288
2
0.000000 0.000000
0.000000 0.000000
Sensor Sensitivity 400.0 V/m/s

Generic velocity response for LENNARTZ LE-3D LITE -north channel
Theoretical 1 LE-3D/vertical paz LENNARTZ
1.0 1
2
-4.44288 -4.44288
-4.44288 4.44288
2
0.000000 0.000000
0.000000 0.000000
Sensor Sensitivity 400.0 V/m/s

Generic velocity response for LENNARTZ LE-3D LITE - east channel
Theoretical 1 LE-3D/vertical paz LENNARTZ
1.0 1
2
-4.44288 -4.44288
-4.44288 4.44288
2
0.000000 0.000000
0.000000 0.000000

Sensor Sensitivity 400.0 V/m/s

Reftek 72A-02 WITH GAIN OF 32
(Gain of unity: 1.1444e-4 V/bit)

Serial No.	channel	V/Bit
274	z	3.576e-6
274	n	3.576e-6
274	e	3.576e-6
331	z	3.576e-6
331	n	3.576e-6
331	e	3.576e-6
333	z	3.576e-6
333	n	3.576e-6
333	e	3.576e-6

Reftek 72A-08 with a gain of unity.

Serial No.	Channel	V/Bit
1115	z	1.907e-6
1115	n	1.907e-6
1115	e	1.907e-6

Earth Data PR2400 24 bit recorder

Serial No.	channel	V/Bit
240	z	9.537e-7
240	n	9.537e-7
240	e	9.537e-7

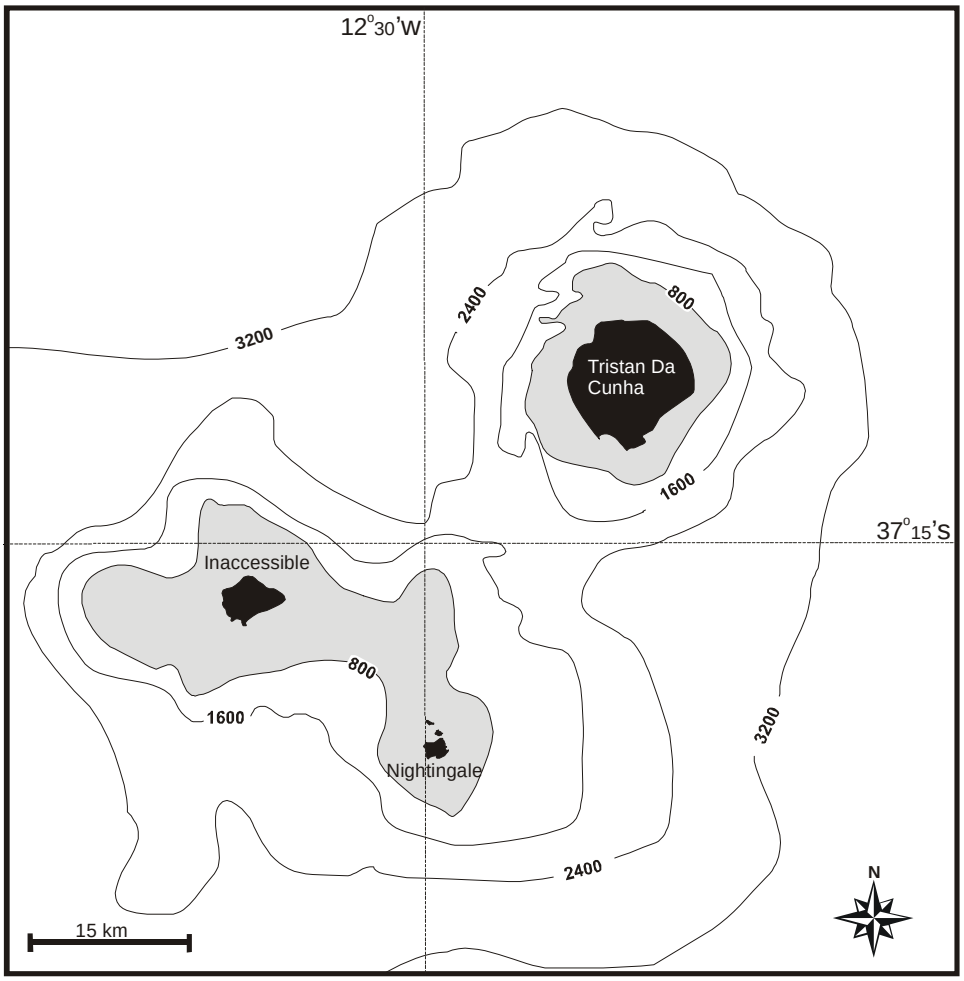

Figure 1 Bathymetry in the vicinity of Tristan Da Cuhna, with the areas between 800 and 0mbsl shaded in grey. (Based on data from Admiralty chart 1769).

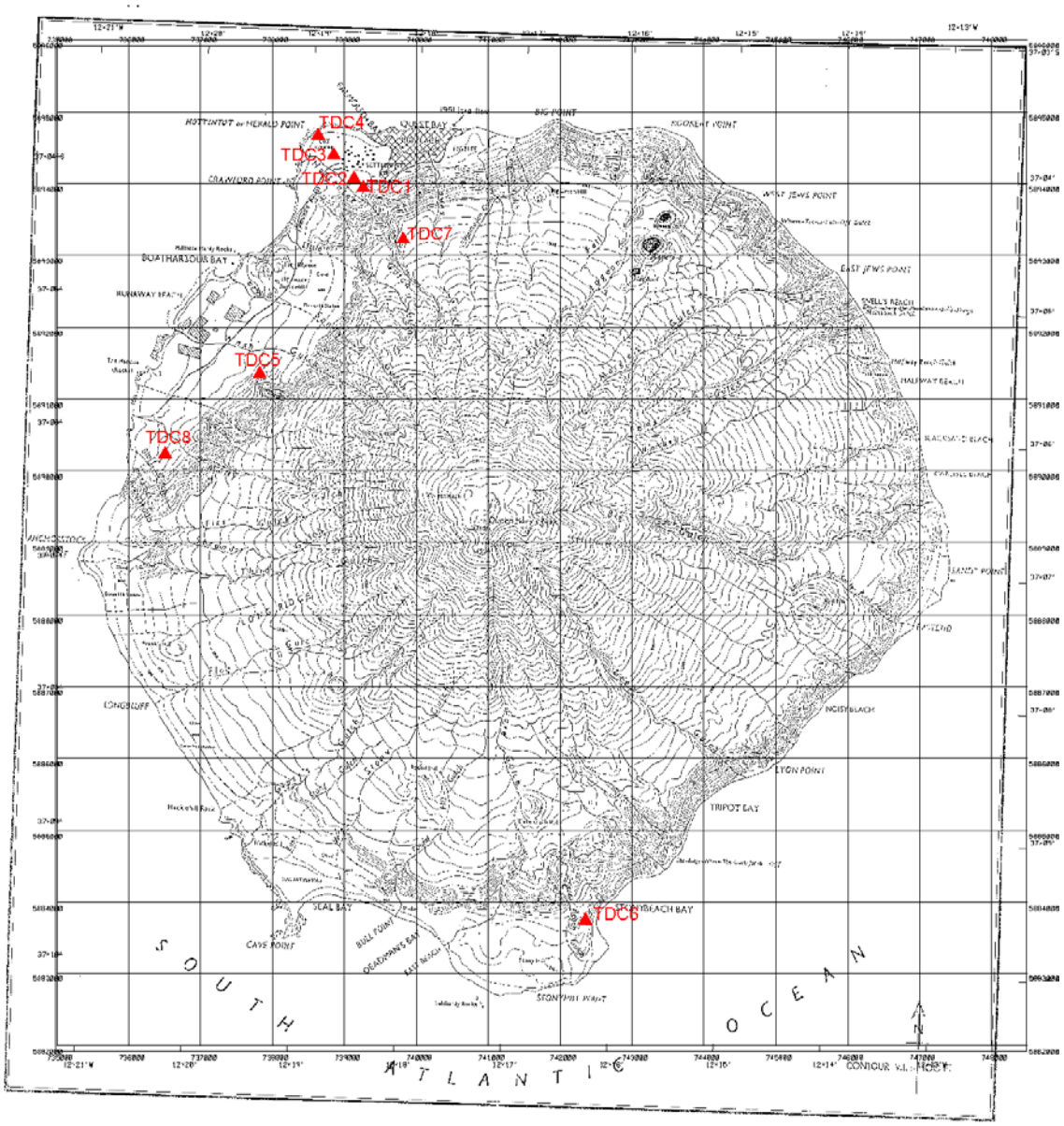

Figure 2. Map of Tristan Da Cuhna. Station installed during the site survey are marked by red triangles.

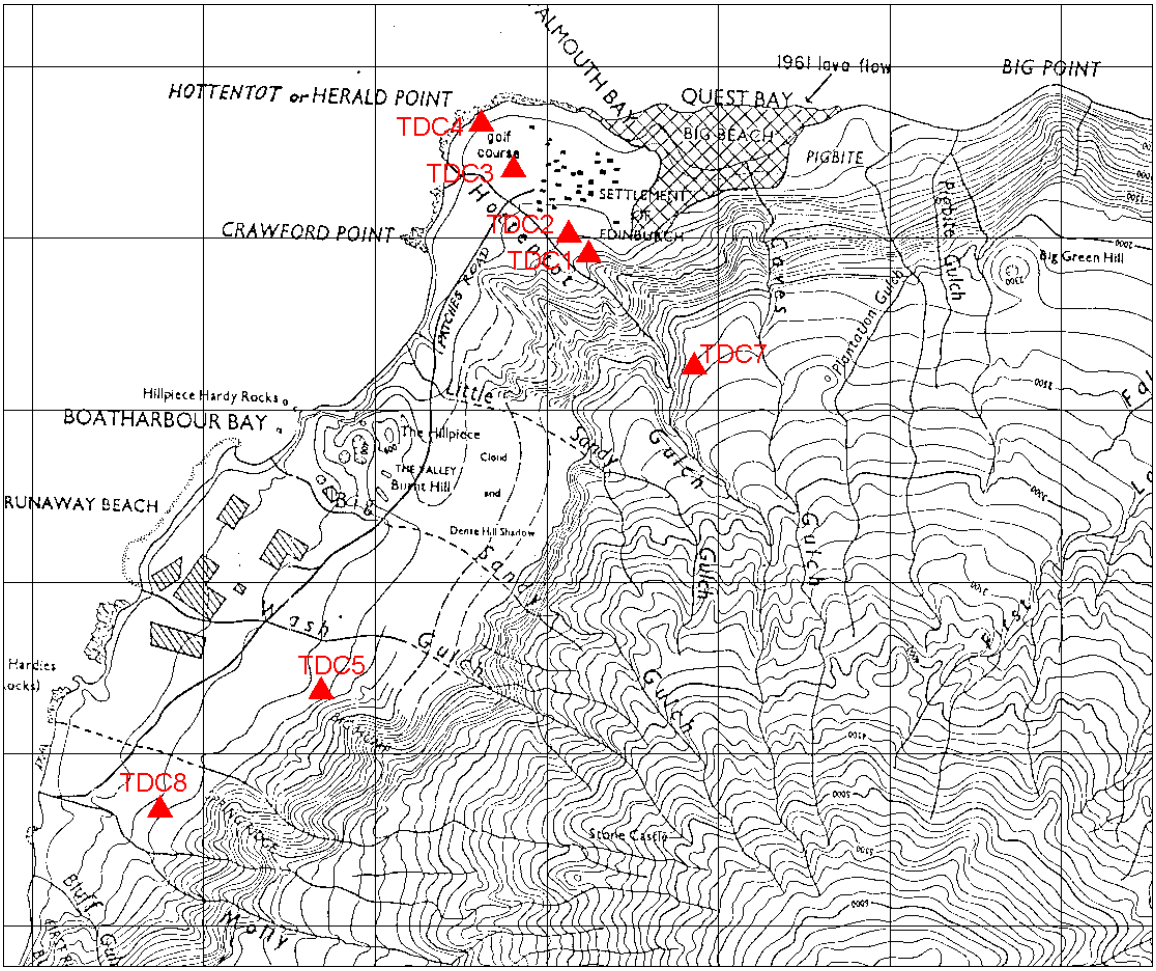

Figure 3. Northwest coastal plain showing seismic stations TDC1-TDC5 and TDC7-TDC8 (red triangles). Grid squares are 1km.

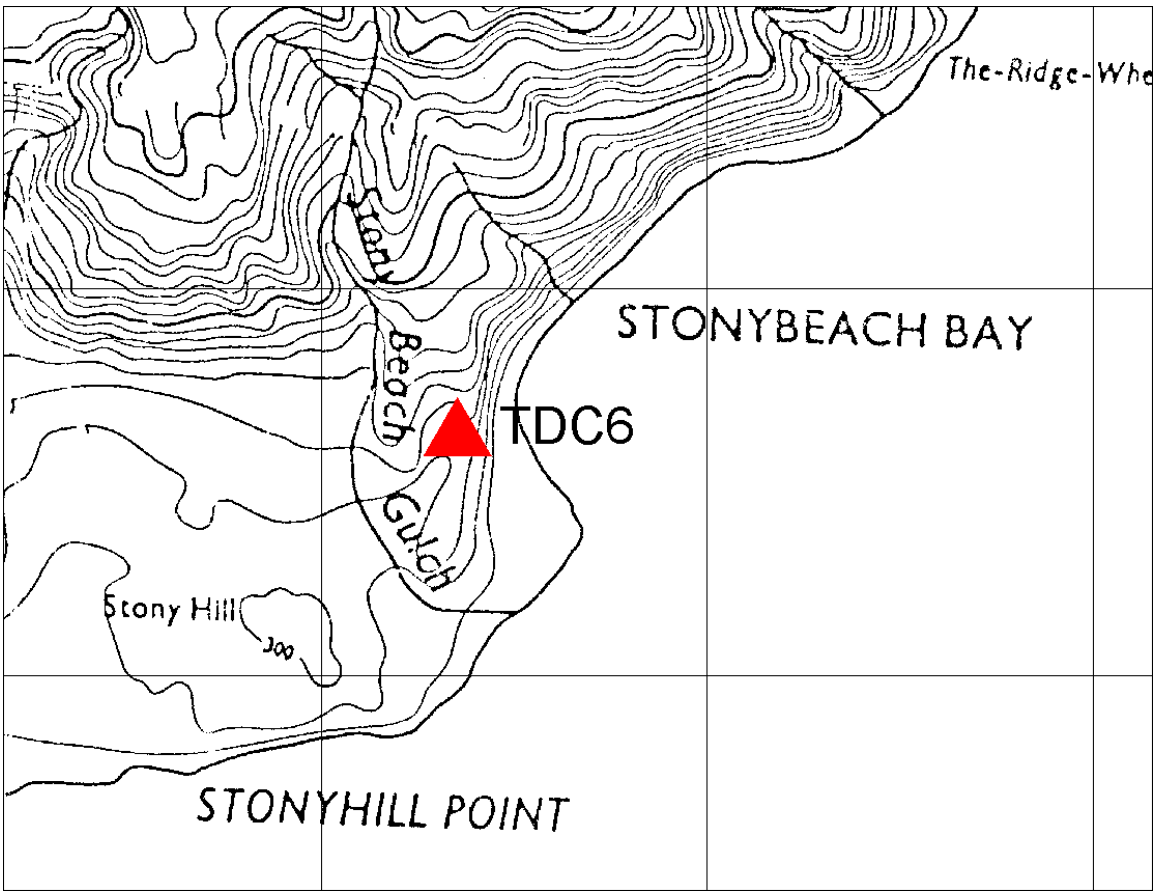

Figure 4. Map showing southern station, TDC6, at Stoneybeach.

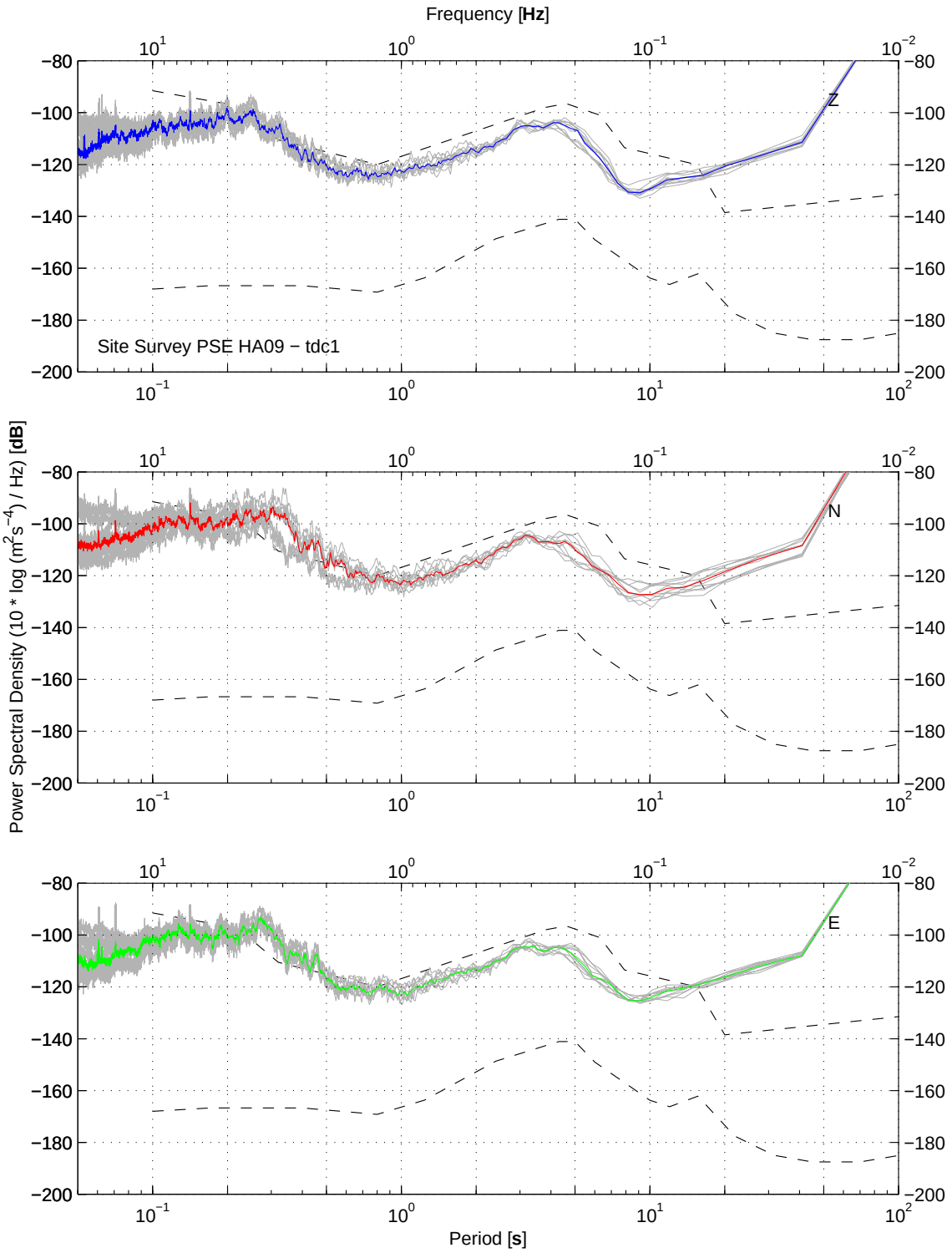

Figure 5. Power spectral density estimates for each component of ground motion at station TDC1 using overlapping 8192-point windows. Ten data segments of length 10.5 minutes were used for both day (0600-1759) and night (1800-0559). Median values for all segments are shown by blue, red and green lines. The dashed lines show the USGS low and high noise models.

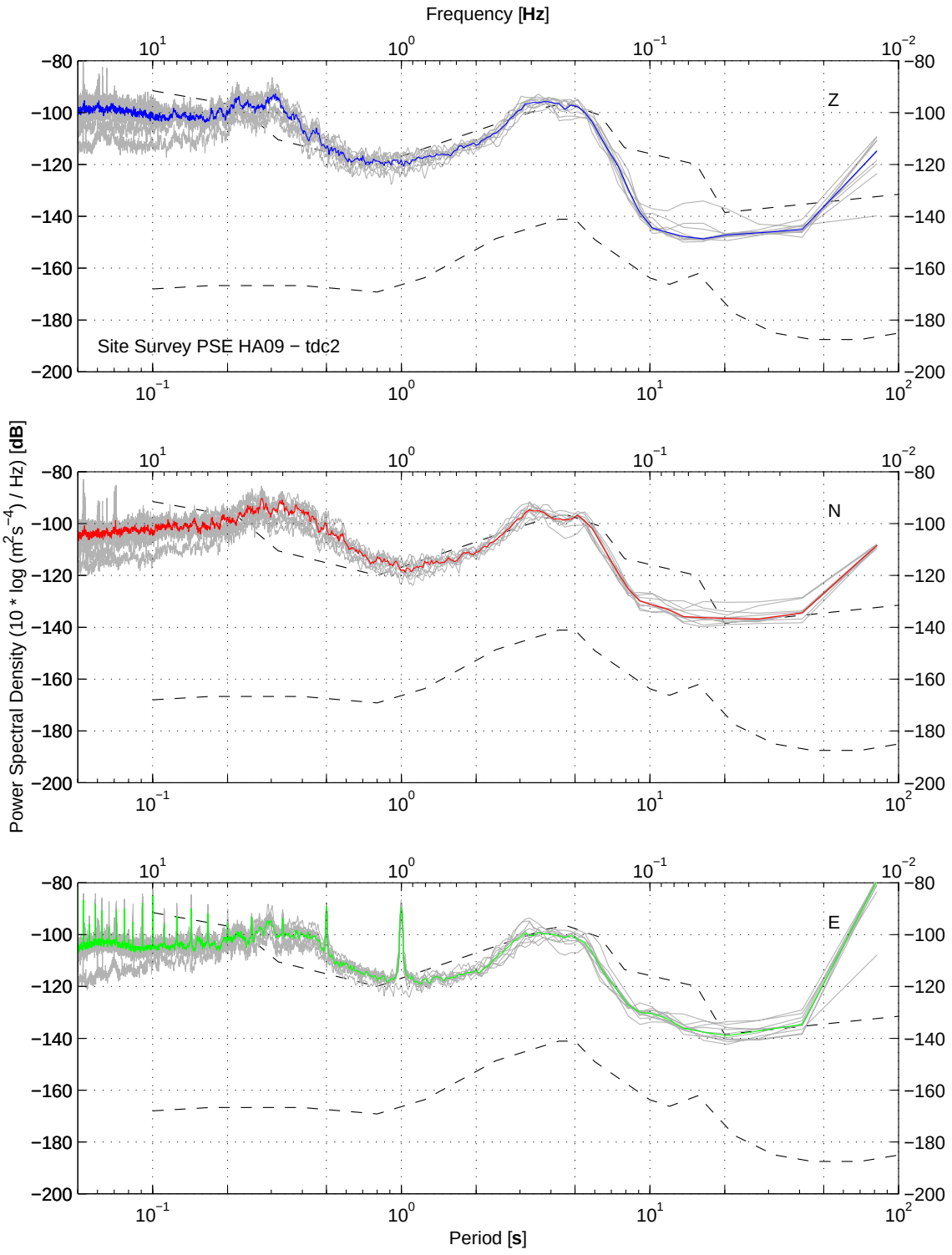

Figure 6. Power spectral density estimates for each component of ground motion at station TDC2.

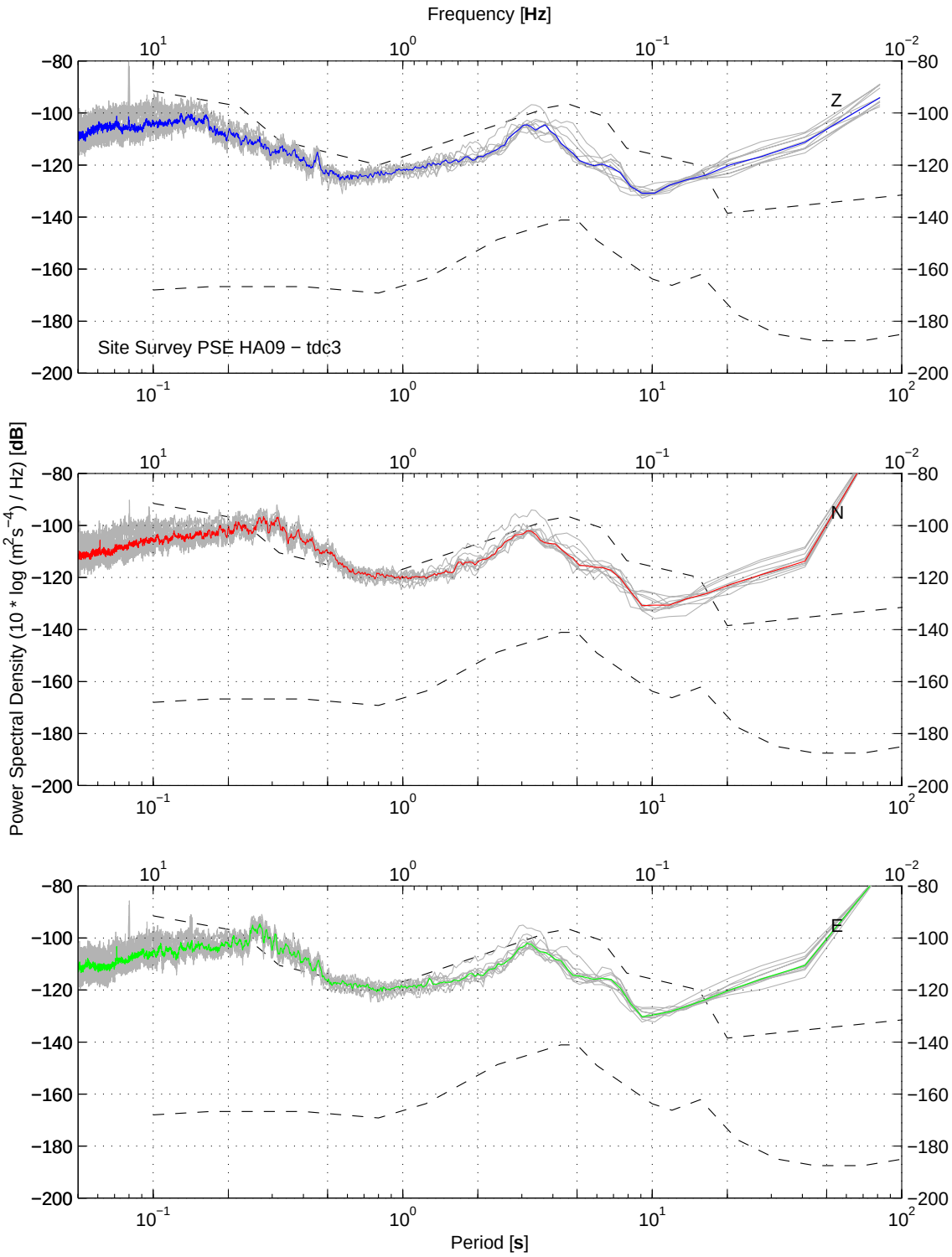

Figure 7. Power spectral density estimates for each component of ground motion at station TDC3.

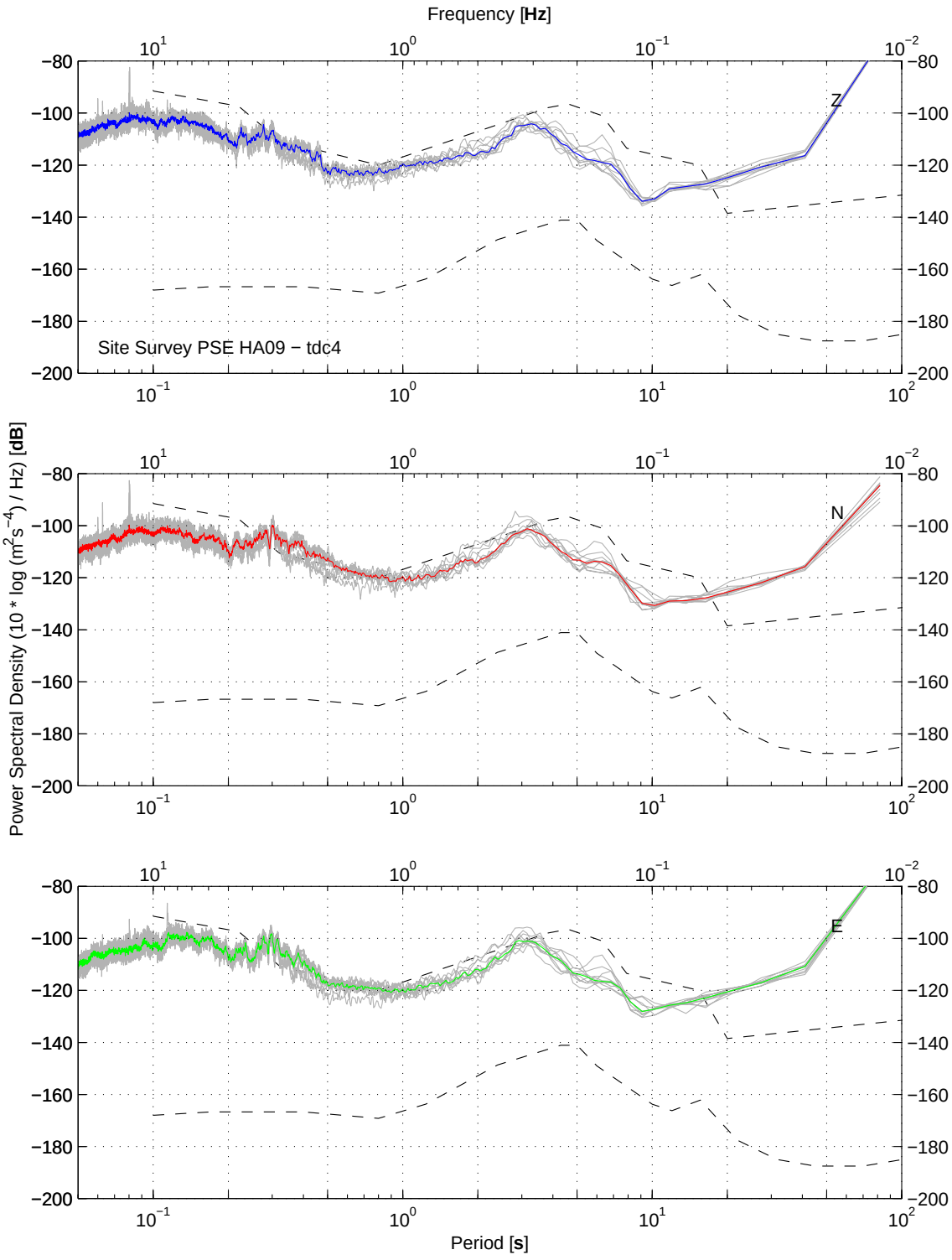

Figure 8. Power spectral density estimates for each component of ground motion at station TDC4.

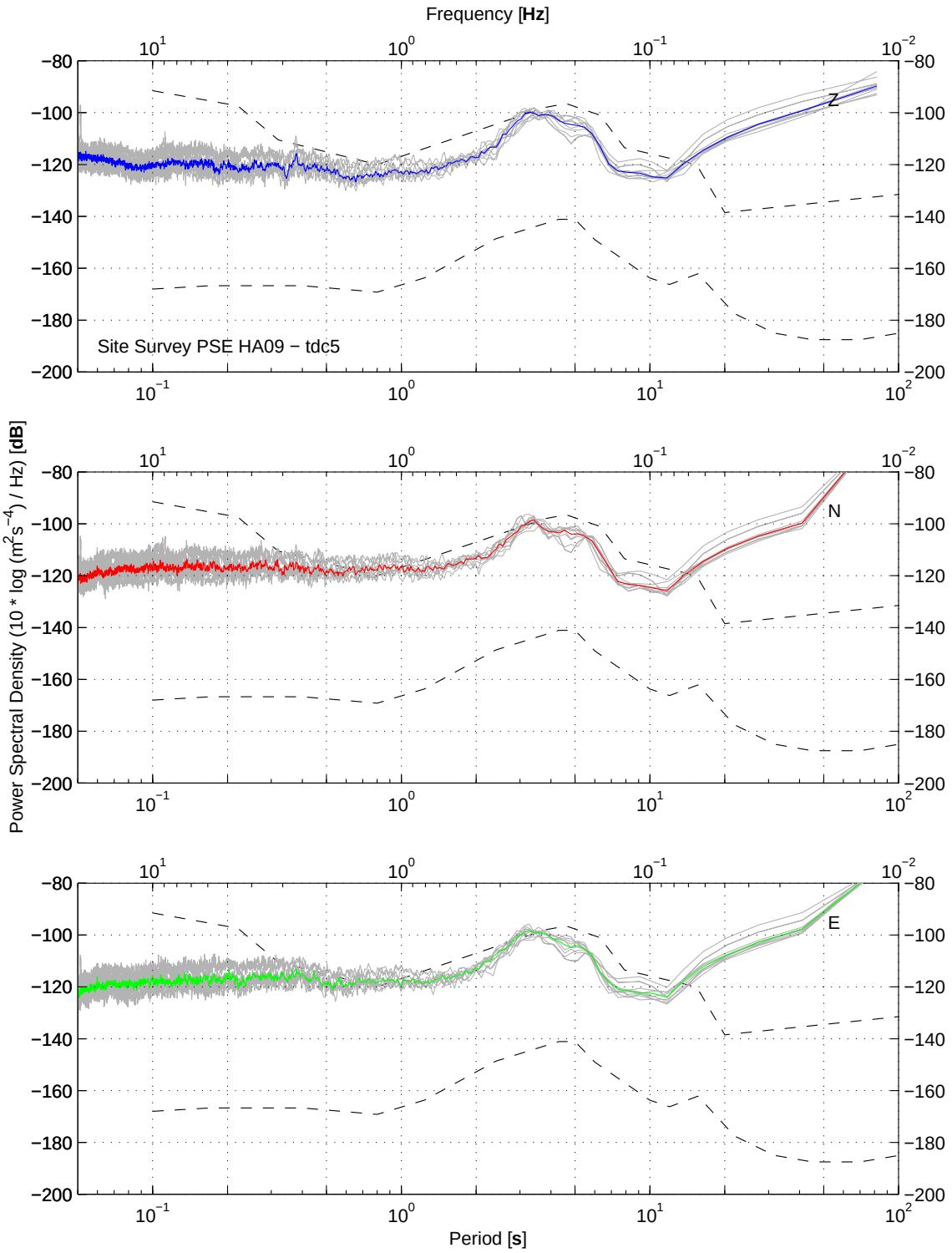

Figure 9. Power spectral density estimates for each component of ground motion at station TDC5.

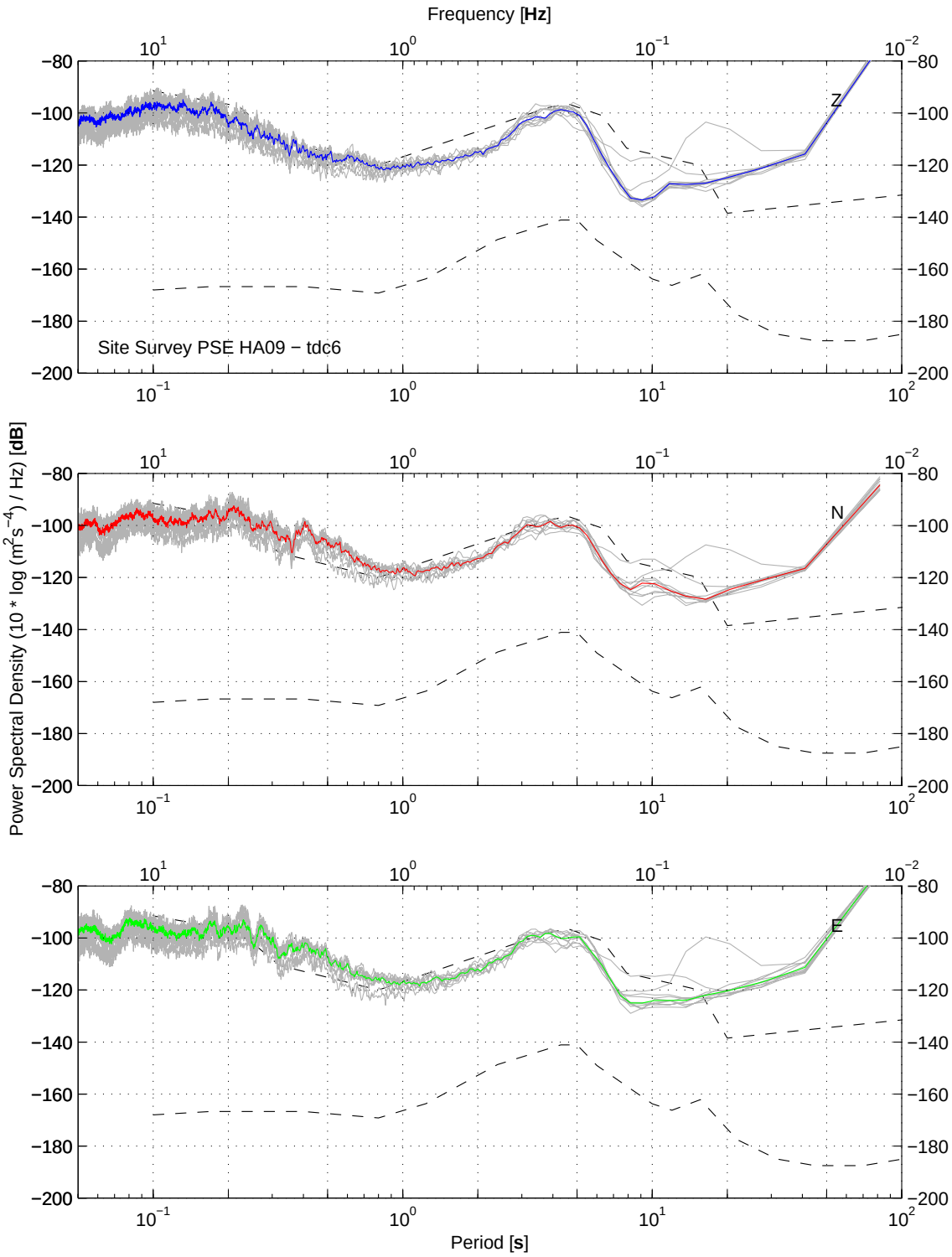

Figure 10. Power spectral density estimates for each component of ground motion at station TDC6.

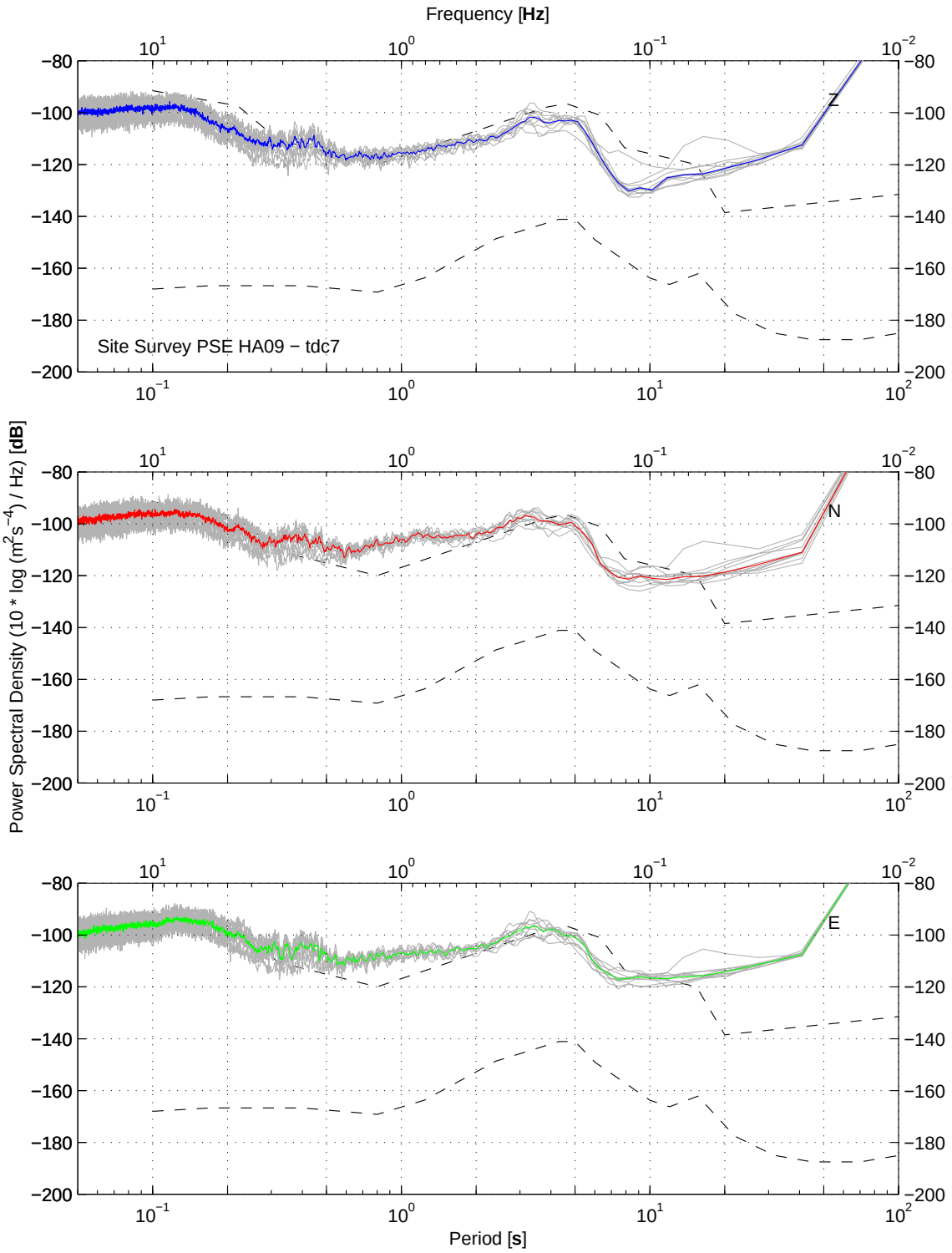

Figure 11. Power spectral density estimates for each component of ground motion at station TDC7.

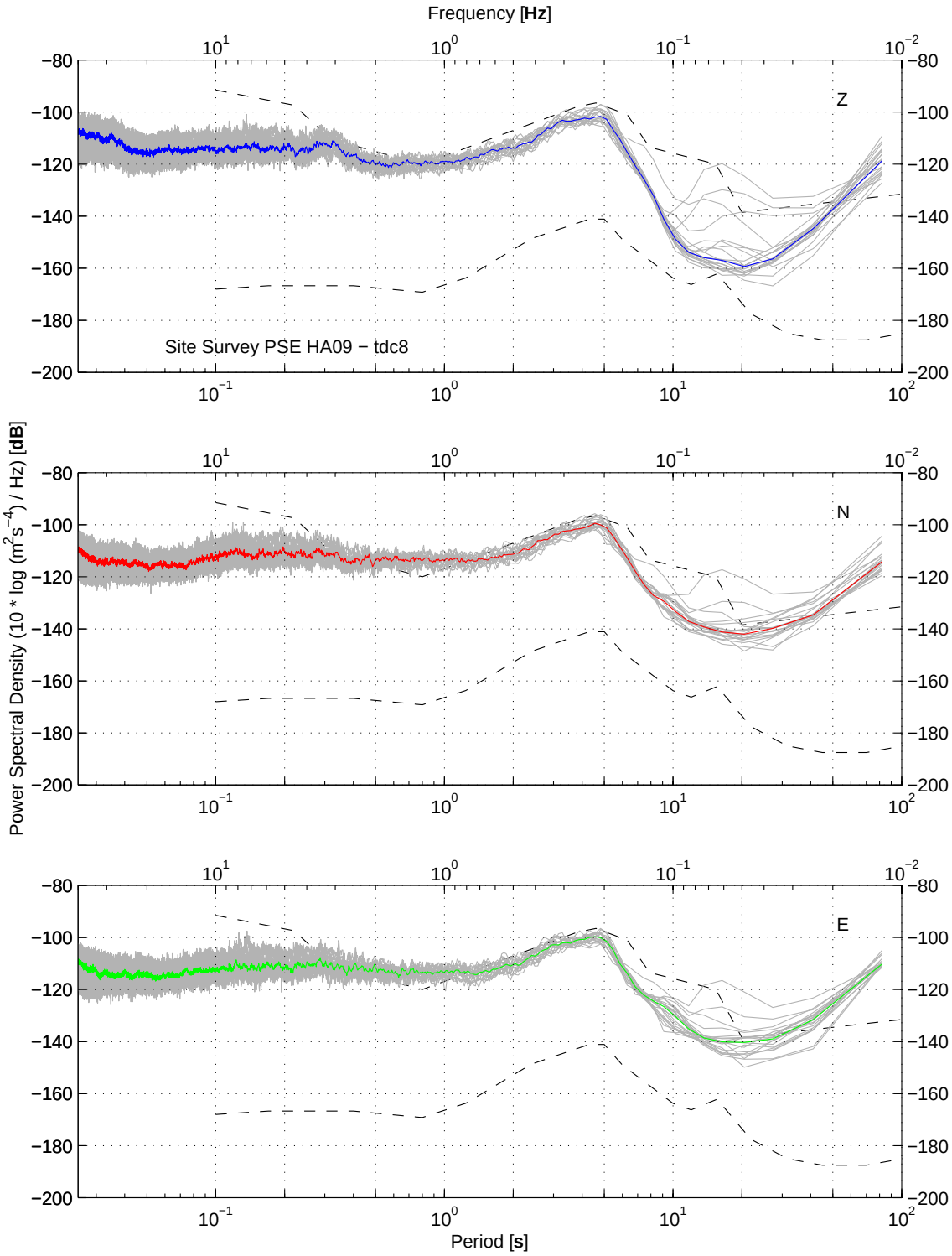

Figure 12. Power spectral density estimates for each component of ground motion at station TDC8.

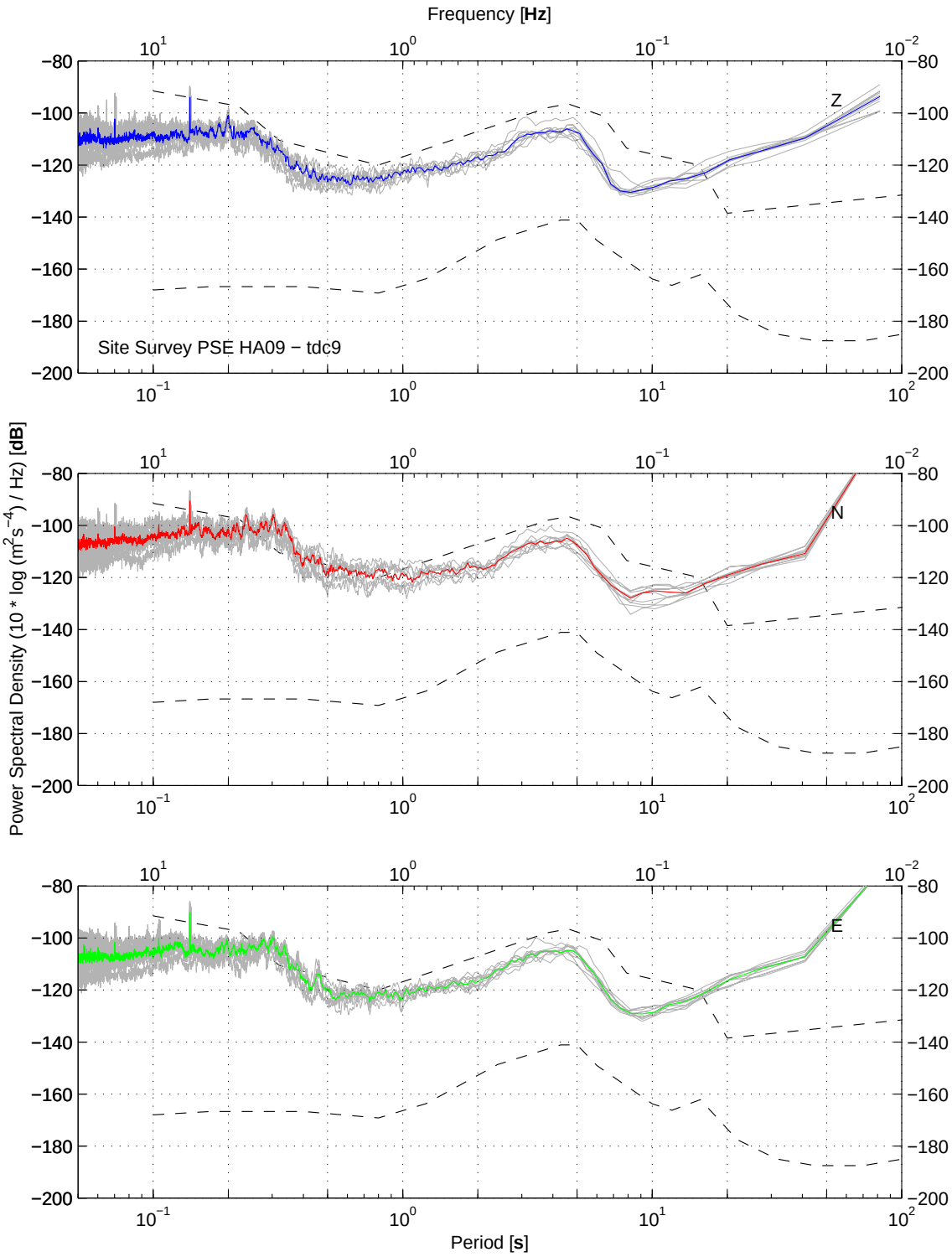

Figure 13. Power spectral density estimates for each component of ground motion at station TDC9.

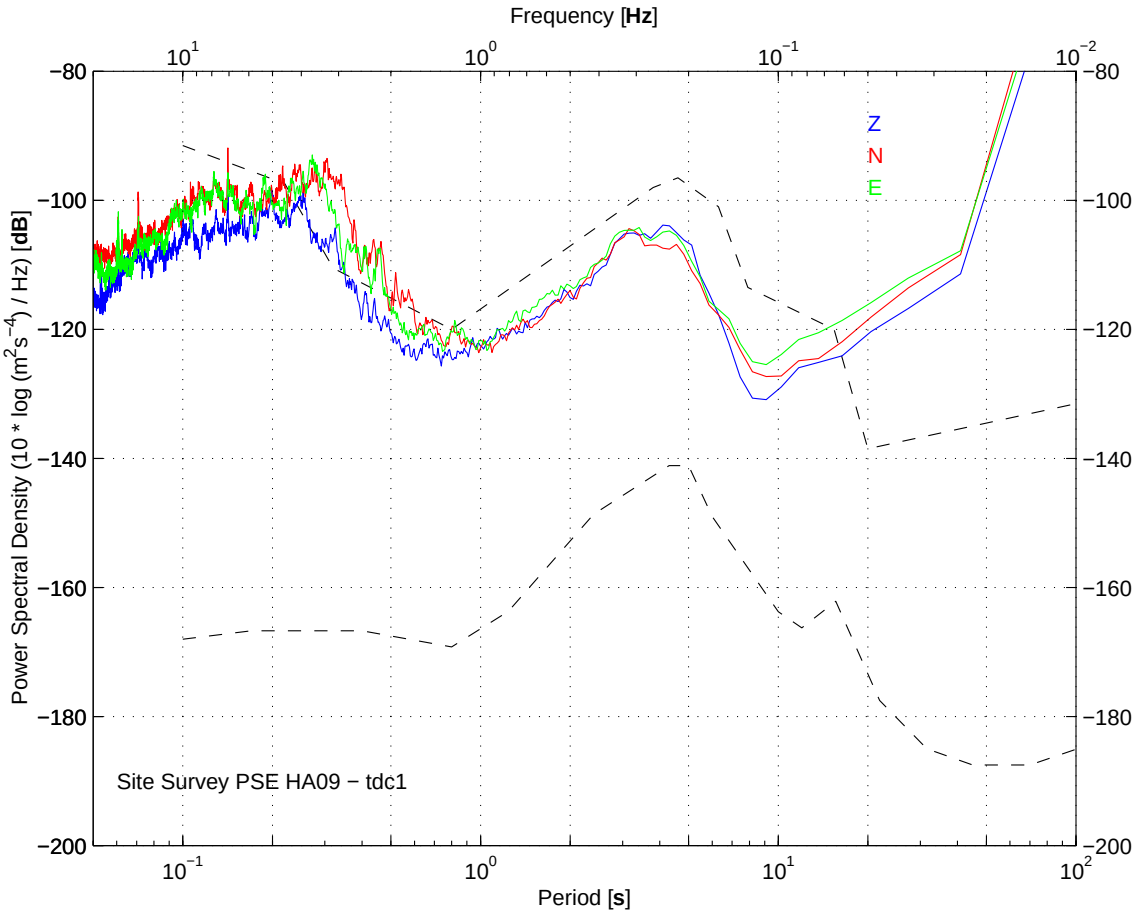

Figure 14. Composite noise curves, determined from the median value of all estimates for each component of ground acceleration at station TDC1, vertical (blue), north-south (red) and east-west (green).

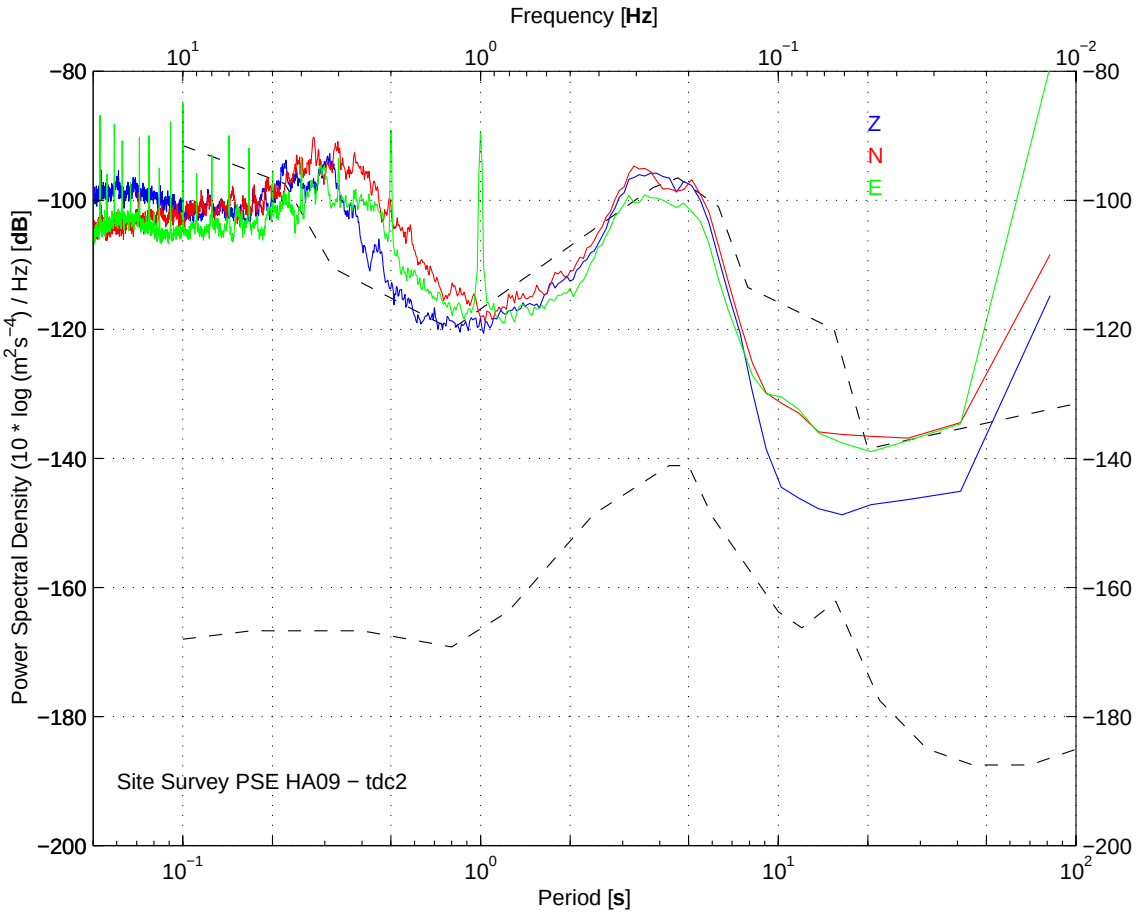

Figure 15. Composite noise curves, determined from the median value of all estimates for each component of ground acceleration at station TDC2, vertical (blue), north-south (red) and east-west (green).

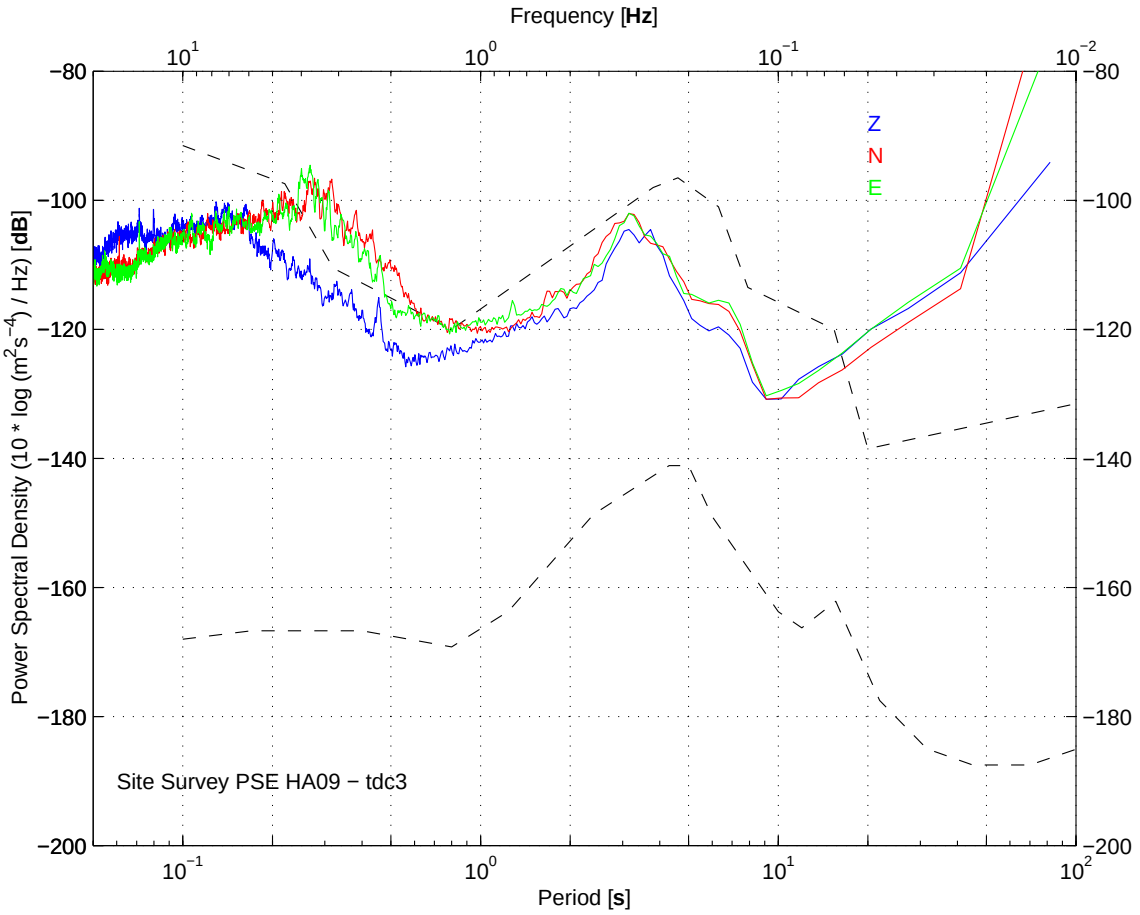

Figure 16. Composite noise curves, determined from the median value of all estimates for each component of ground acceleration at station TDC3, vertical (blue), north-south (red) and east-west (green).

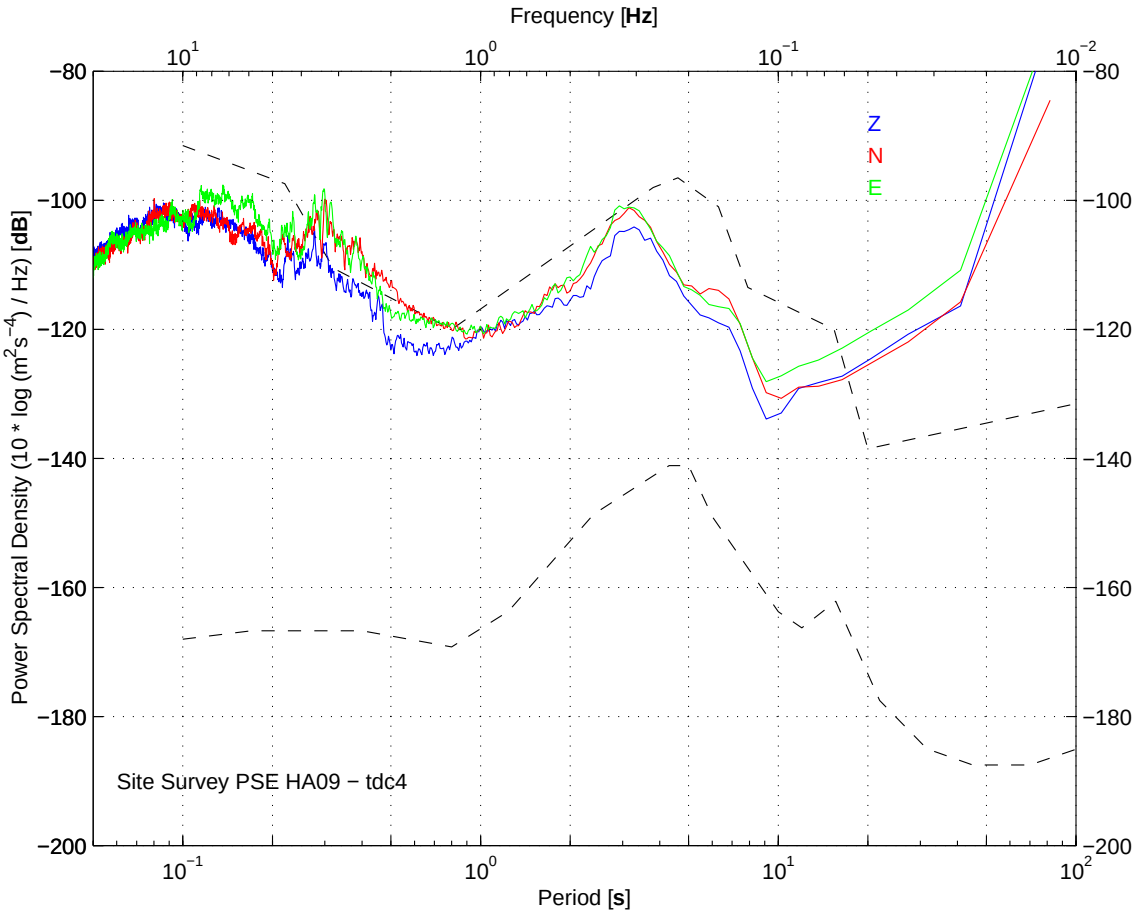

Figure 17. Composite noise curves, determined from the median value of all estimates for each component of ground acceleration at station TDC4, vertical (blue), north-south (red) and east-west (green).

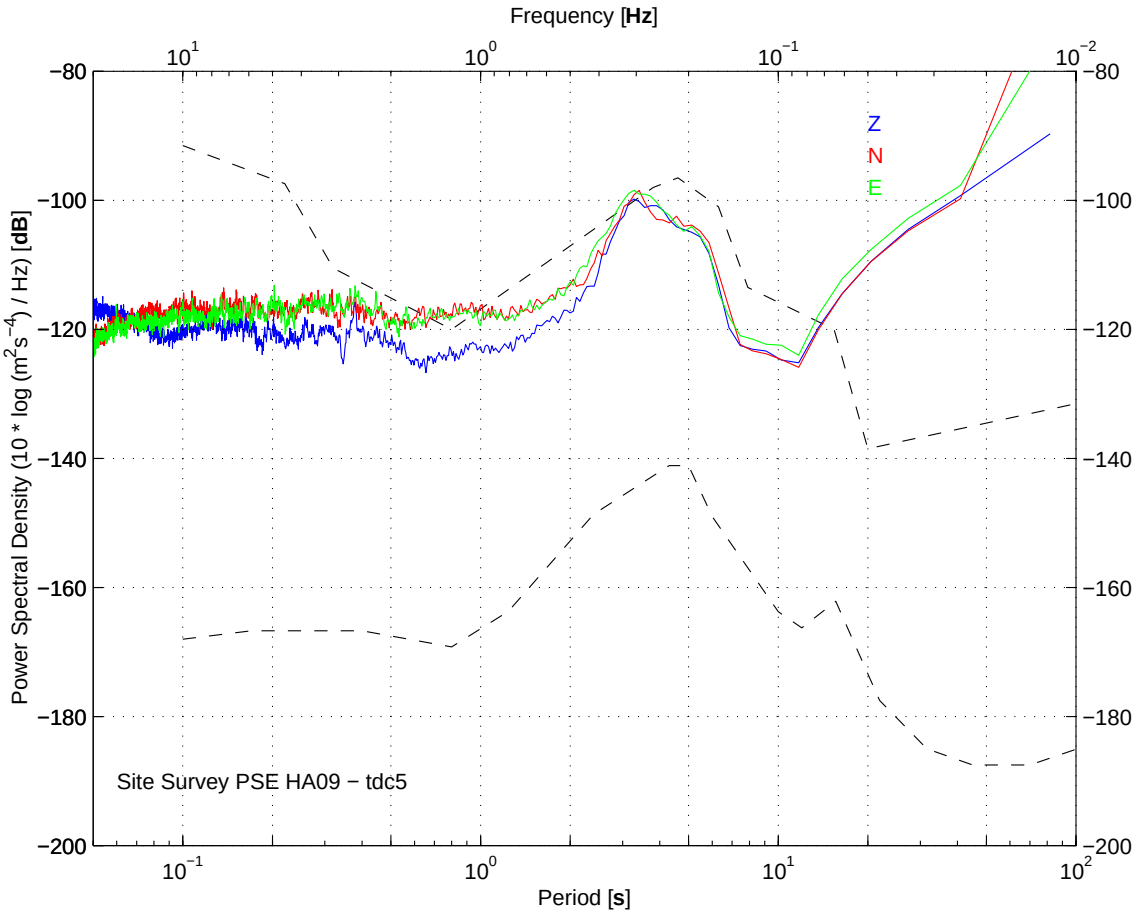

Figure 18. Composite noise curves, determined from the median value of all estimates for each component of ground acceleration at station TDC5, vertical (blue), north-south (red) and east-west (green).

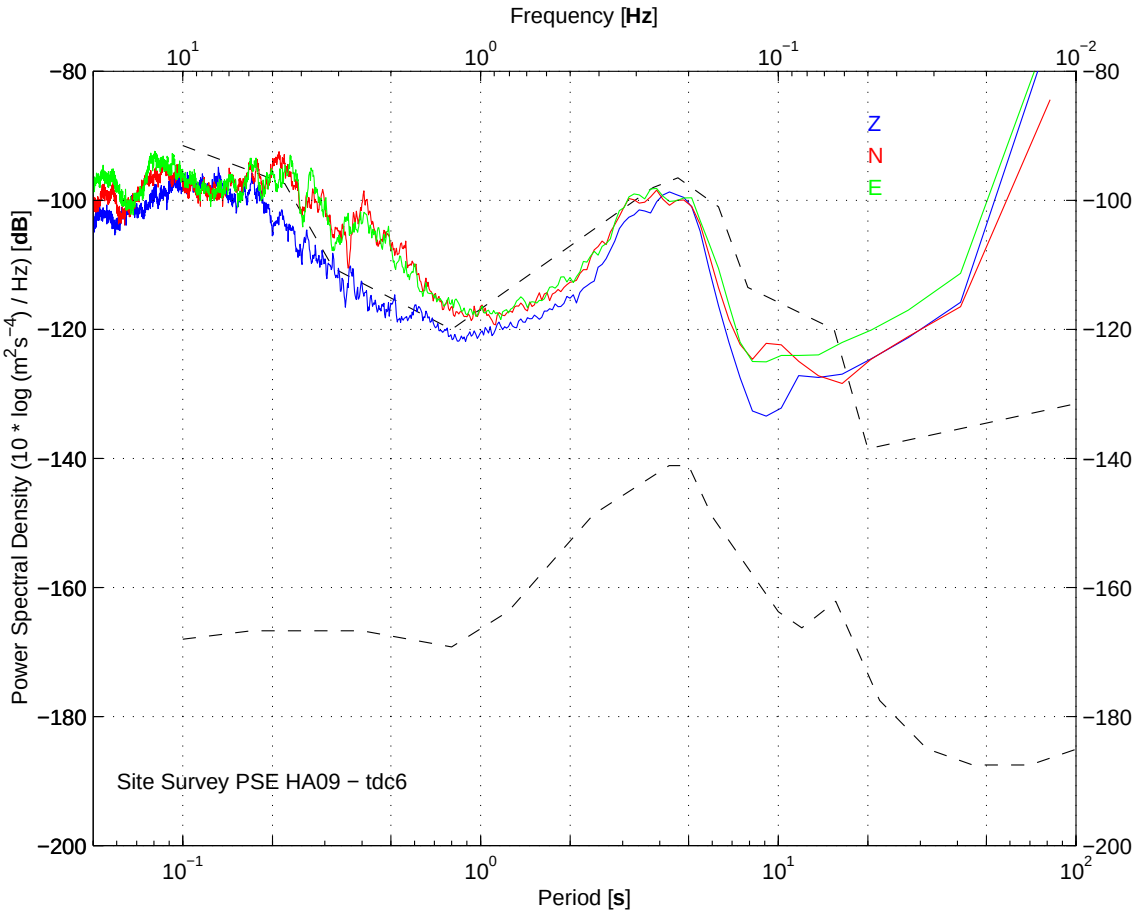

Figure 19. Composite noise curves, determined from the median value of all estimates for each component of ground acceleration at station TDC6, vertical (blue), north-south (red) and east-west (green).

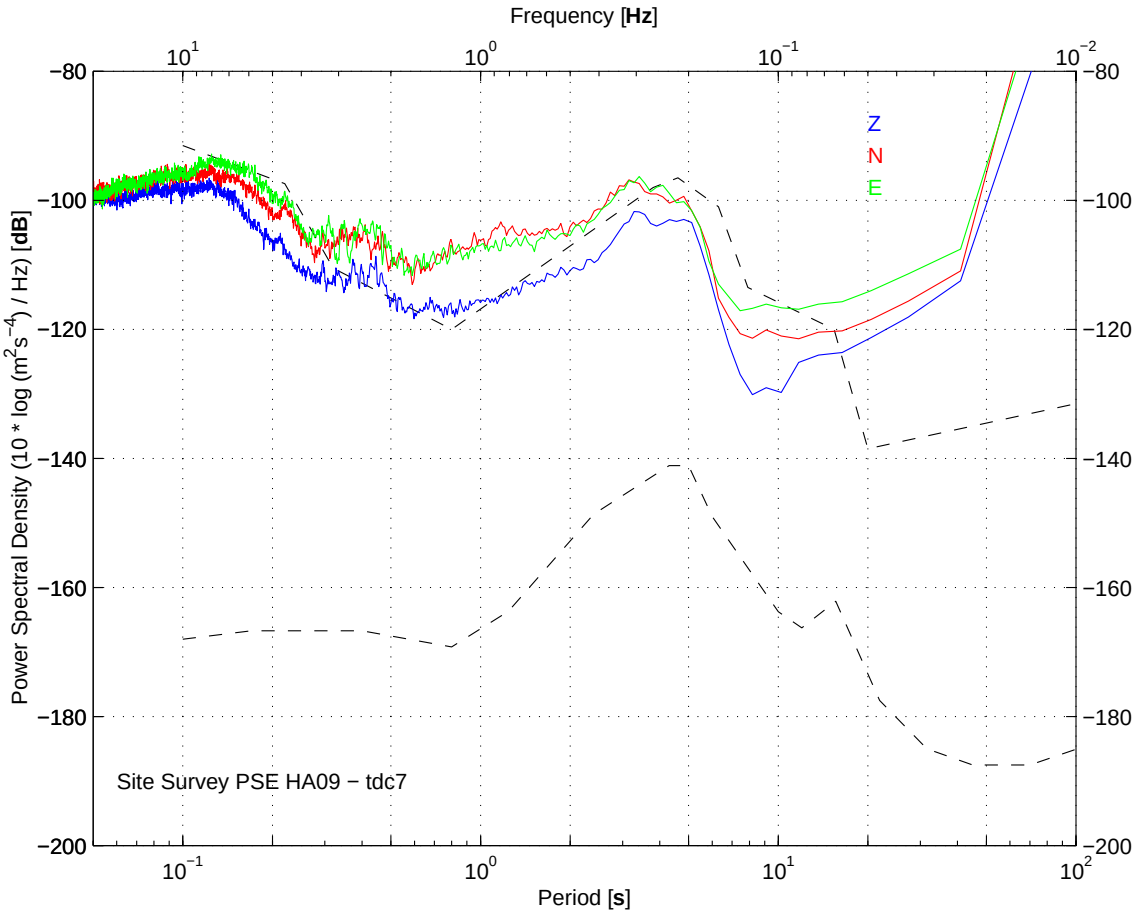

Figure 20. Composite noise curves, determined from the median value of all estimates for each component of ground acceleration at station TDC7, vertical (blue), north-south (red) and east-west (green).

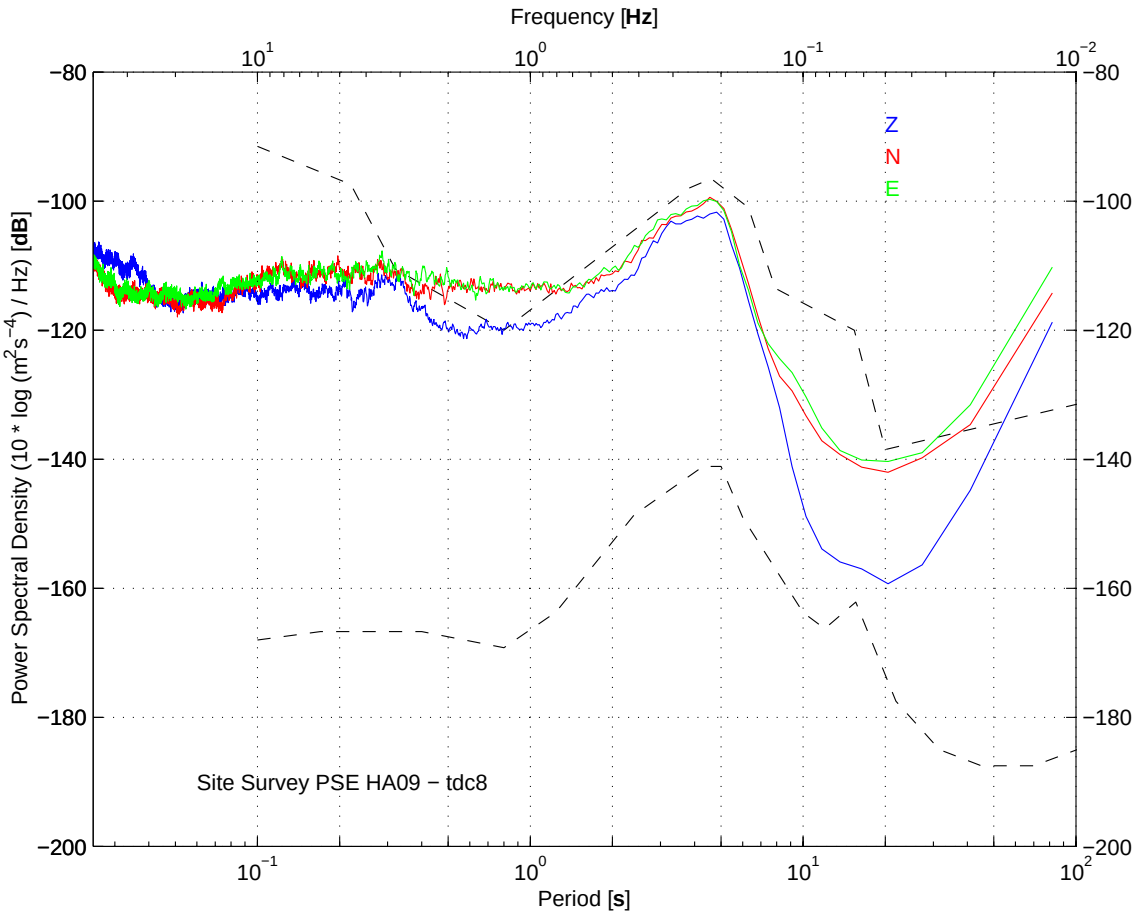

Figure 21. Composite noise curves, determined from the median value of all estimates for each component of ground acceleration at station TDC8, vertical (blue), north-south (red) and east-west (green).

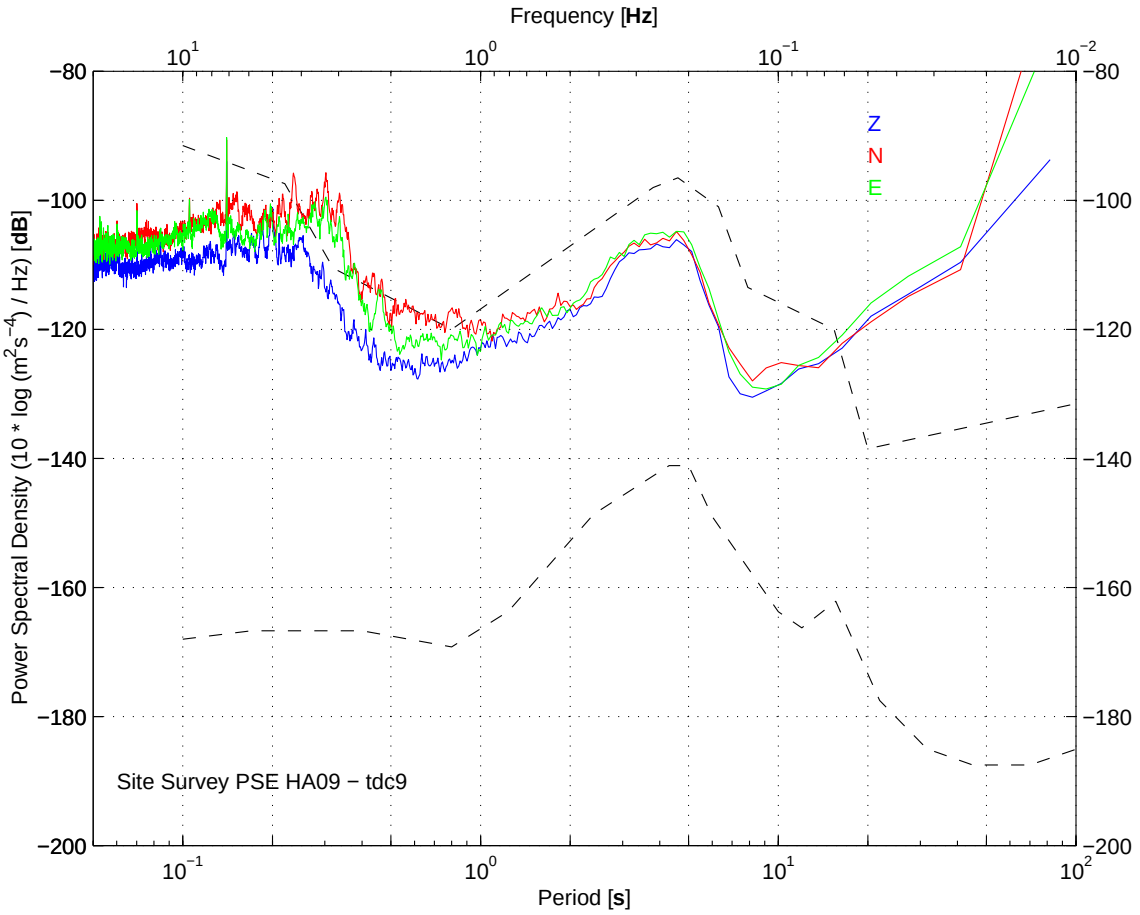

Figure 22. Composite noise curves, determined from the median value of all estimates for each component of ground acceleration at station TDC9, vertical (blue), north-south (red) and east-west (green).

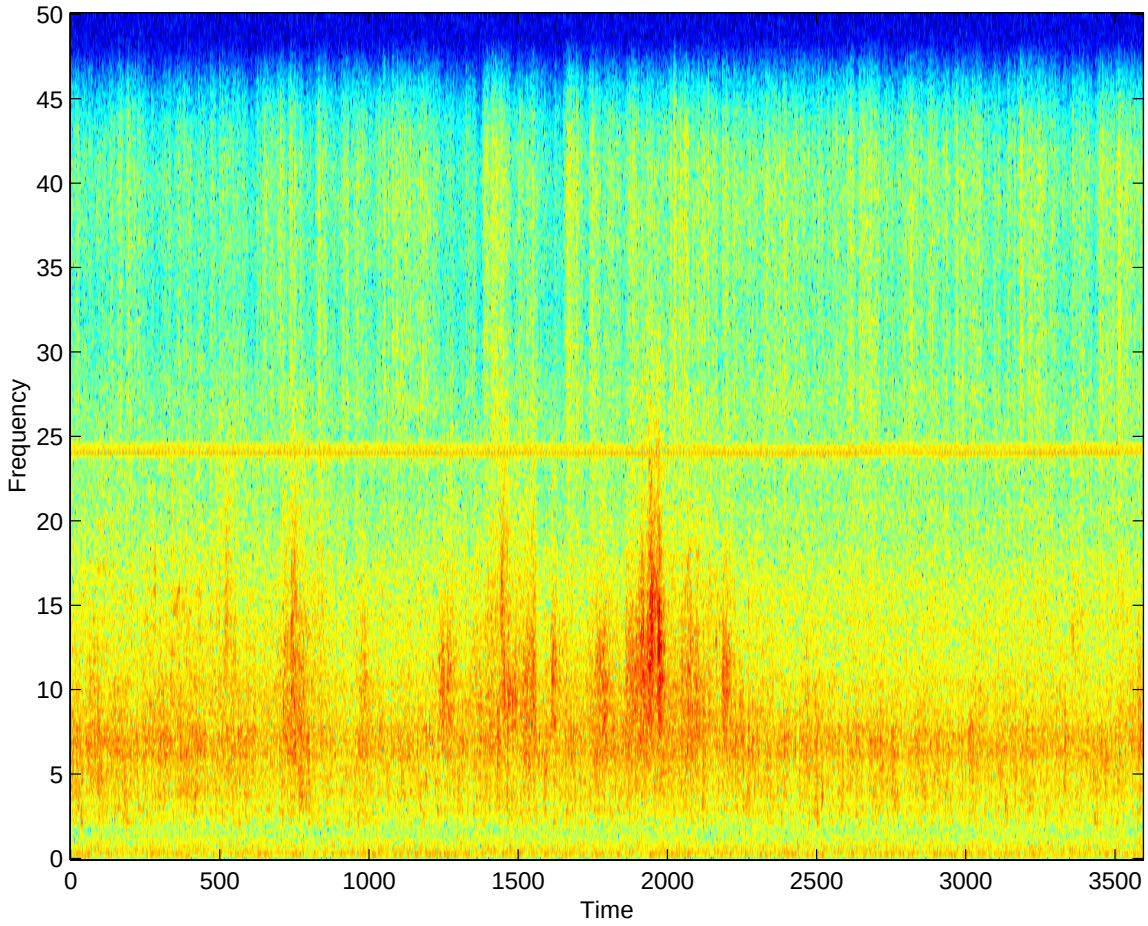

Figure 23. Spectrogram for 60 minutes of data from station TDC3 starting at 1200 on 8 November, showing high frequency signals due to cars and other cultural noise sources.

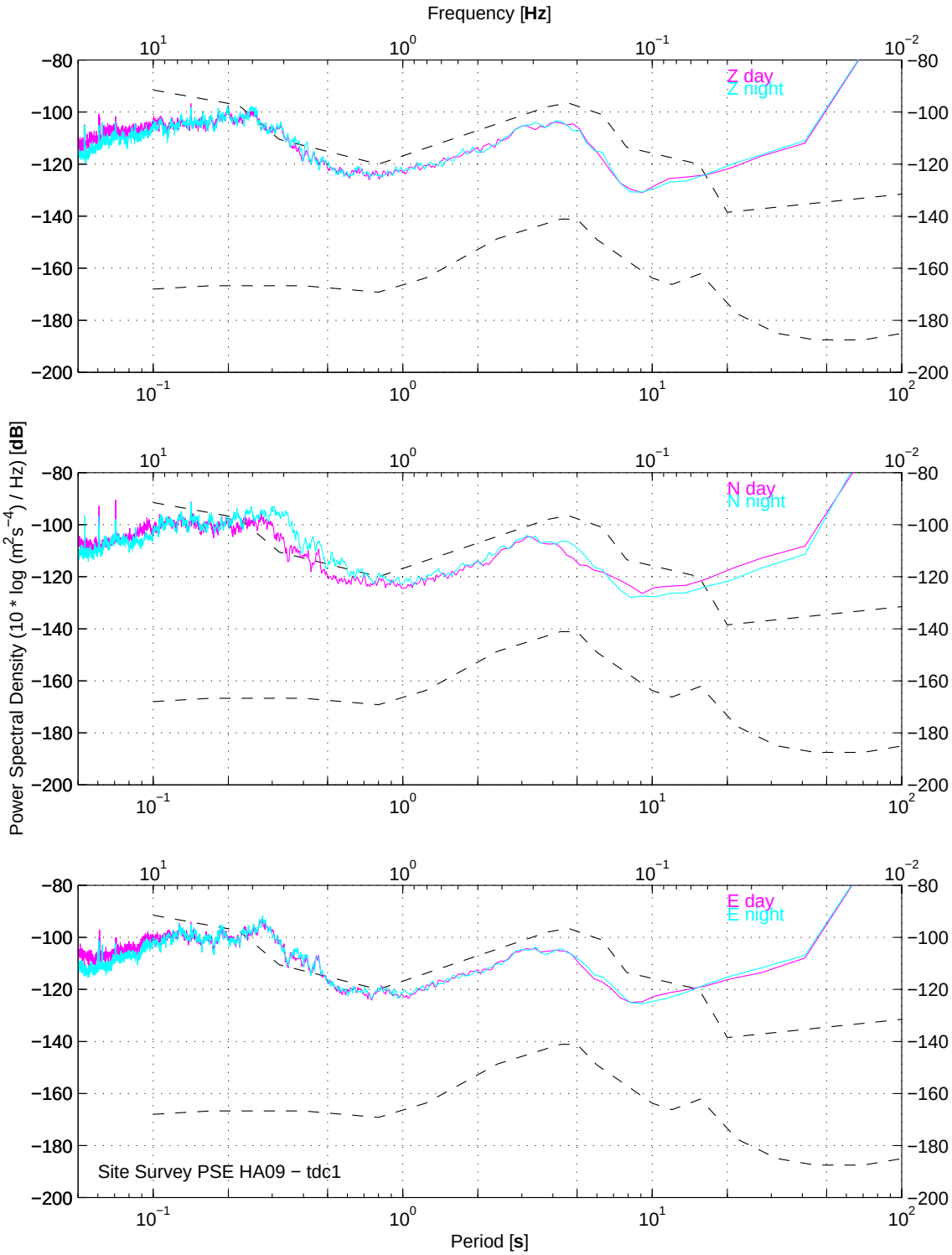

Figure 24. Median power spectral density estimates for each component of ground acceleration at station TDC1 for the day (magenta) and night (blue) data.

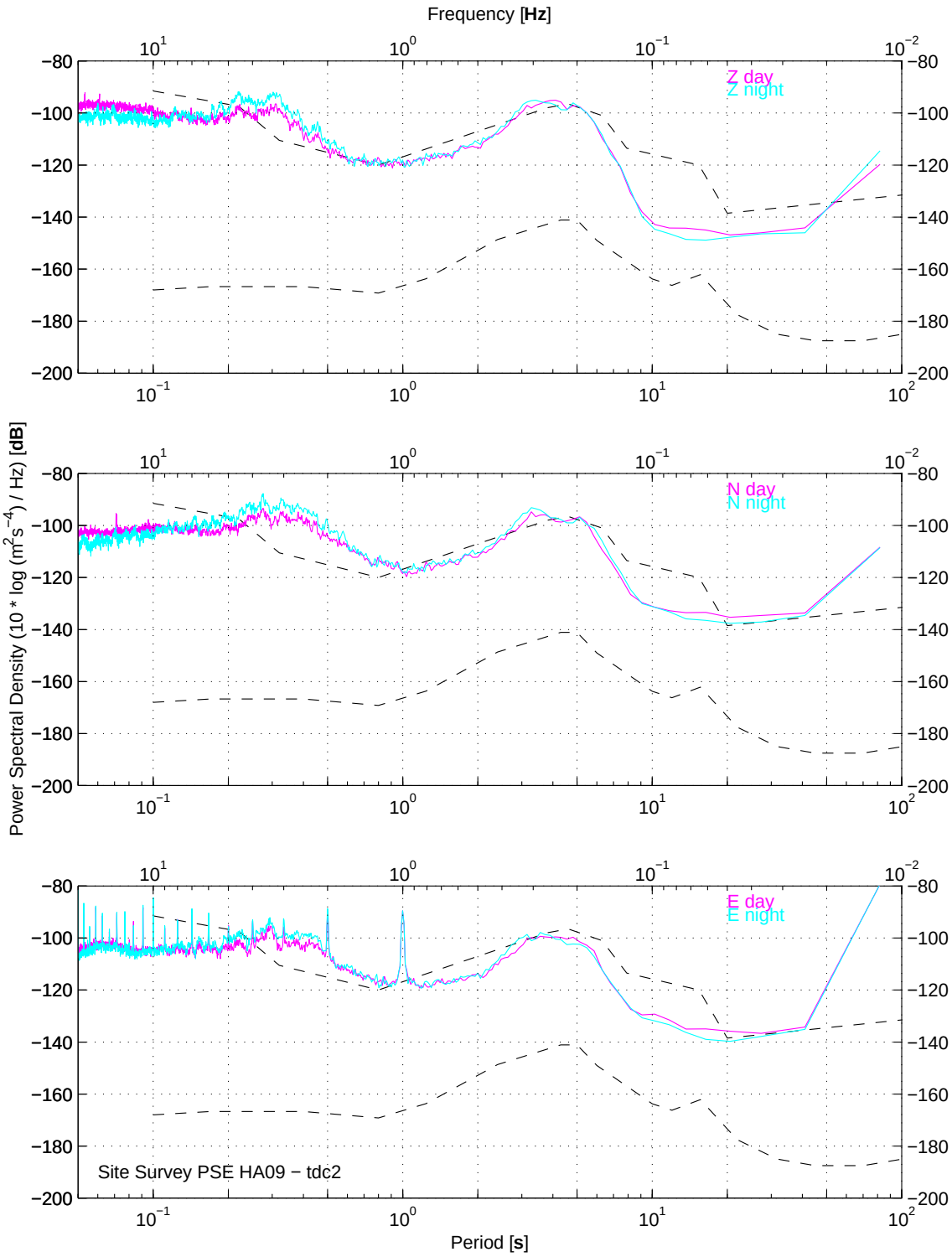

Figure 25. Median power spectral density estimates for each component of ground acceleration at station TDC2 for the day (magenta) and night (blue) data.

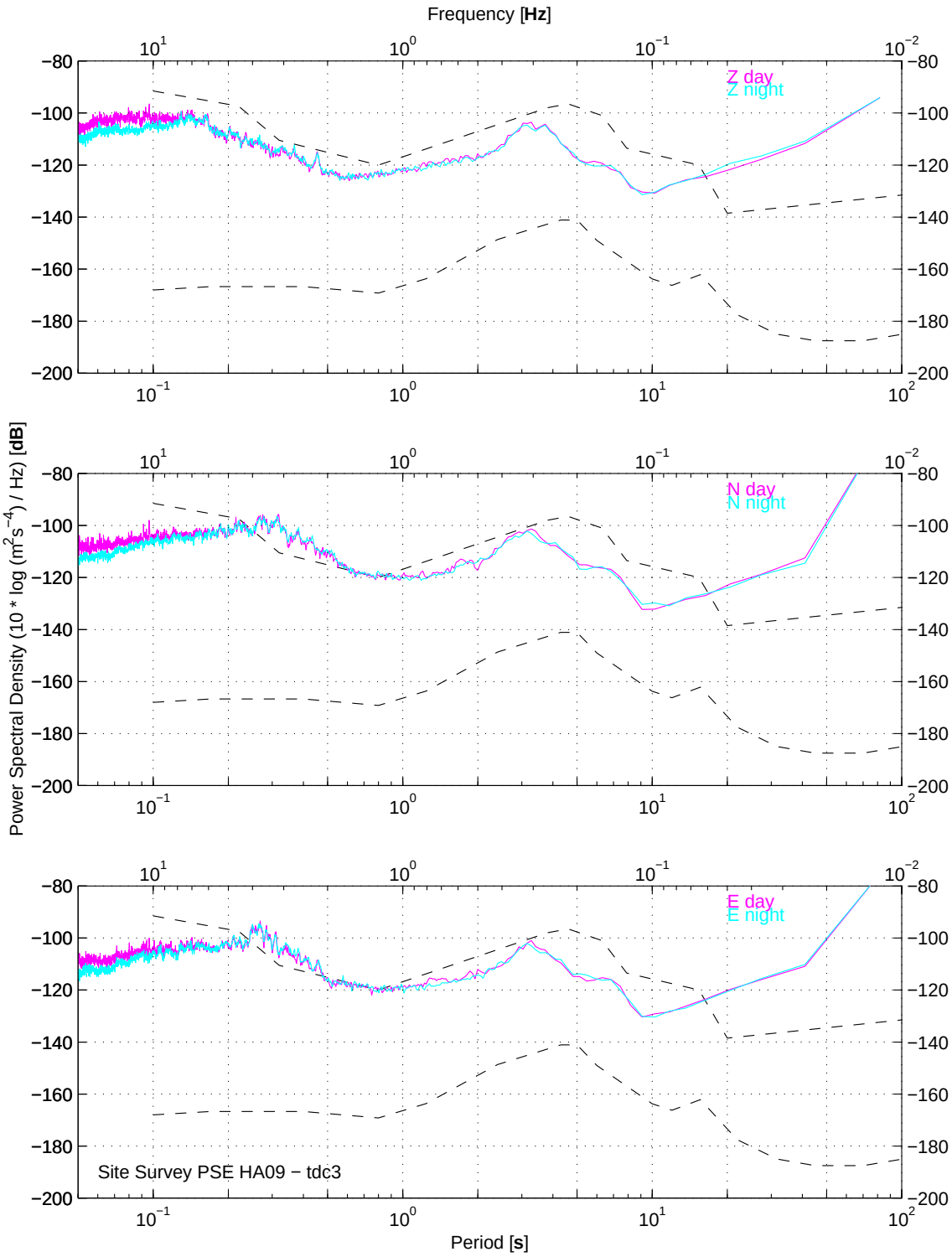

Figure 26. Median power spectral density estimates for each component of ground acceleration at station TDC3 for the day (magenta) and night (blue) data.

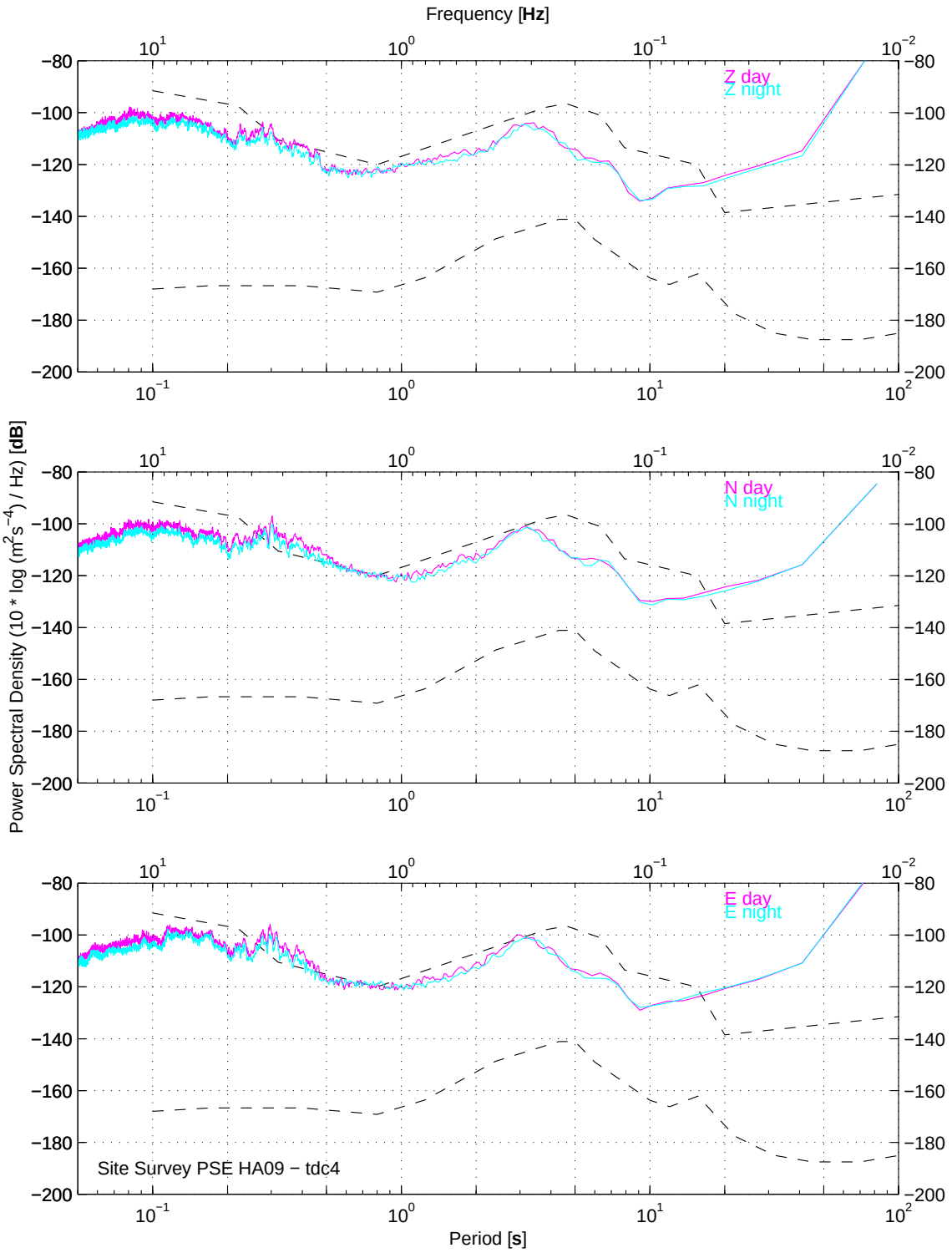

Figure 27. Median power spectral density estimates for each component of ground acceleration at station TDC4 for the day (magenta) and night (blue) data.

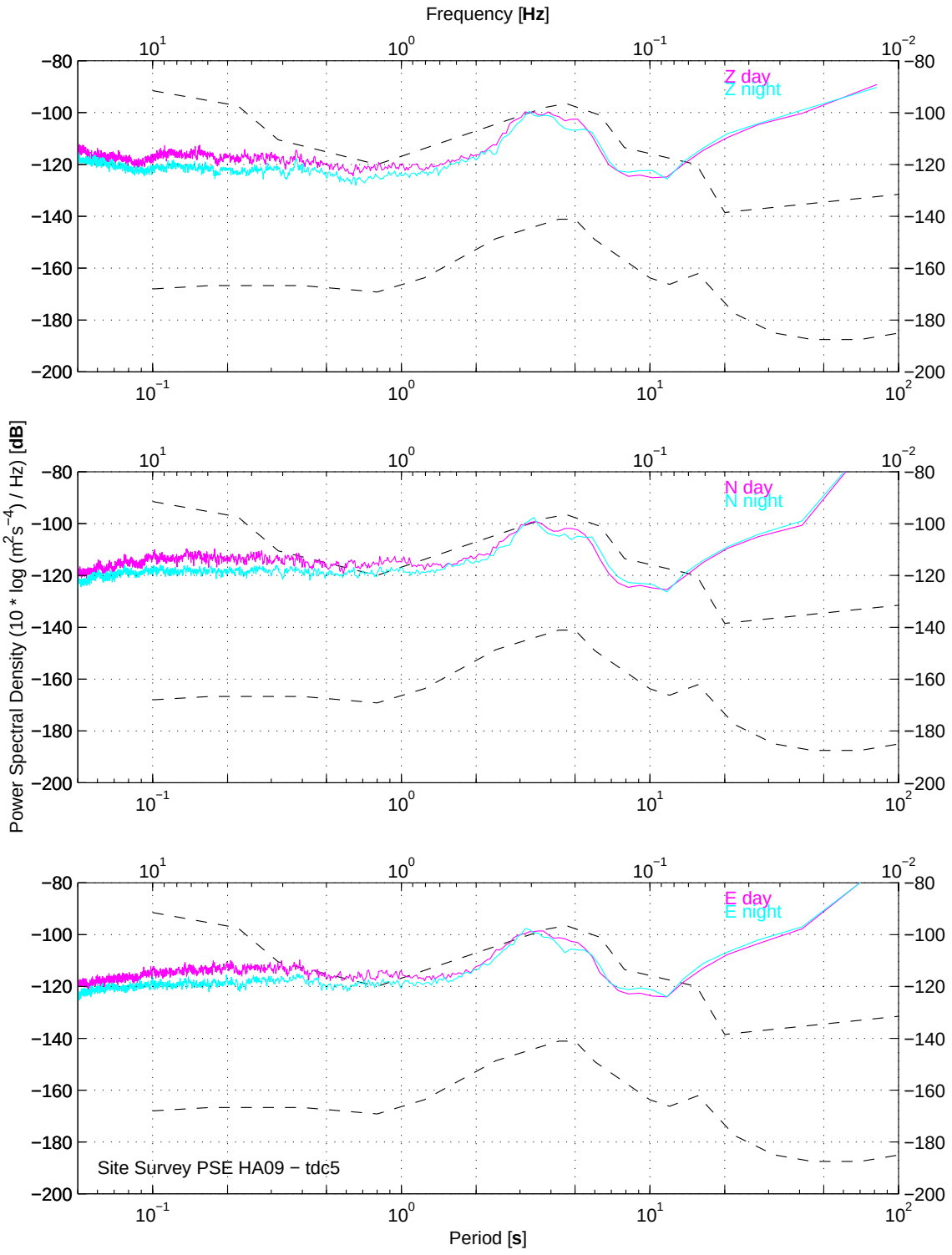

Figure 28. Median power spectral density estimates for each component of ground acceleration at station TDC5 for the day (magenta) and night (blue) data.

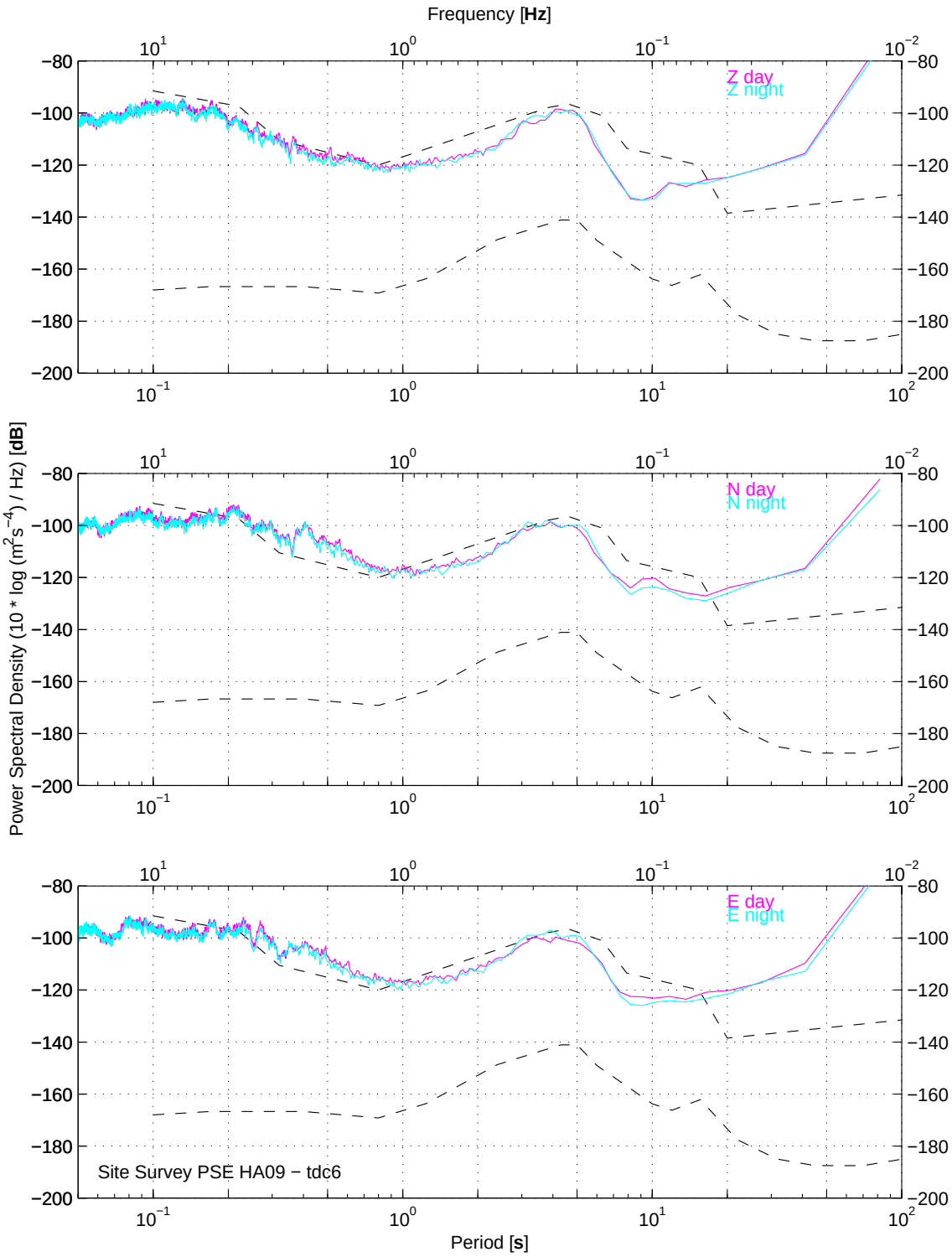

Figure 29. Median power spectral density estimates for each component of ground acceleration at station TDC6 for the day (magenta) and night (blue) data.

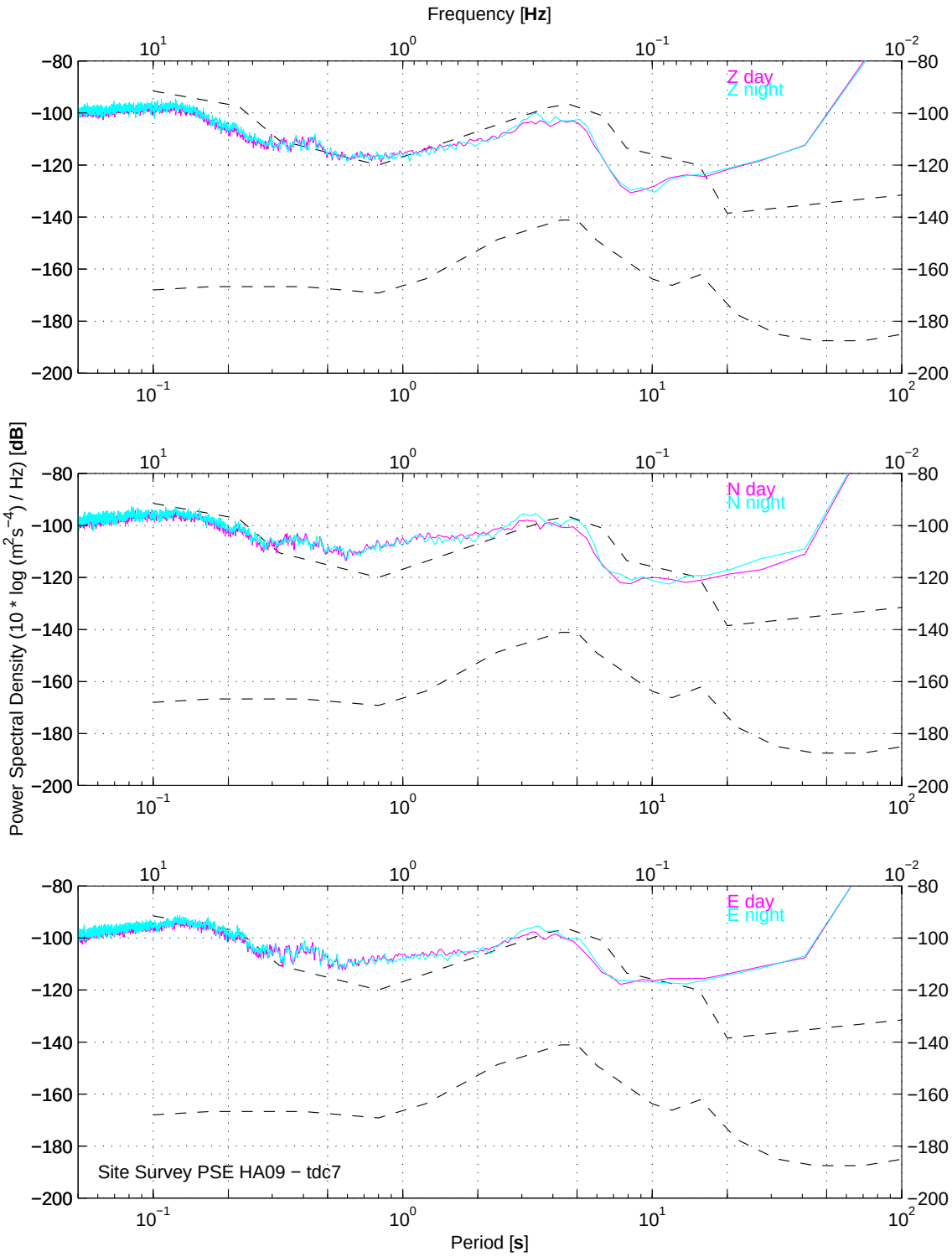

Figure 30. Median power spectral density estimates for each component of ground acceleration at station TDC7 for the day (magenta) and night (blue) data.

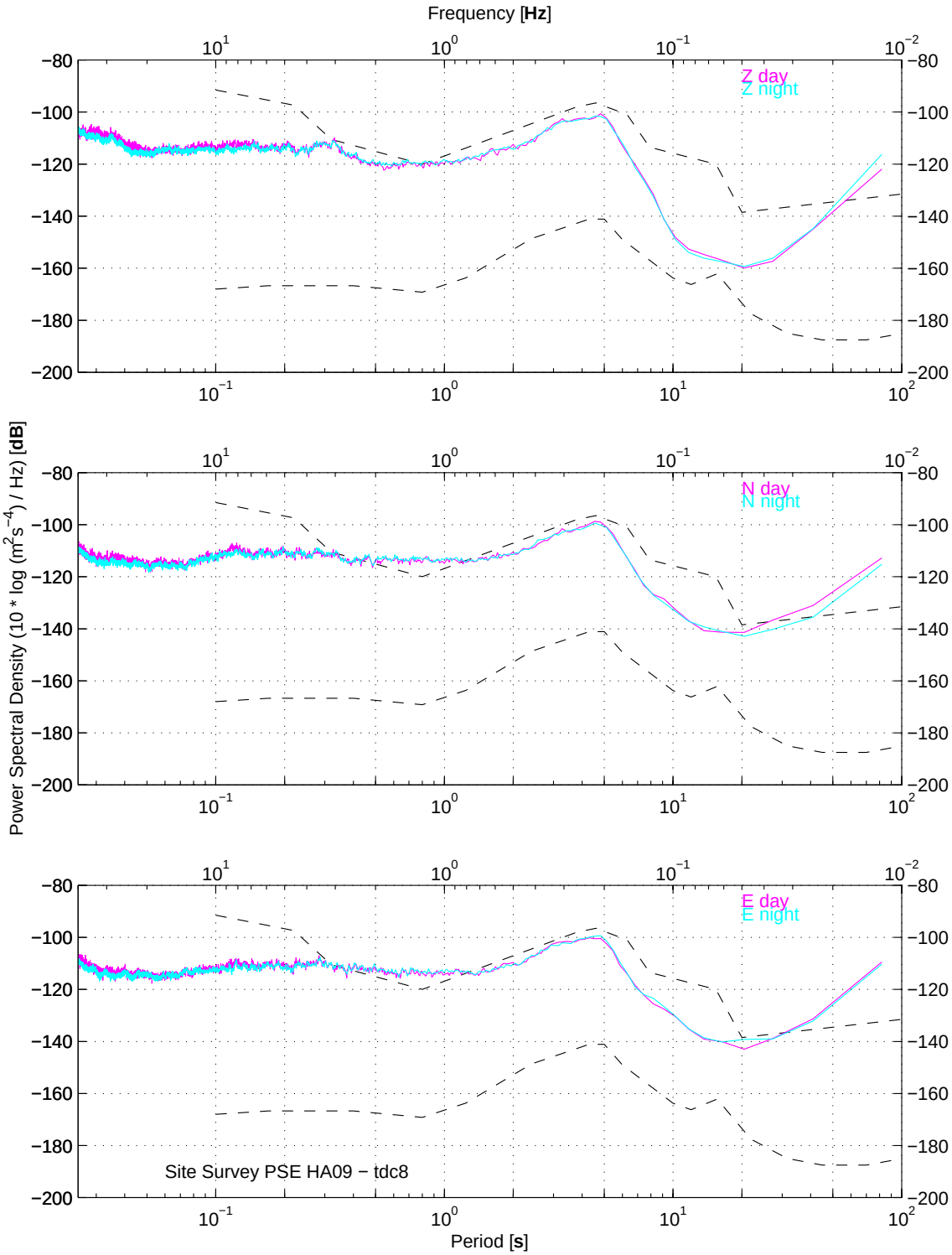

Figure 31. Median power spectral density estimates for each component of ground acceleration at station TDC8 for the day (magenta) and night (blue) data.

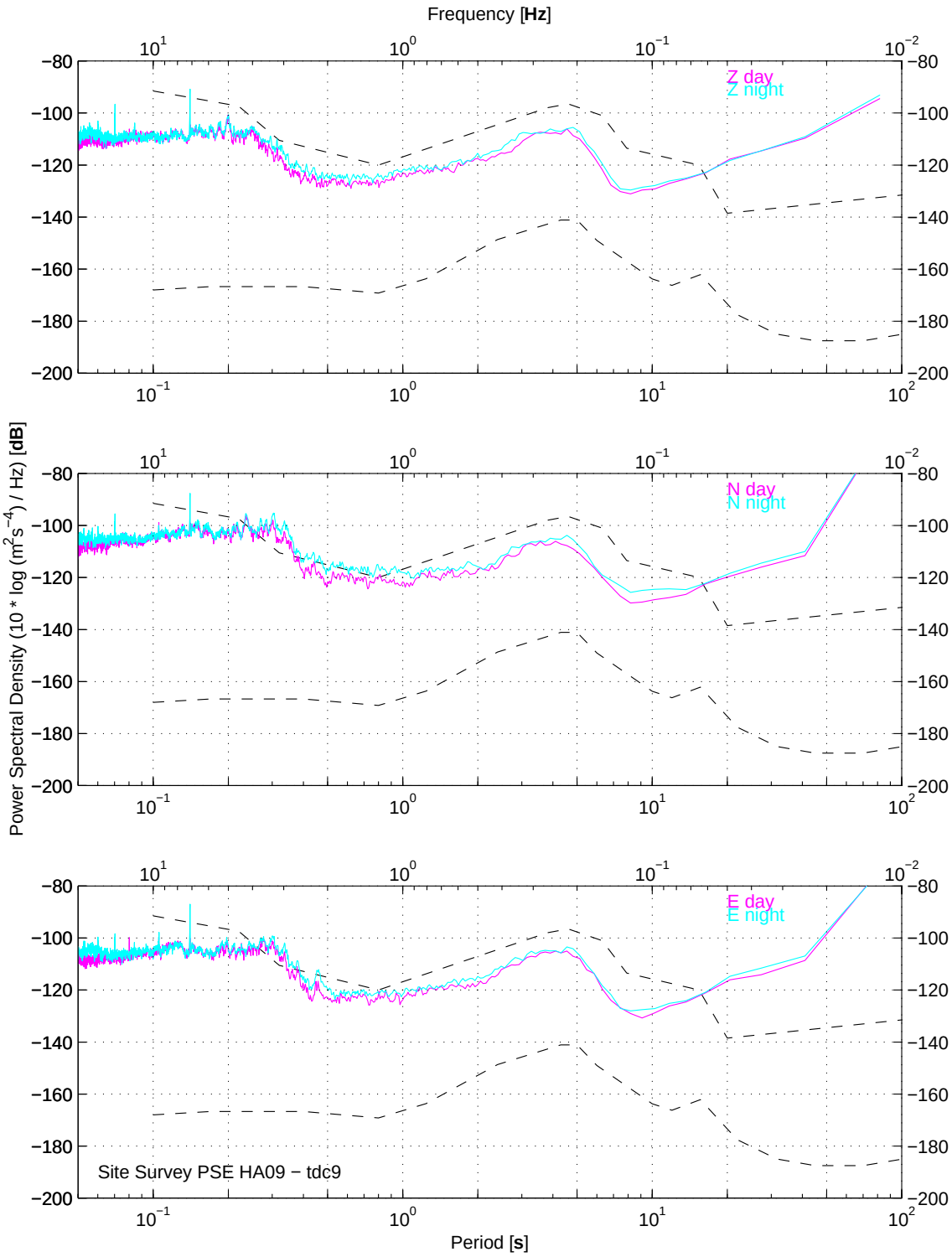

Figure 32. Median power spectral density estimates for each component of ground acceleration at station TDC9 for the day (magenta) and night (blue) data.

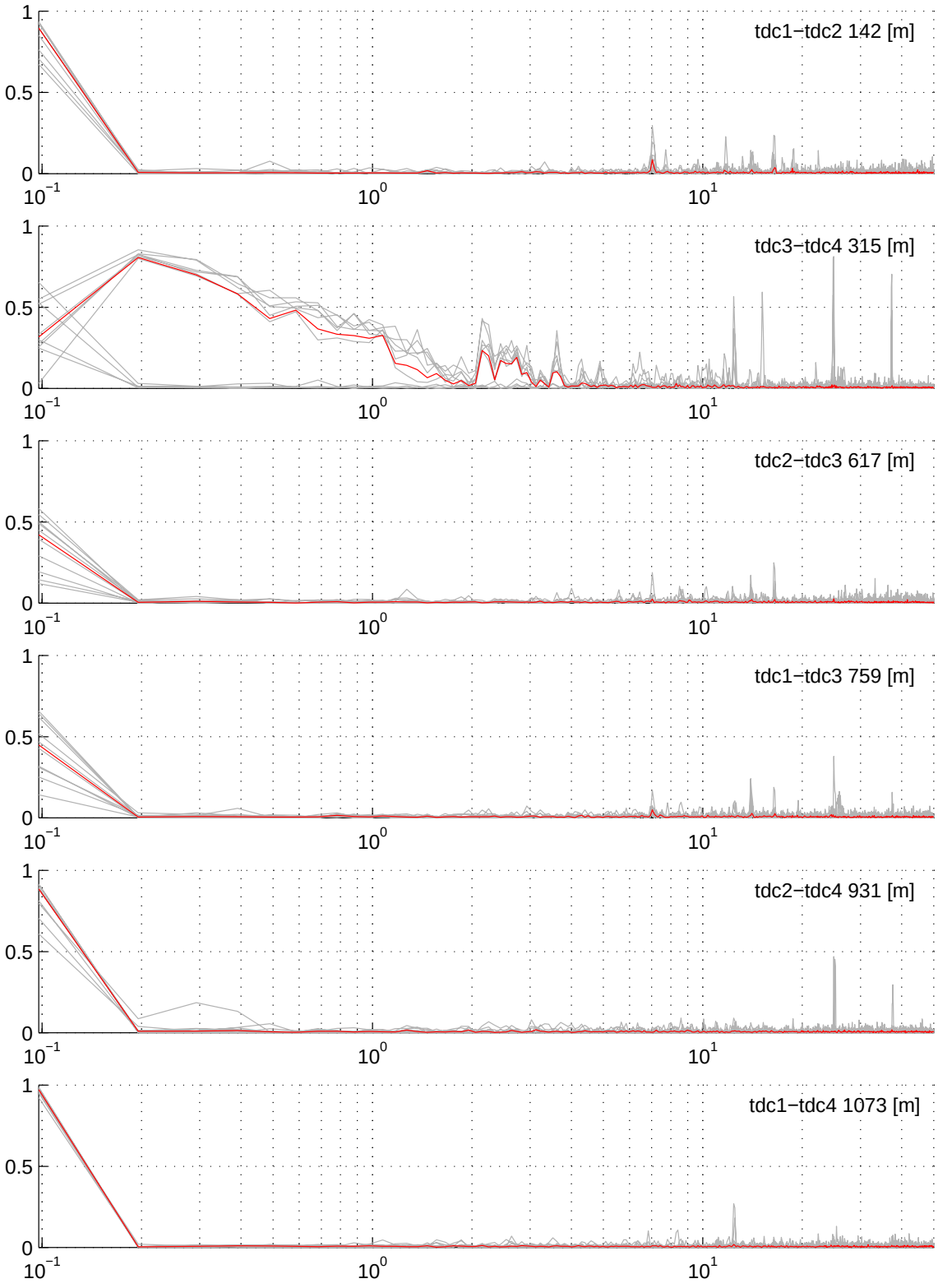

Figure 33. Coherence of the vertical components of ground motion at individual stations pairs from TDC1 to TDC4, for five randomly selected noise segments (grey) and the median value (red).

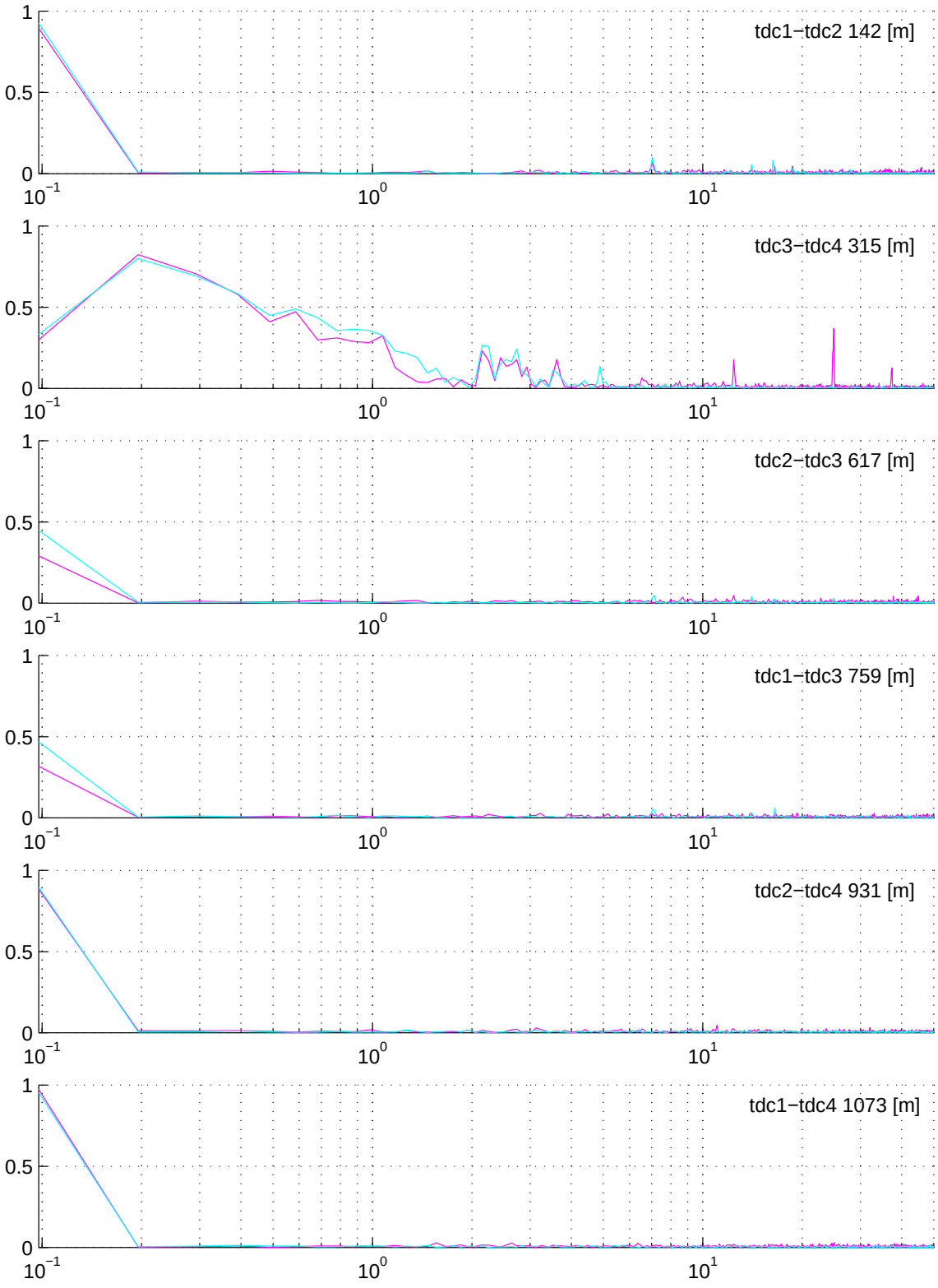

Figure 34. Median values of coherence of the vertical components of ground motion at individual stations pairs from TDC1 to TDC4, for day (magenta) and night (blue).

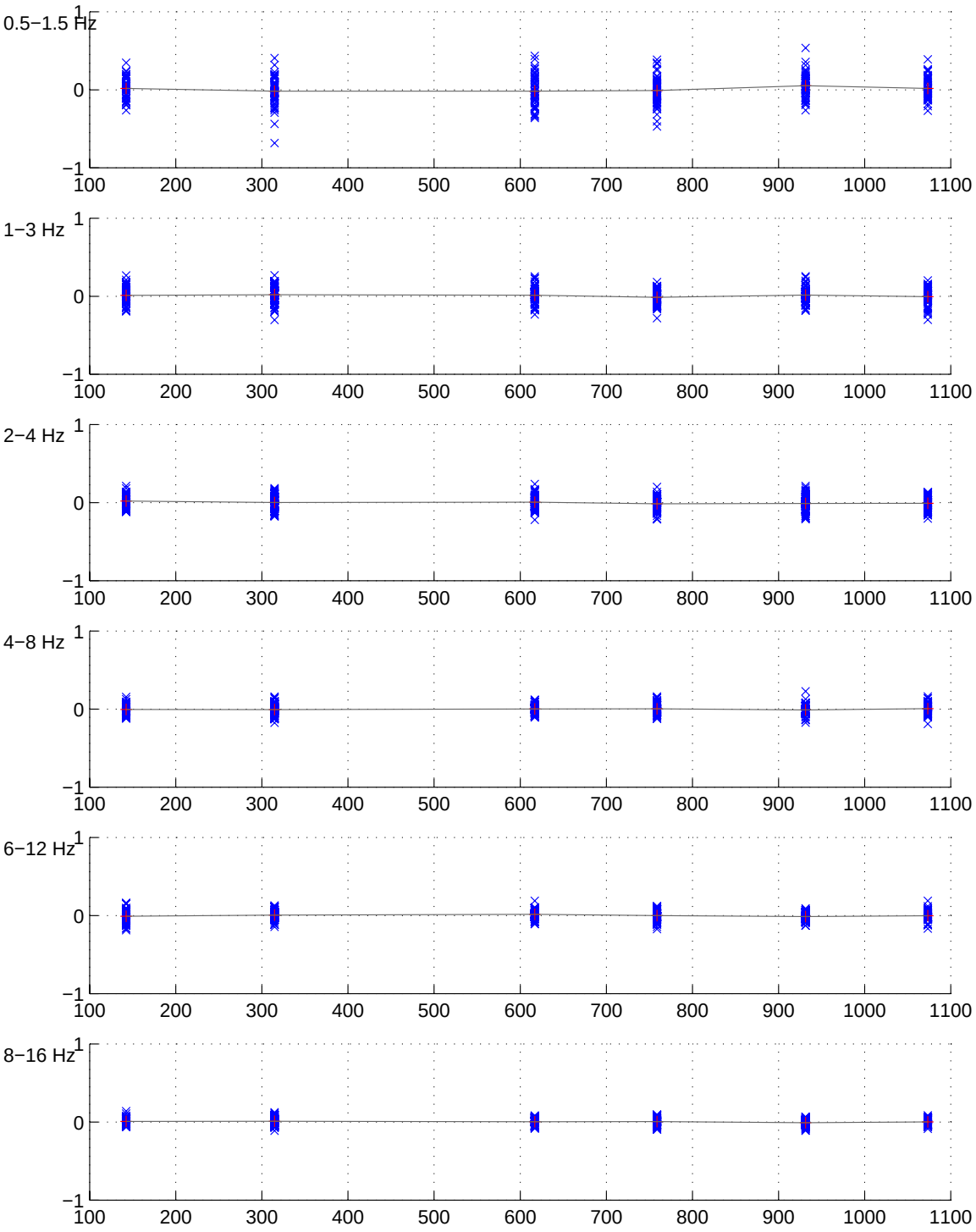

Figure 35. Cross correlation functions for individual station pairs in six discrete frequency bands shown as a function of distance.

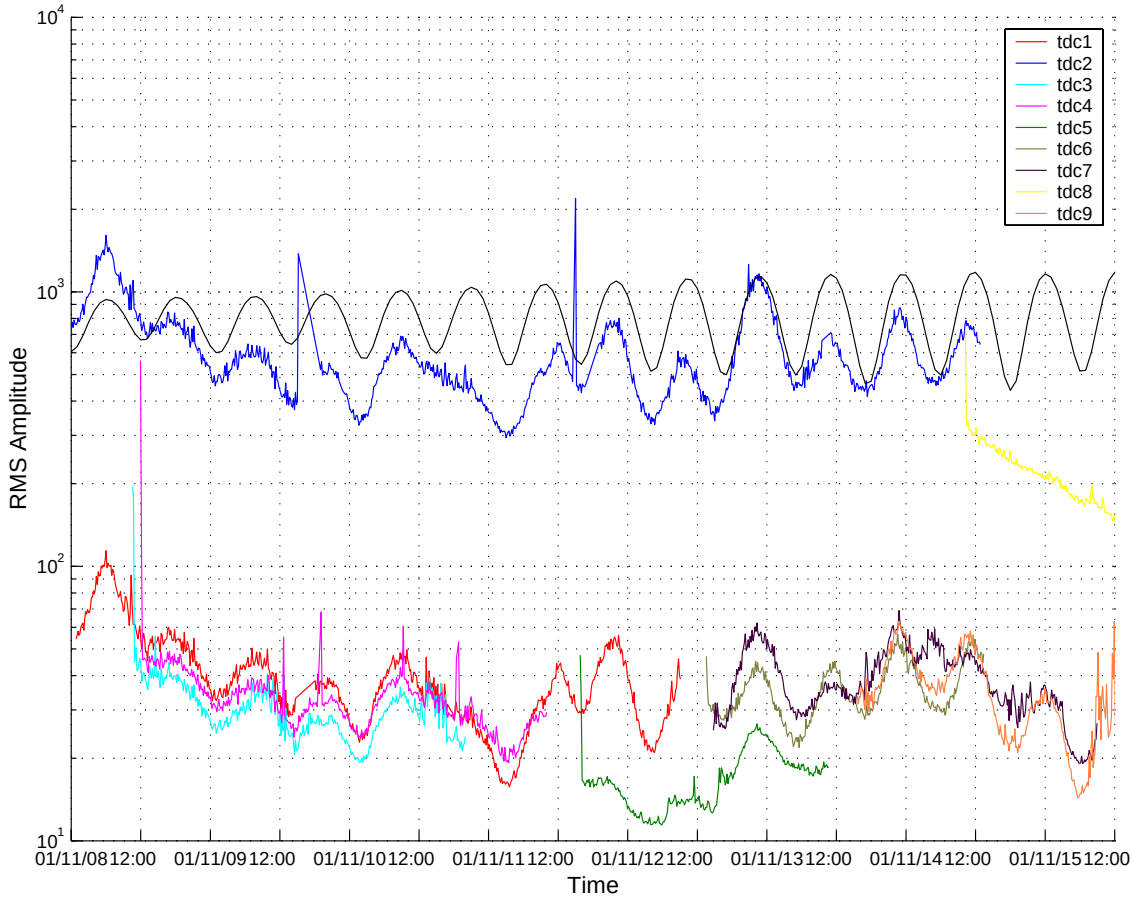

Figure 36. RMS amplitude measurements at each station shown as a function of time. Also shown are the tidal predications for Tristan Da Cuhna (black).

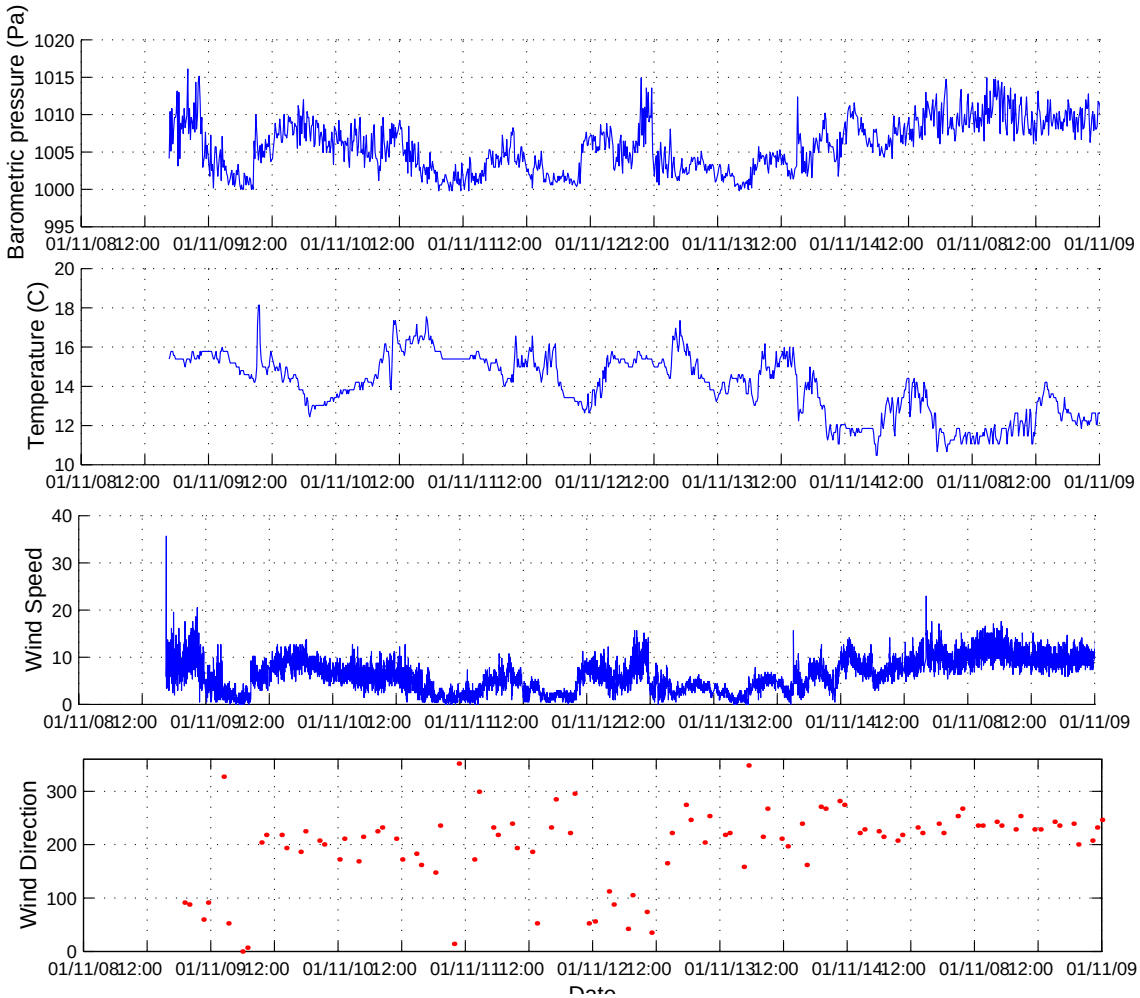

Figure 37. Environmental parameters recorded during the site survey, pressure, temperature, wind speed and direction.

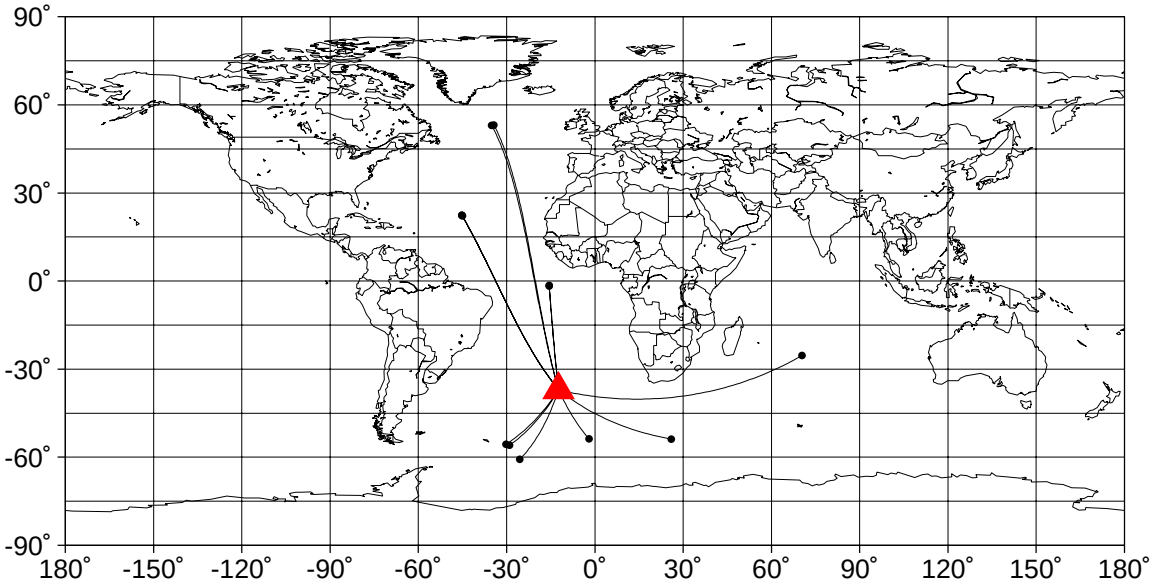

Figure 38. Epicenters for seismo-acoustic events (black circles) listed in Table 3. Great circles between source and receiver show approximate raypaths.

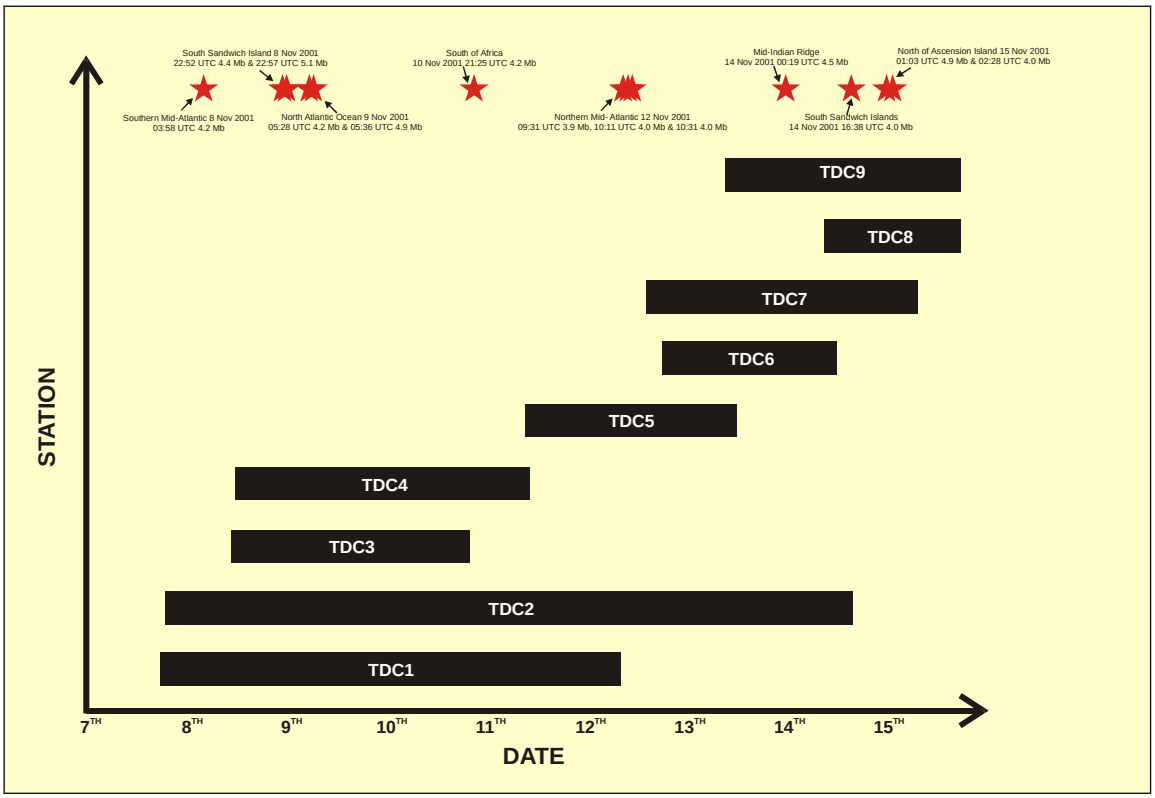

Figure 39. Schematic depicting the periods of operation of each of the stations deployed during the site survey on Tristan Da Cuhna. Also shown are the origin times of the seismo-acoustic events listed in Table 3.

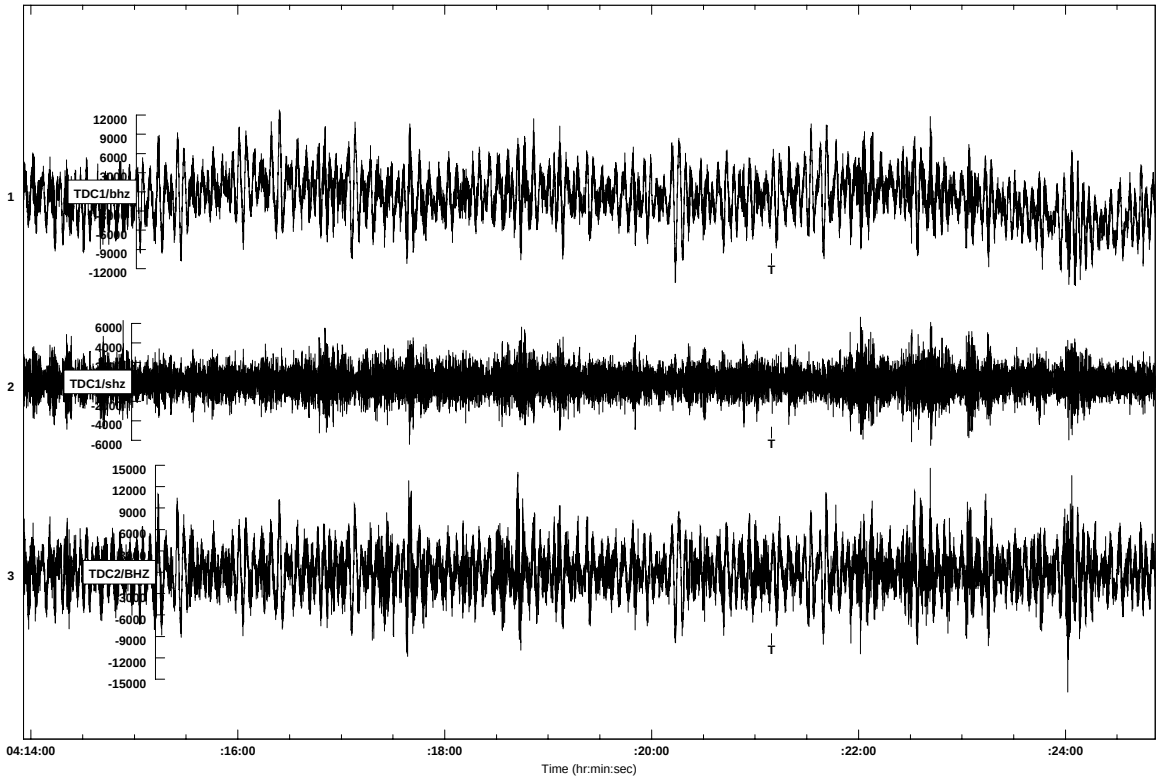

Figure 40. Windowed seismograms of the vertical component of ground velocity recorded at stations TDC1 and TDC2 showing the expected T-phase arrival from the magnitude 4.2 Southern Mid-Atlantic on 8 November event at 03:58

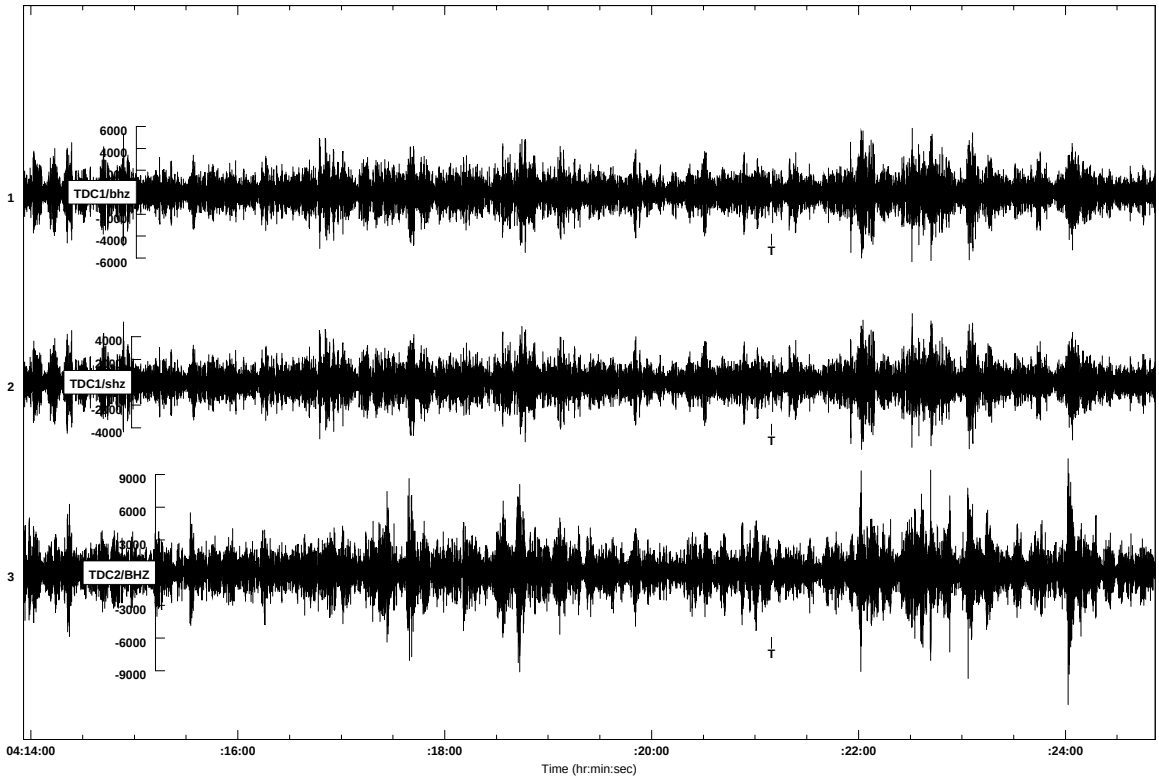

Figure 41. Seismograms shown in Figure 40 filtered with a 4th order Butterworth filter with a pass-band of 3-7 Hz.

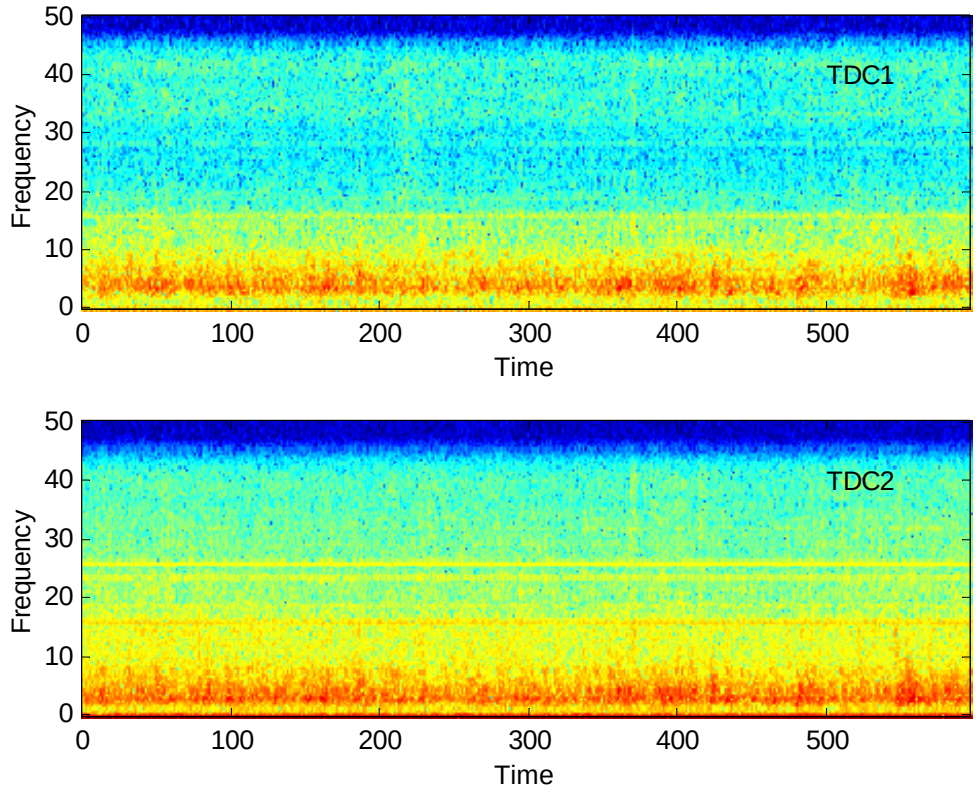

Figure 42. Spectrogram, calculated for the vertical component of ground velocity at stations TDC1 And TDC2, of the expected T-phase arrival for the magnitude 4.2 Southern Mid-Atlantic event on 8 November at 03:58 UTC.

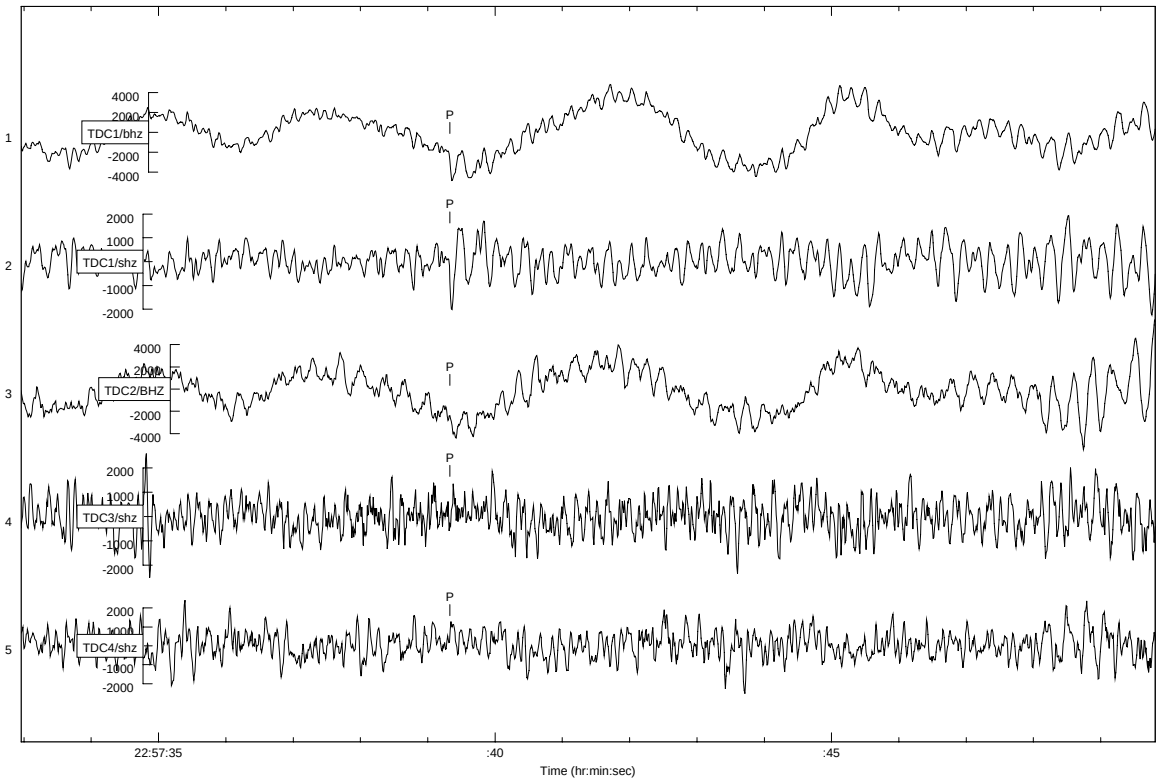

Figure 43. Seismogram showing the P-wave arrival recorded at stations TDC1 to TDC4 for the magnitude 4.4 South Sandwich Island event on 8 November at 22:52 UTC.

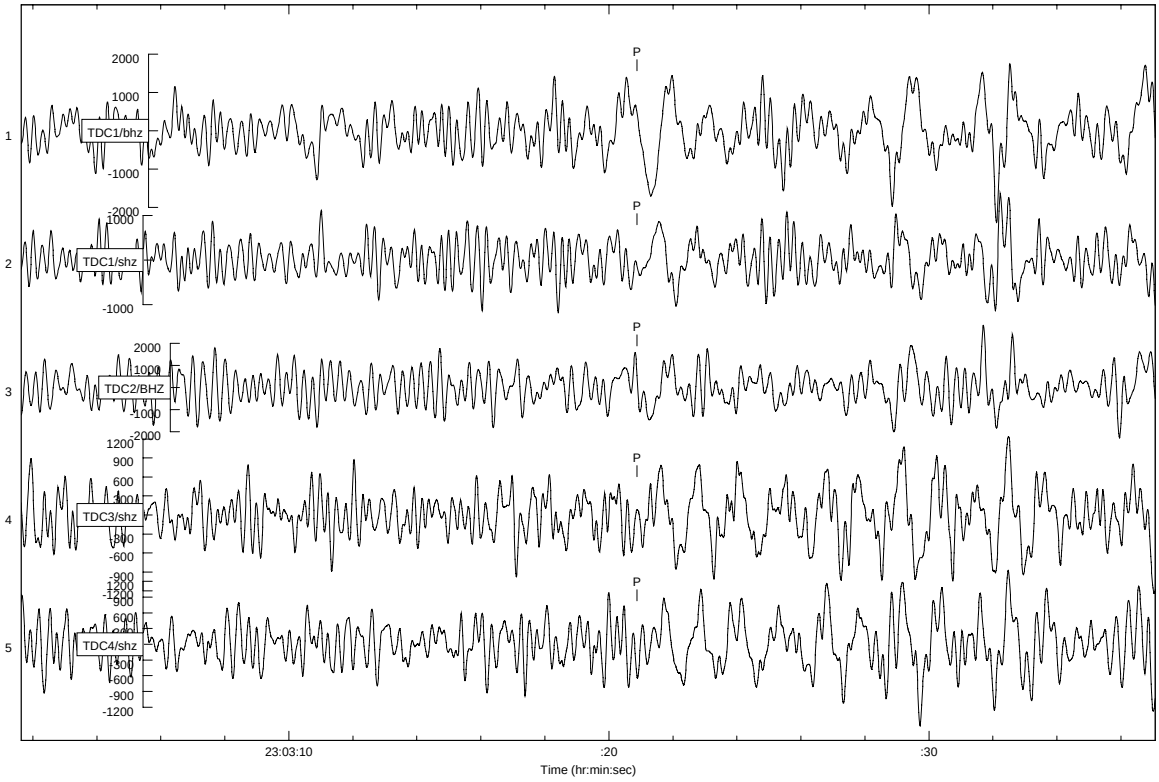

Figure 44. Seismogram showing the P-wave arrival recorded at stations TDC1 to TDC4 for the magnitude 5.1 South Sandwich Island event on 8 November at 22:57 UTC.

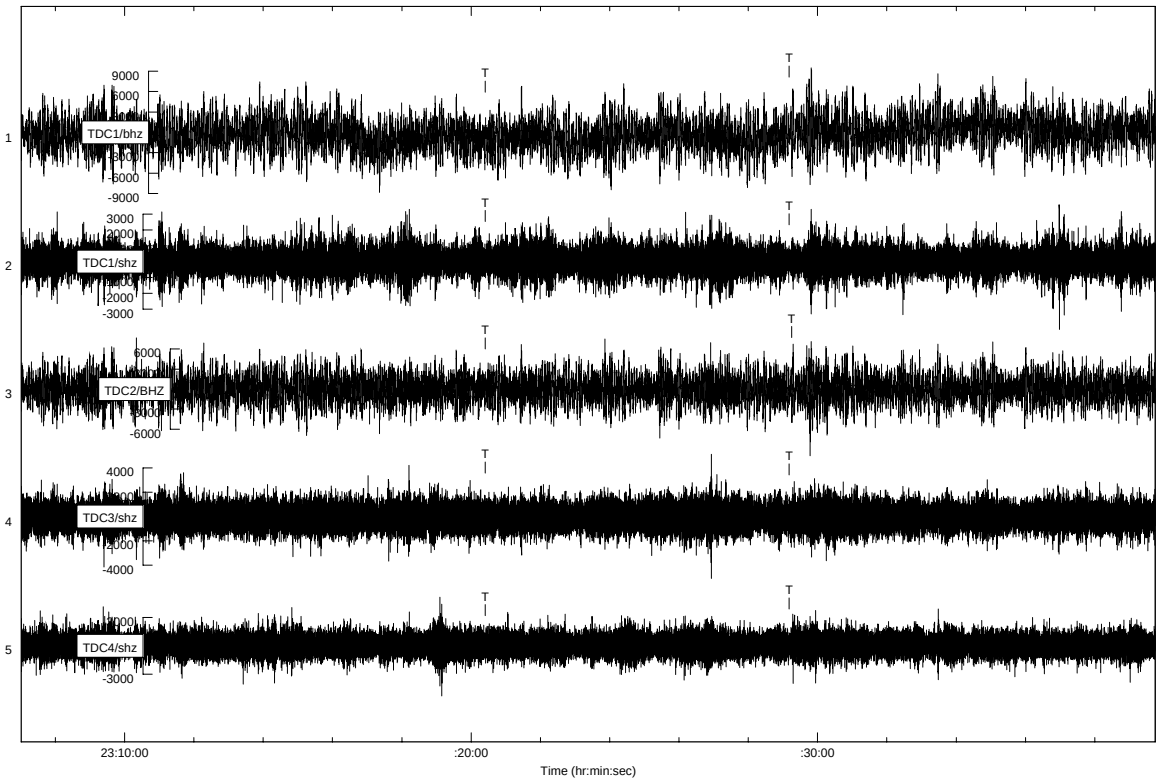

Figure 45. Seismograms of the vertical component of ground velocity recorded at stations TDC1, TDC2, TDC3 and TDC4 showing the expected T-phase arrivals for the magnitude 4.4 and 5.1 South Sandwich Island events on 8 November.

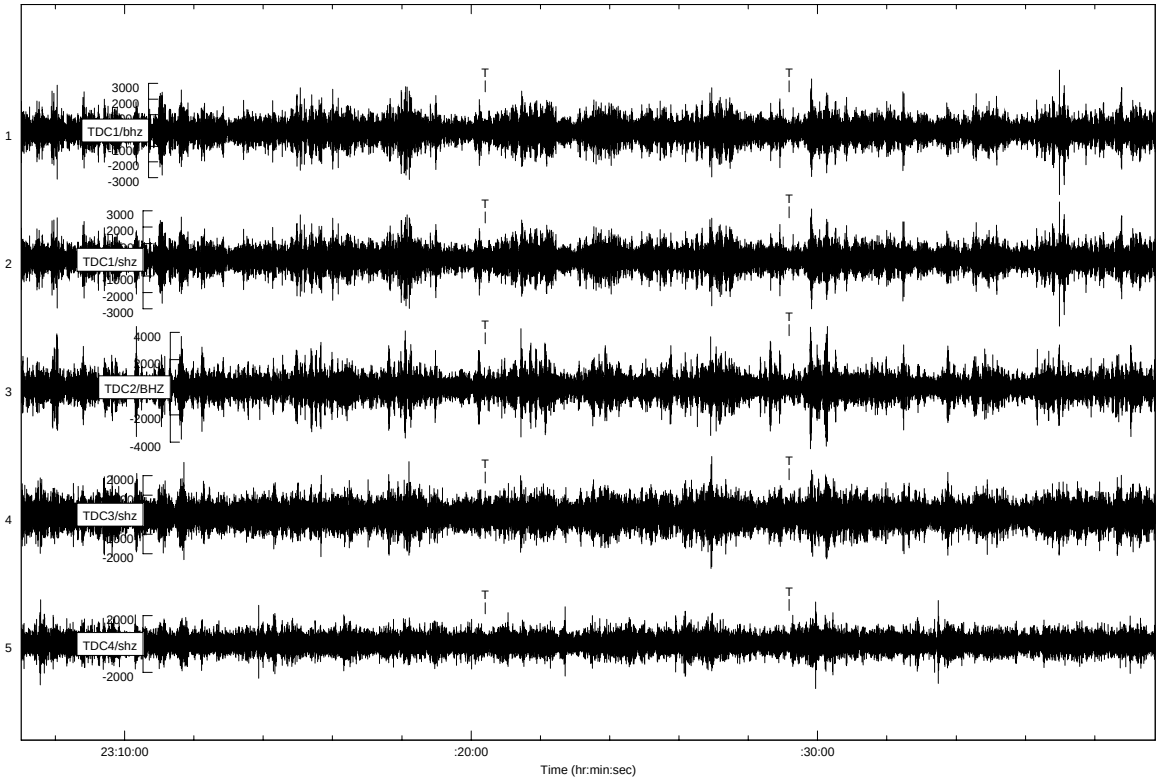

Figure 46. Data shown in Figure 45 filtered with a 4th order Butterworth filter with a pass-band of 3-7 Hz.

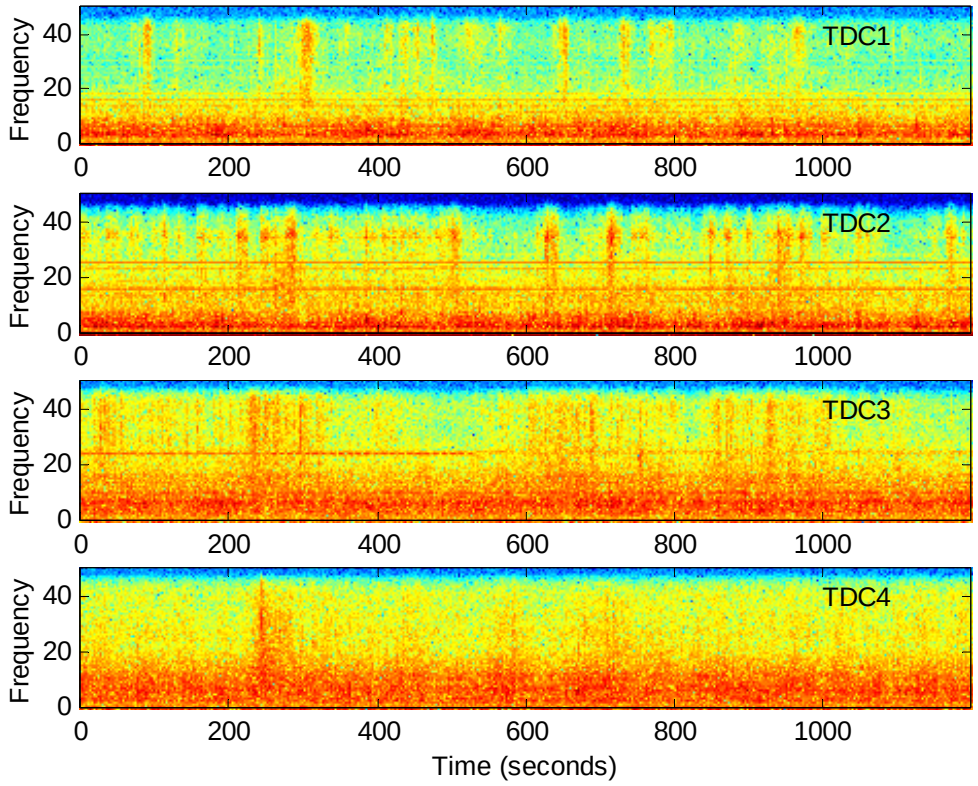

Figure 47. Spectrogram, calculated for the vertical component of ground velocity at stations TDC1, TDC2, TDC3 and TDC4, of the expected T-phase arrivals from the magnitude 4.4 and 5.1 South Sandwich Island events on 8 November.

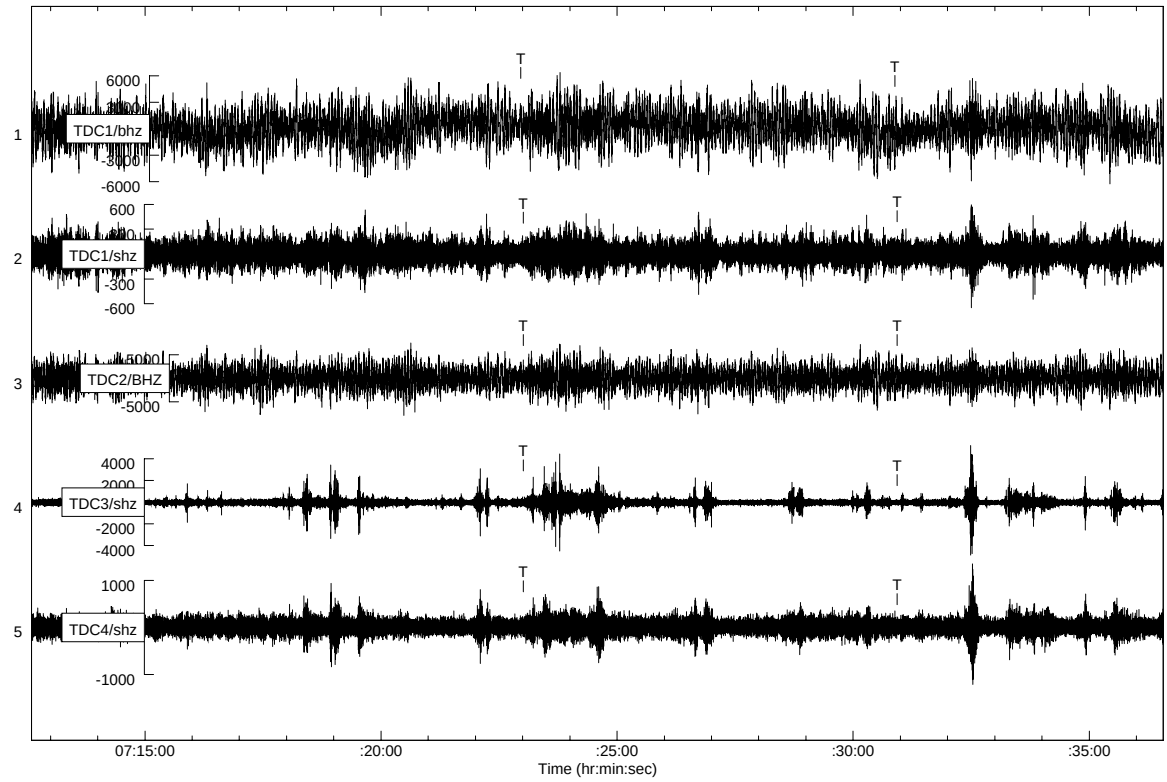

Figure 48. Seismograms of the vertical component of ground velocity recorded at stations TDC1, TDC2, TDC3 and TDC4 showing the expected T-phase arrivals for the magnitude 4.2 and 4.9 North Atlantic Ocean events on 9 November.

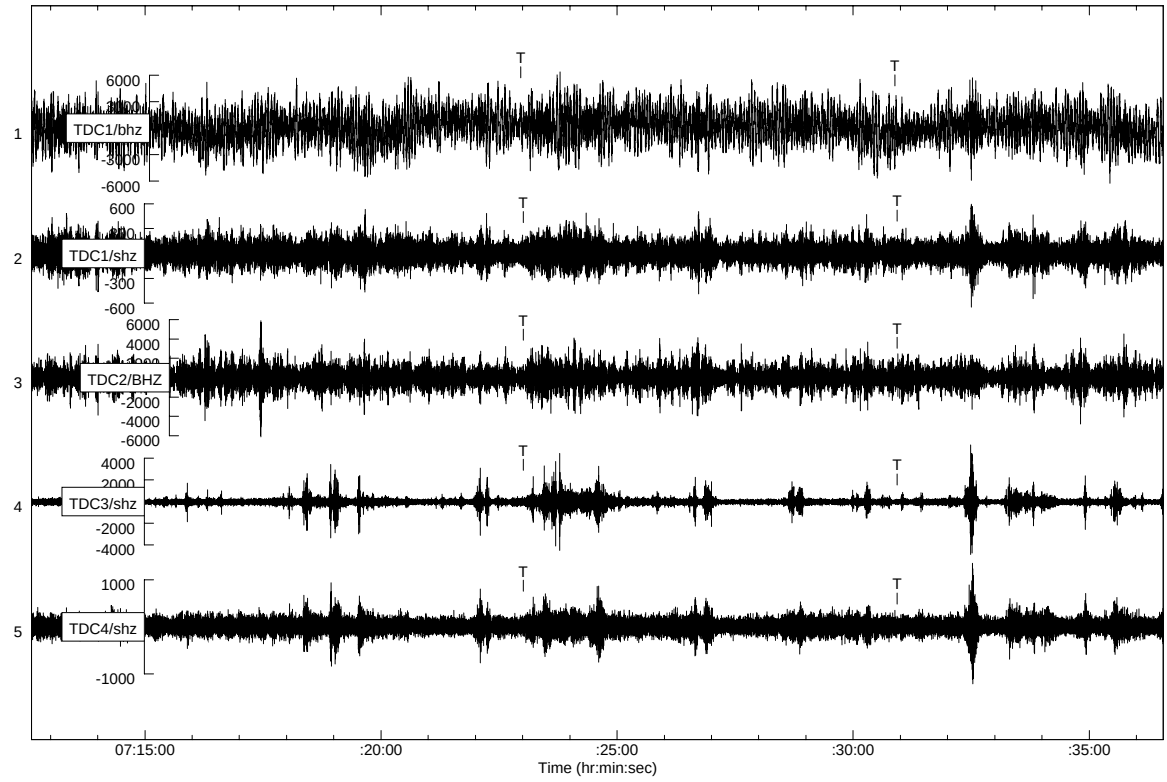

Figure 49. Seismograms shown in Figure48 filtered with a 4th order Butterworth filter with a pass-band of 2-6 Hz.

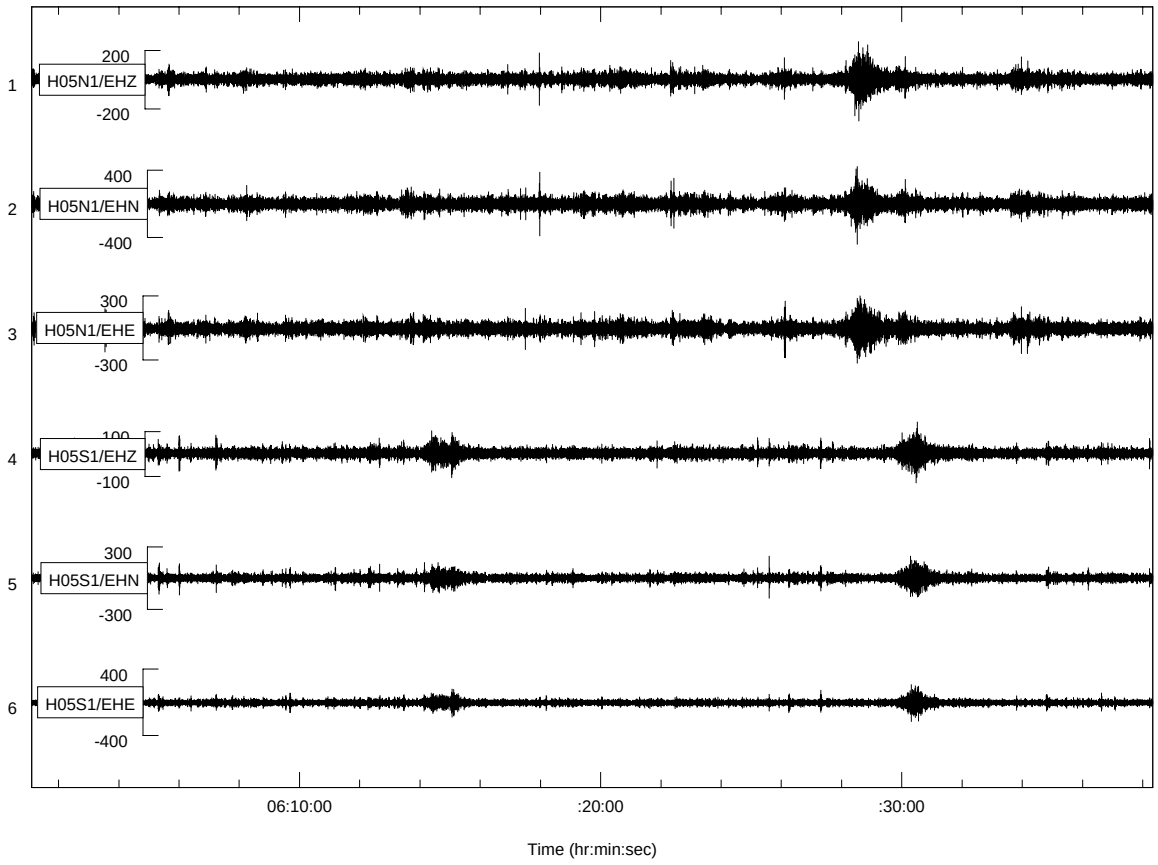

Figure 50. Seismograms showing the T-phase arrivals recorded at IMS station HA05 in Guadeloupe from the magnitude 4.2 and 4.9 North Atlantic Ocean events on 9 November.

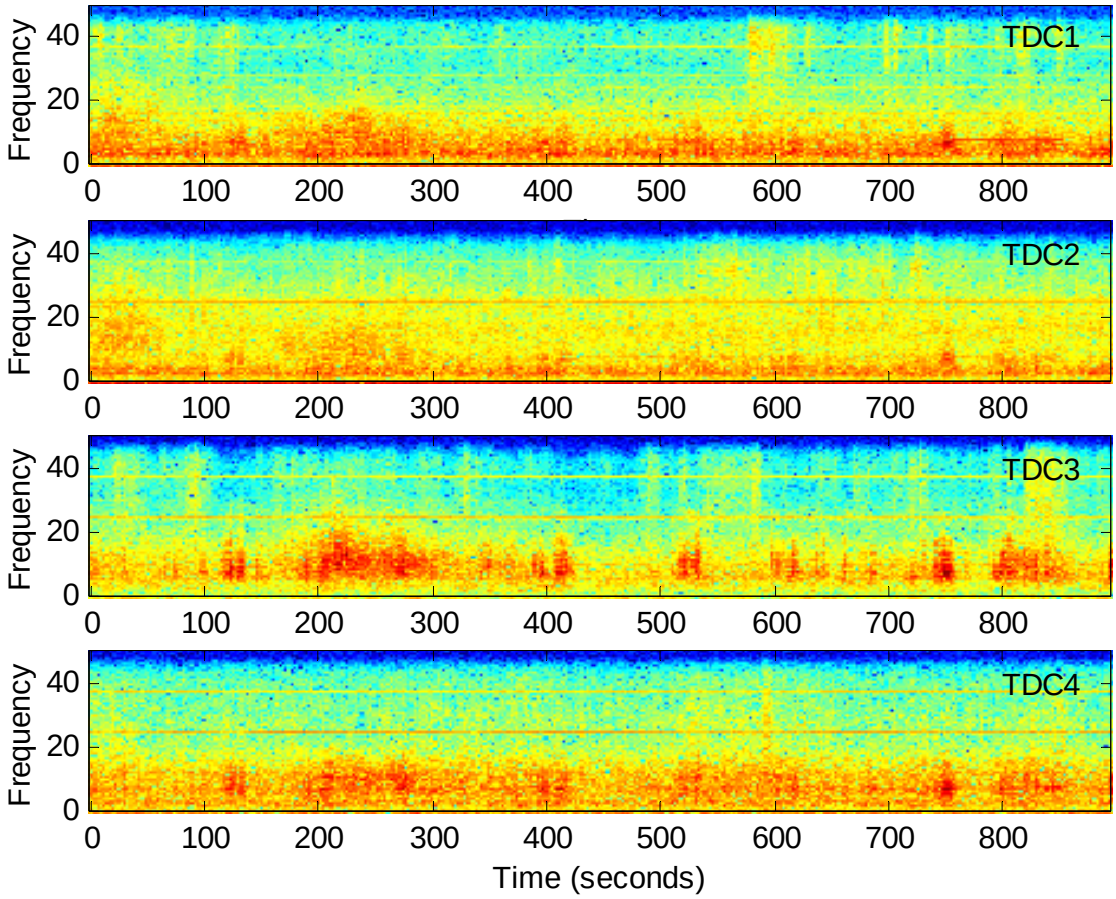

Figure 51. Spectrogram, calculated for the vertical component of ground velocity at stations TDC1, TDC2, TDC3 and TDC4, of the expected T-phase arrivals from the magnitude 4.2 and 4.9 North Atlantic Ocean events on 9 November.

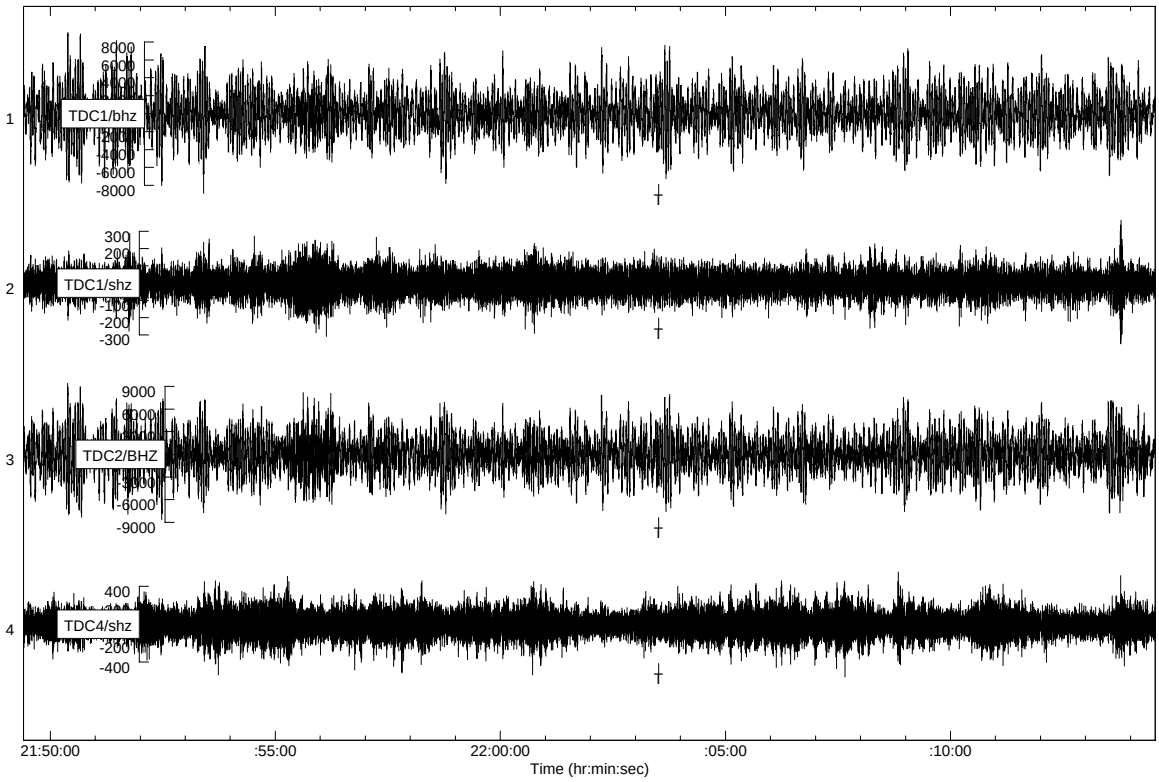

Figure 52. Seismograms of the vertical component of ground velocity recorded at stations TDC1, TDC2 and TDC4 showing the expected T-phase arrivals for the magnitude 4.2 event, South of Africa, on 10 November at 21:25 UTC.

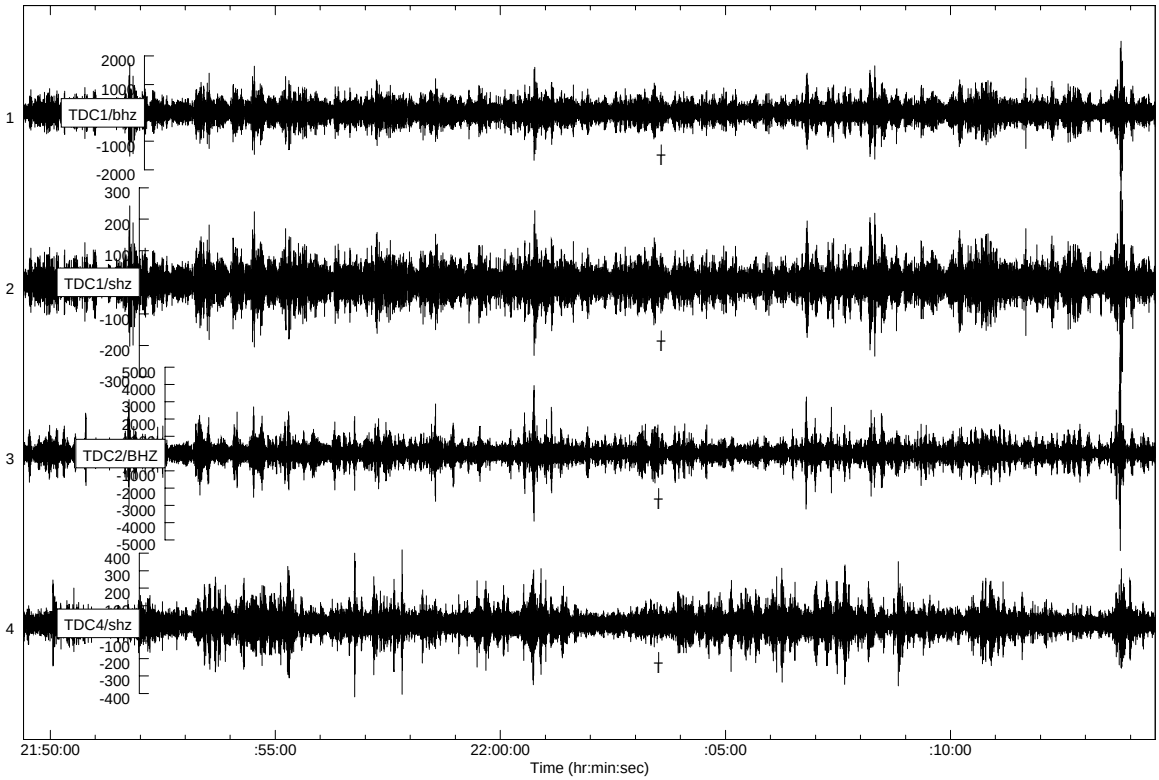

Figure 53. Seismograms shown in Figure 52 filtered with a 4th order Butterworth filter with a pass-band of 3-7 Hz.

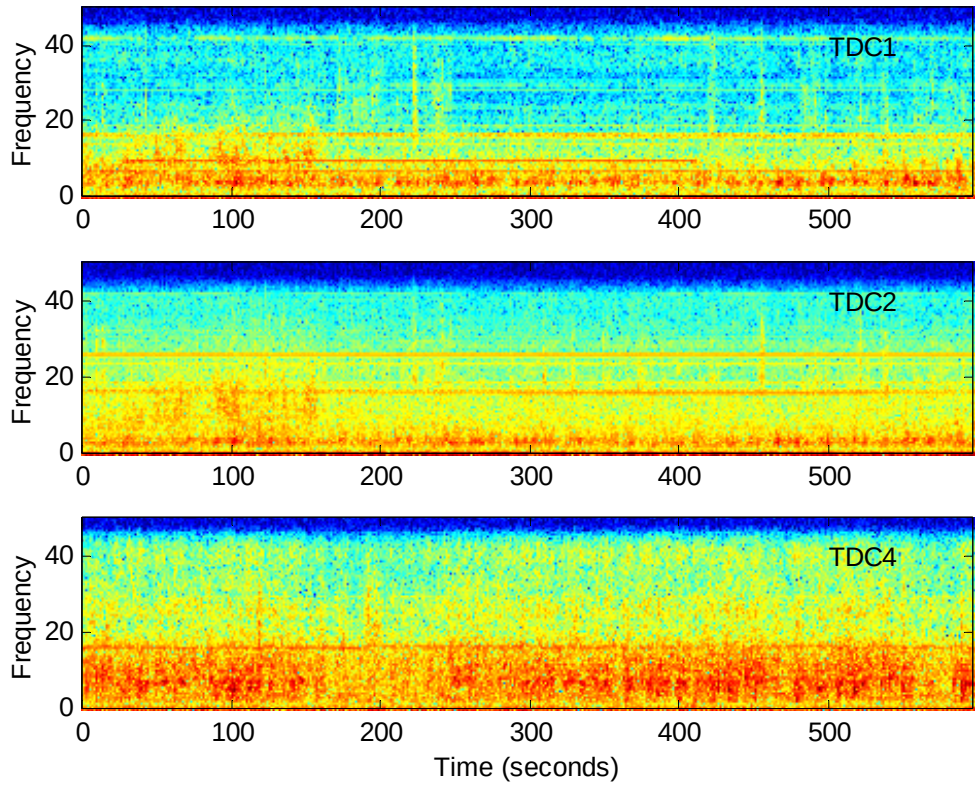

Figure 54. Spectrogram, calculated for the vertical component of ground velocity at stations TDC1, TDC2 and TDC4, of the expected T-phase arrivals from the magnitude 4.2 event, South of Africa, on 10 November at 21:25 UTC.

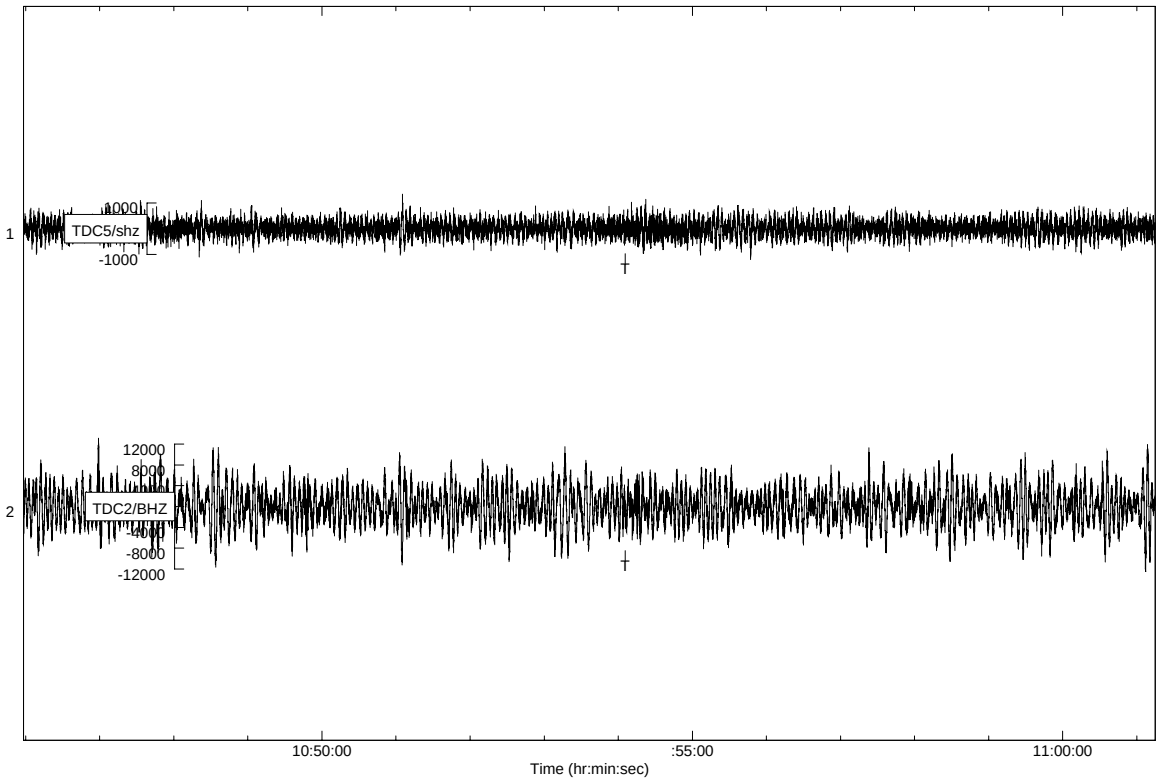

Figure 55. Seismograms of the vertical component of ground velocity recorded at stations TDC2 and TDC5 showing the expected T-phase arrival for the magnitude 3.9 Northern Mid-Atlantic event on 12 November at 09:31 UTC.

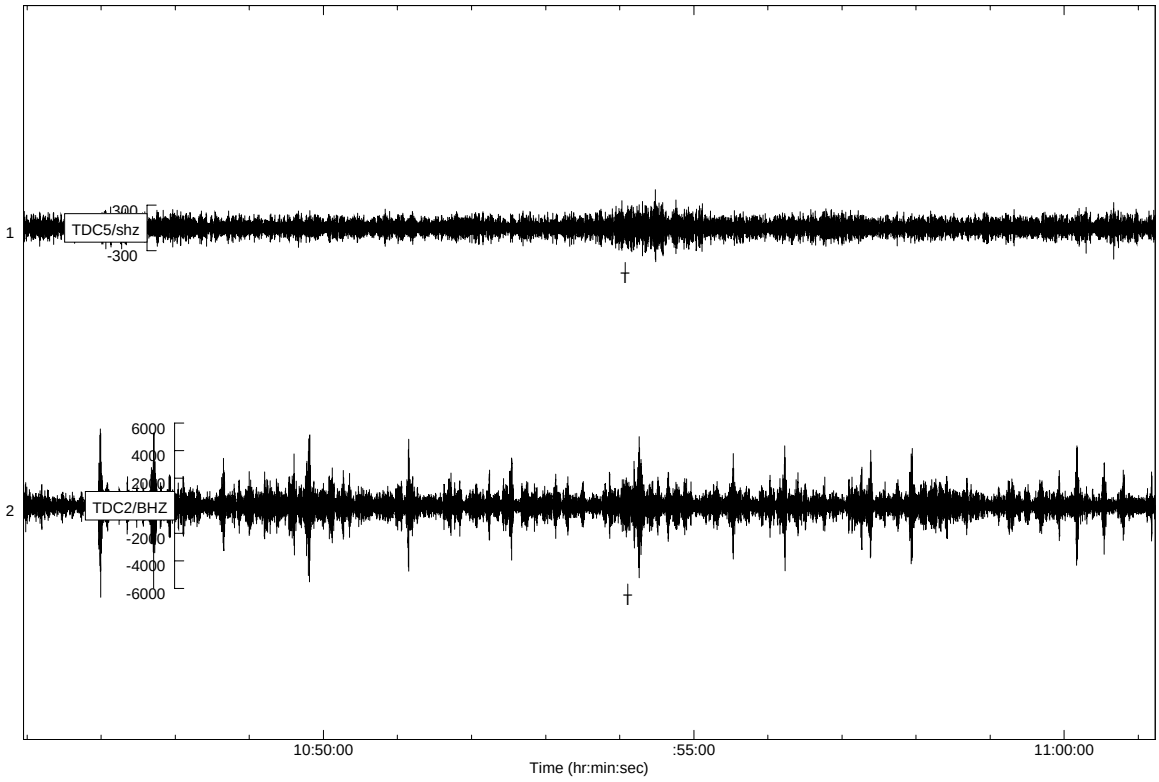

Figure 56. Seismograms shown in Figure 55 filtered with a 4th order Butterworth filter with a pass-band of 2-6 Hz.

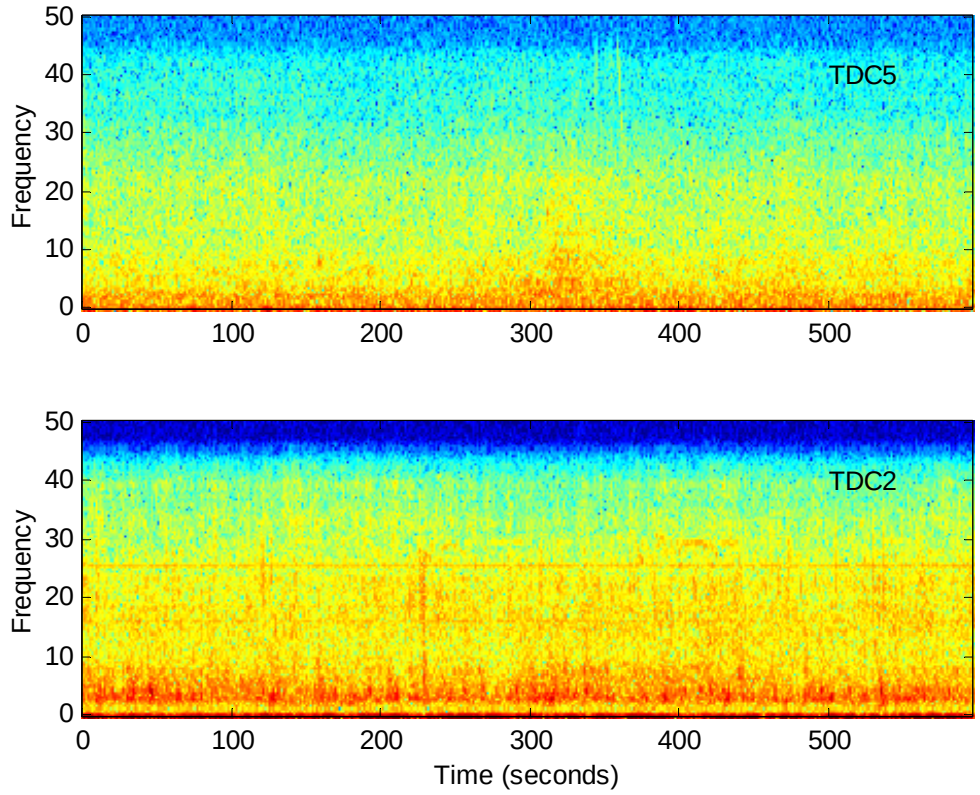

Figure 57. Spectrogram, calculated for the vertical component of ground velocity at stations TDC5 and TDC2, of the expected T-phase arrivals from the magnitude 3.9 Northern Mid-Atlantic event on 12 November at 09:31 UTC.

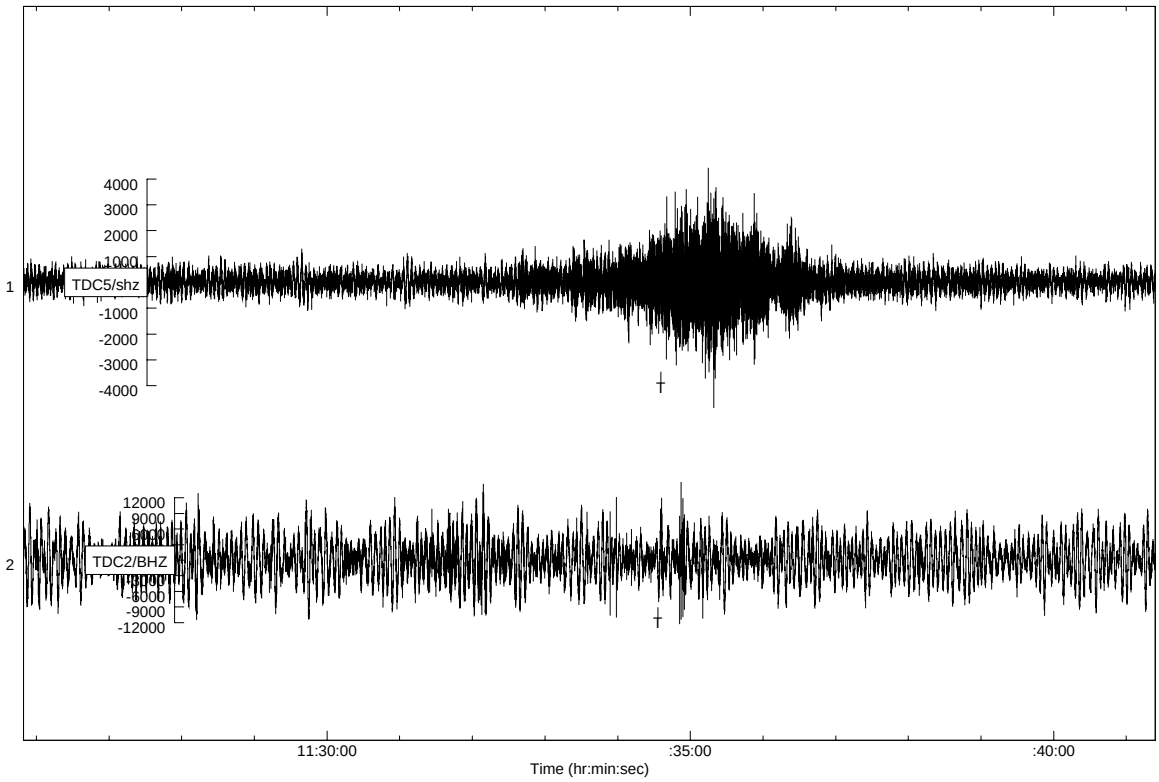

Figure 58. Seismograms of the vertical component of ground velocity recorded at stations TDC2 and TDC5 showing the expected T-phase arrival for the magnitude 4.0 Northern Mid-Atlantic event on 12 November at 10:11 UTC.

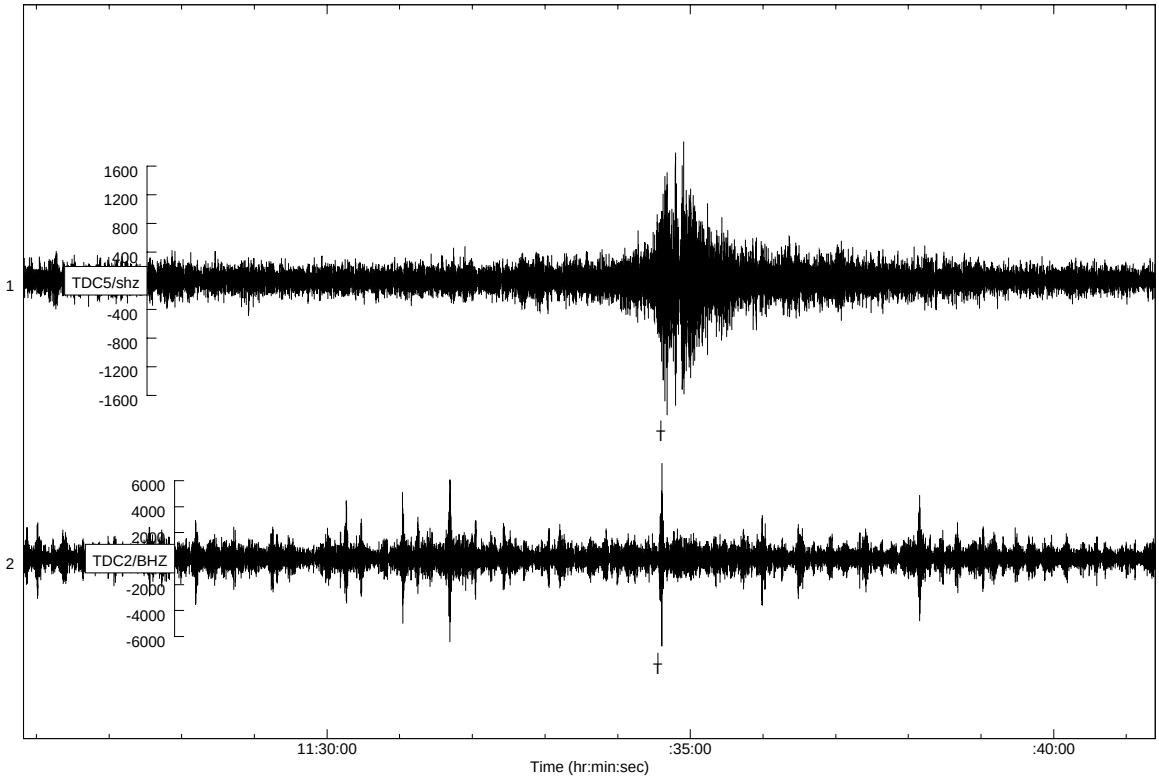

Figure 59. Seismograms shown in Figure 58 filtered with a 4th order Butterworth filter with a pass-band of 2-6 Hz.

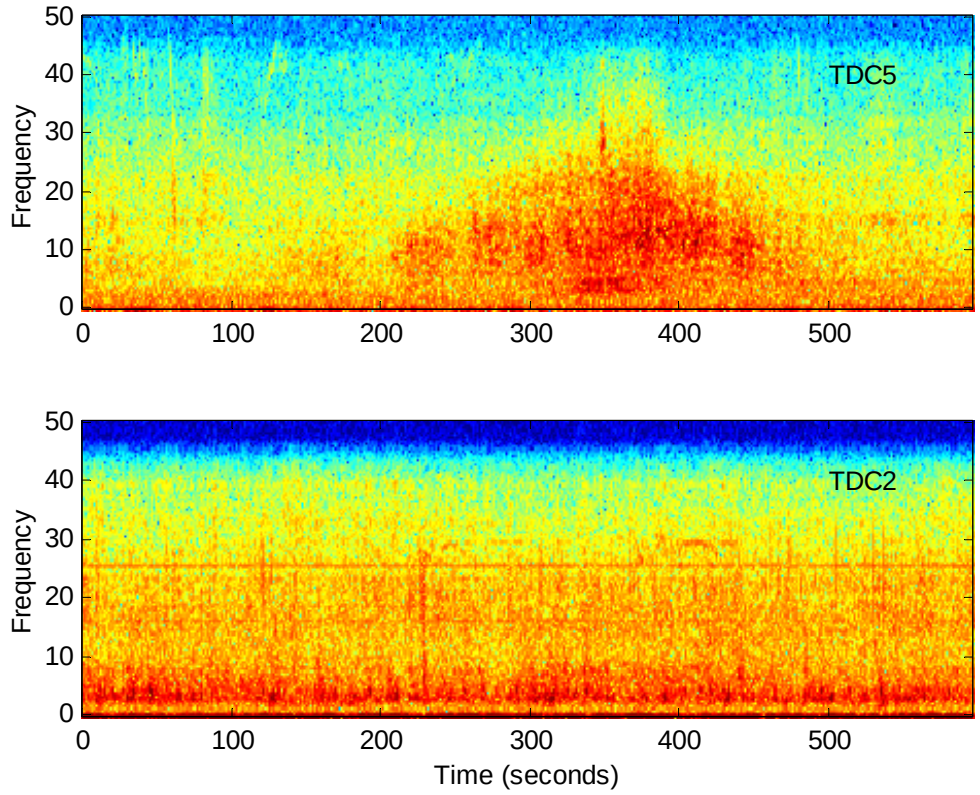

Figure 60. Spectrogram, calculated for the vertical component of ground velocity at stations TDC5 and TDC2, of the expected T-phase arrivals from the magnitude 4.0 Northern Mid-Atlantic event on 12 November at 10:11 UTC.

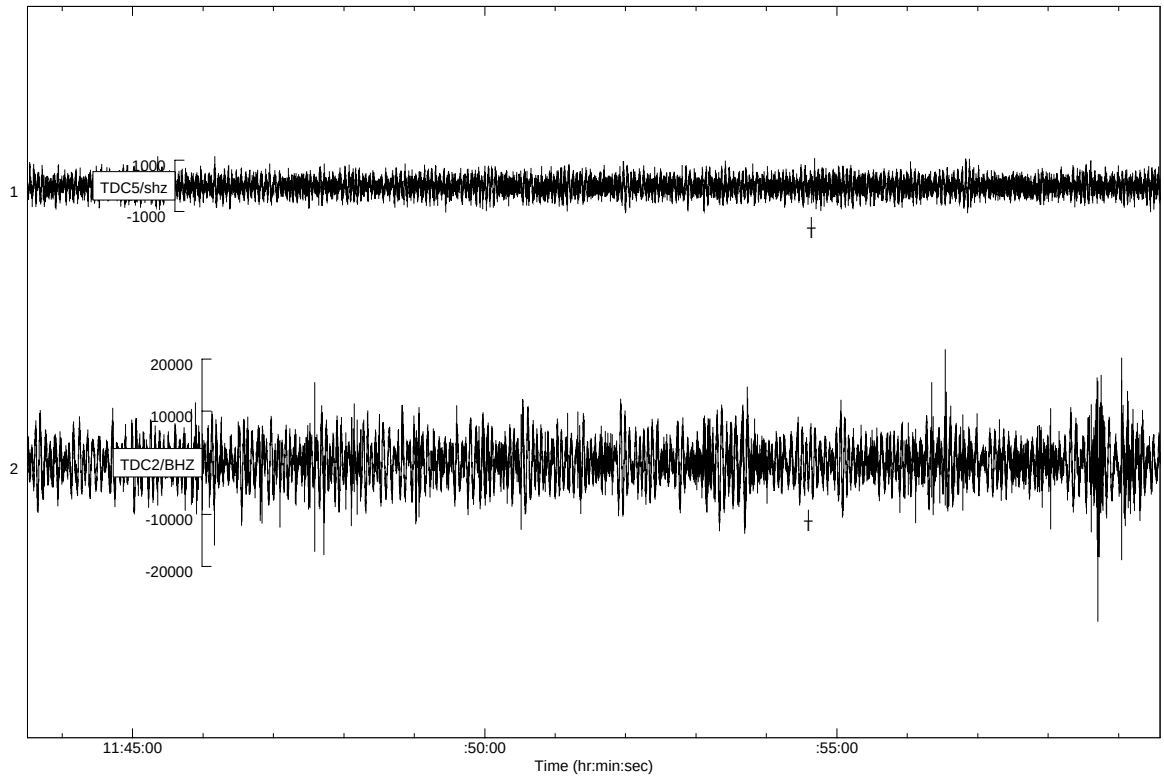

Figure 61. Seismograms of the vertical component of ground velocity recorded at stations TDC2 and TDC5 showing the expected T-phase arrival for the magnitude 4.0 Northern Mid-Atlantic event on 12 November at 10:31 UTC.

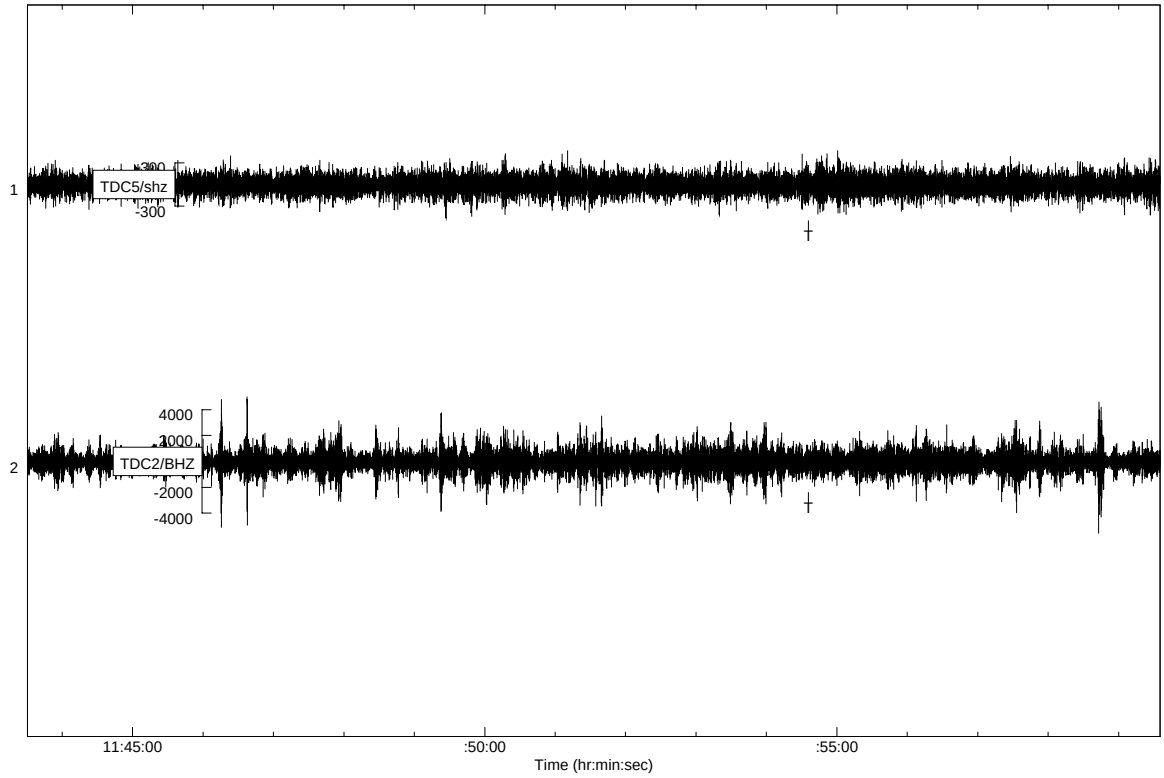

Figure 62. Seismograms shown in Figure 61 filtered with a 4th order Butterworth filter with a pass-band of 2-6 Hz.

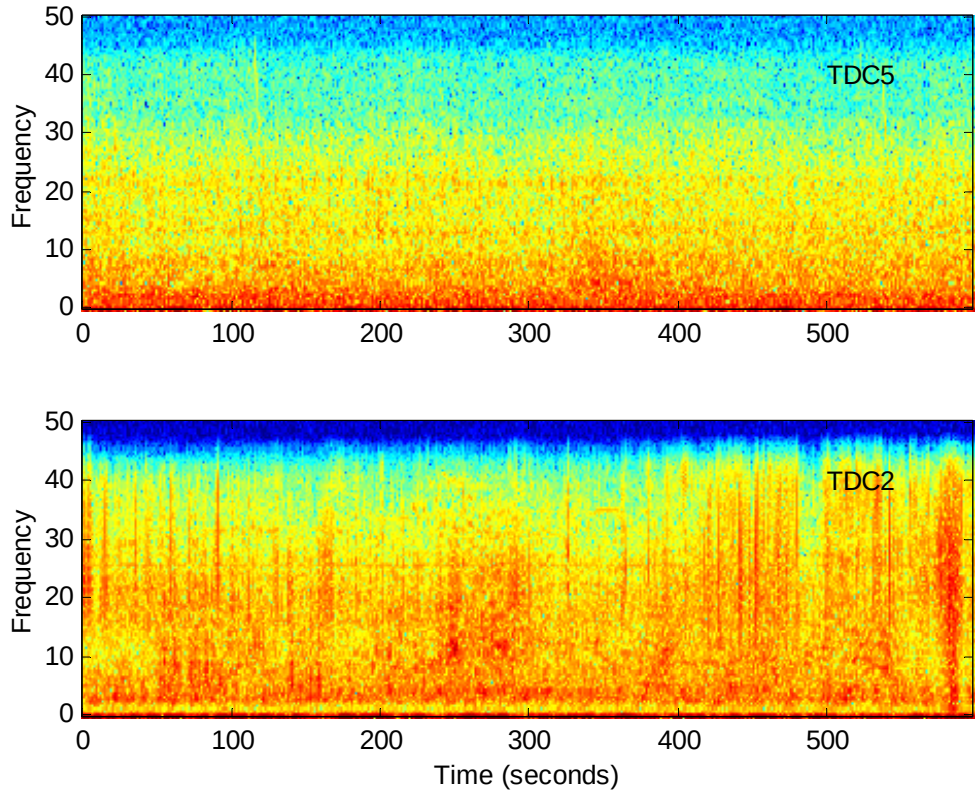

Figure 63. Spectrogram, calculated for the vertical component of ground velocity at stations TDC5 and TDC2, of the expected T-phase arrivals from the magnitude 4.0 Northern Mid-Atlantic event on 12 November at 10:31 UTC.

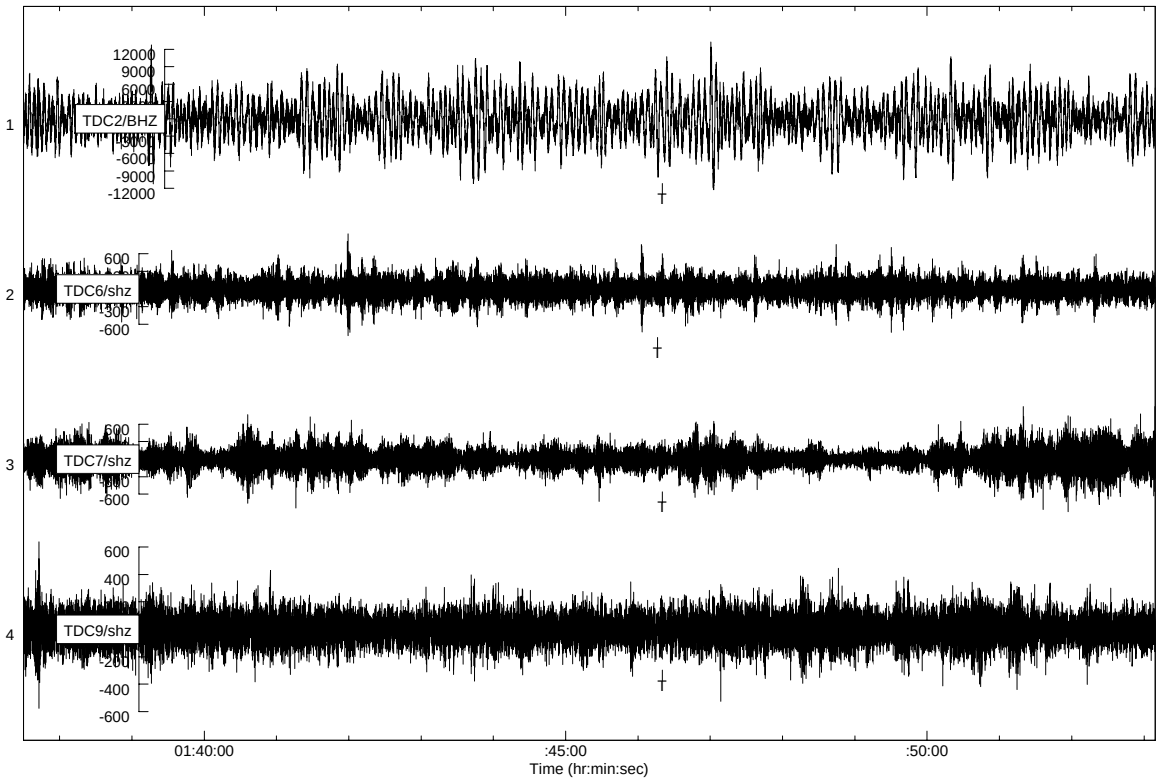

Figure 64. Seismograms of the vertical component of ground velocity recorded at stations TDC2, TDC6, TDC7 and TDC9 showing the expected T-phase arrival for the magnitude 4.5 Mid-Indian Ridge event on 14 November at 00:19 UTC.

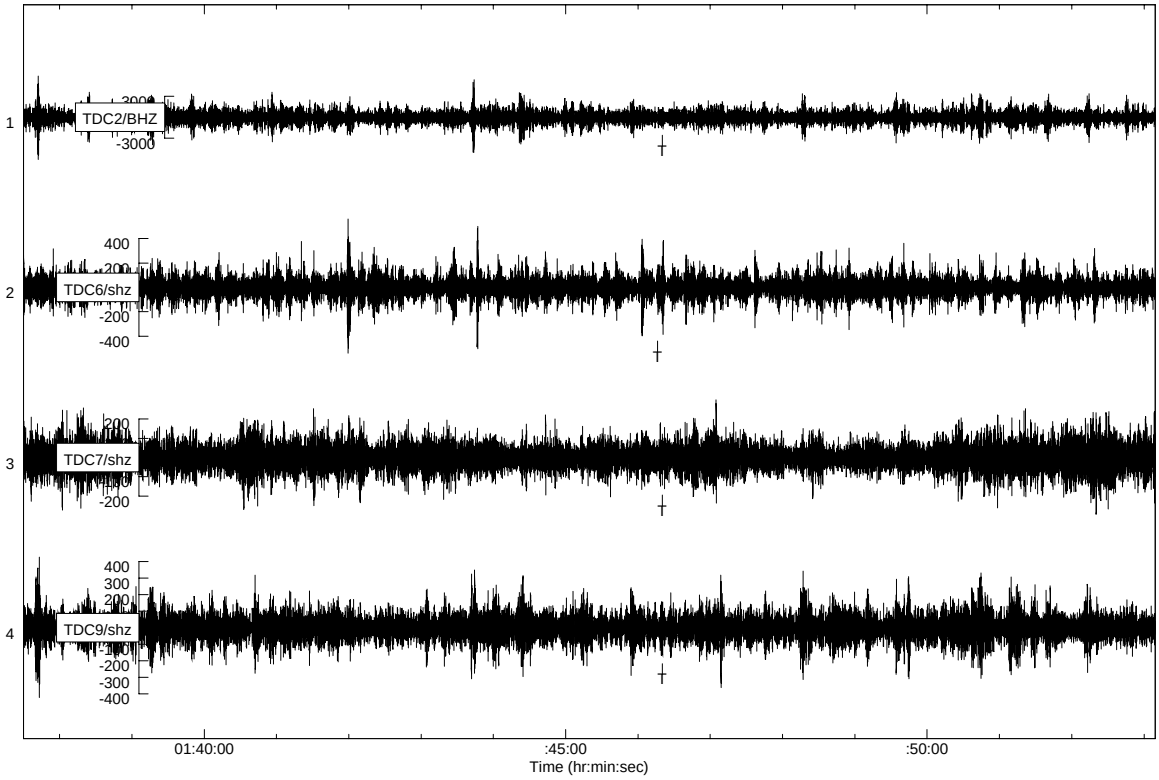

Figure 65. Seismograms shown in Figure 64 filtered with a 4th order Butterworth filter with a pass-band of 2-6 Hz.

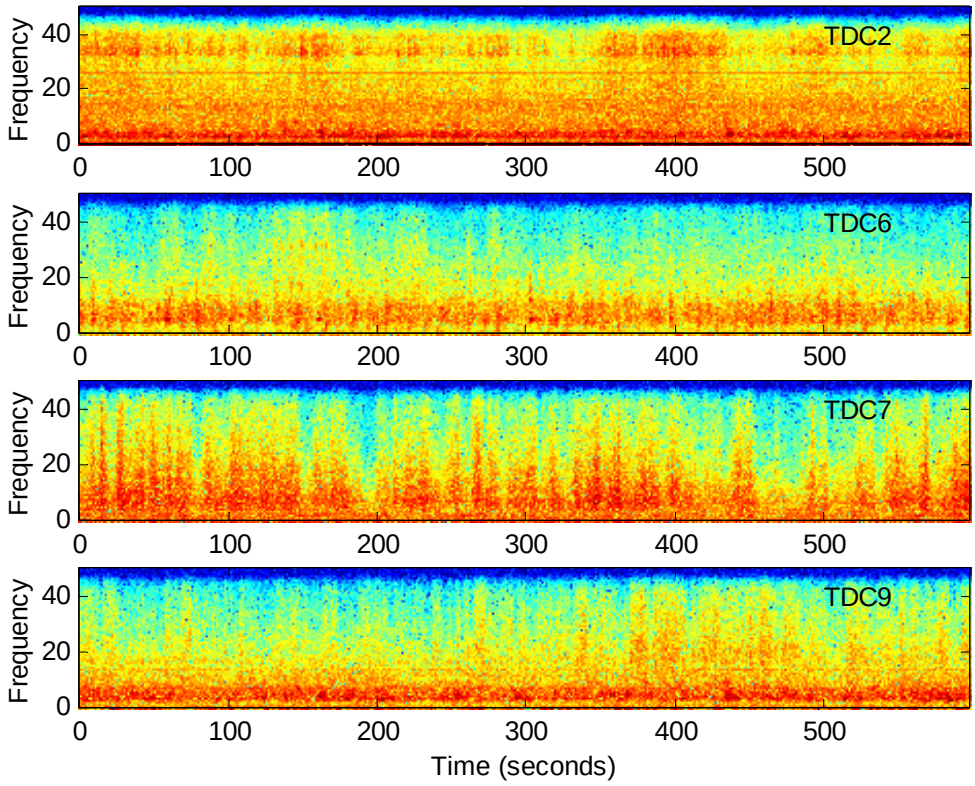

Figure 66. Spectrogram, calculated for the vertical component of ground velocity at stations TDC2, TDC6, TDC7 and TDC9, of the expected T-phase arrivals from the magnitude 4.5 Mid-Indian Ridge on 14 November at 00:19 UTC.

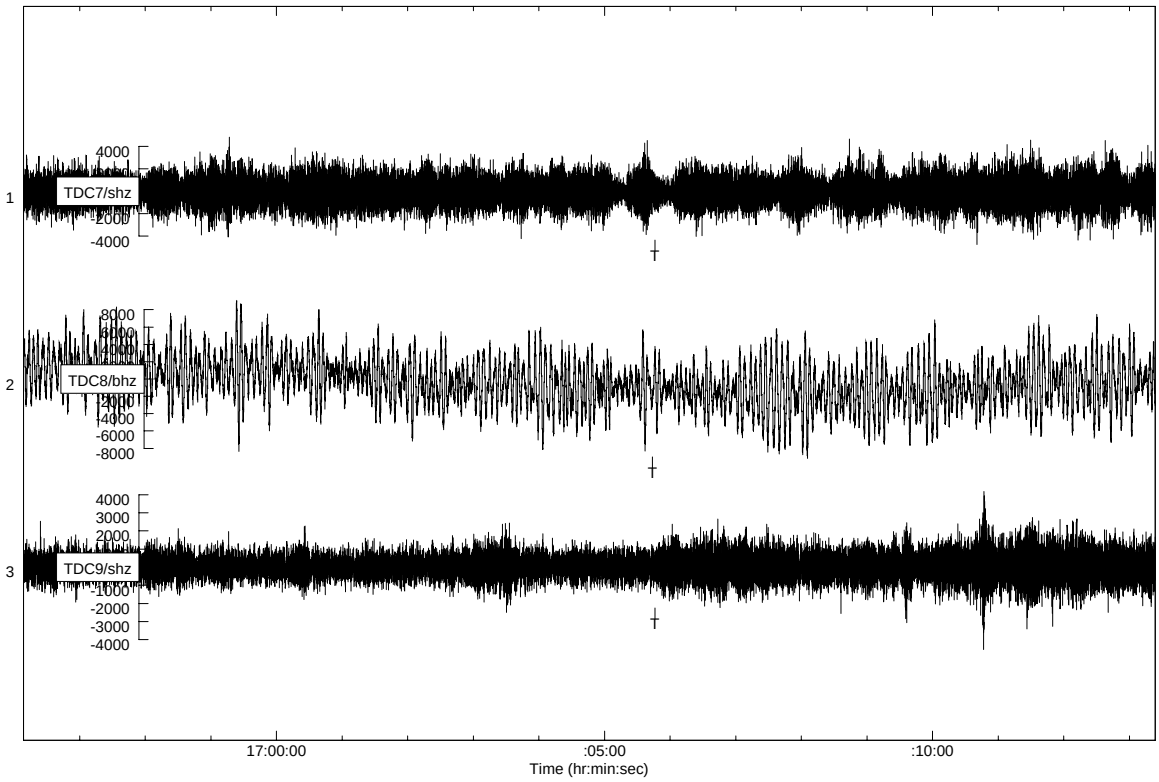

Figure 67. Seismograms of the vertical component of ground velocity recorded at stations TDC7, TDC8 and TDC9 showing the expected T-phase arrival for the magnitude 4.0 South Sandwich Islan event on 14 November at 16:38 UTC.

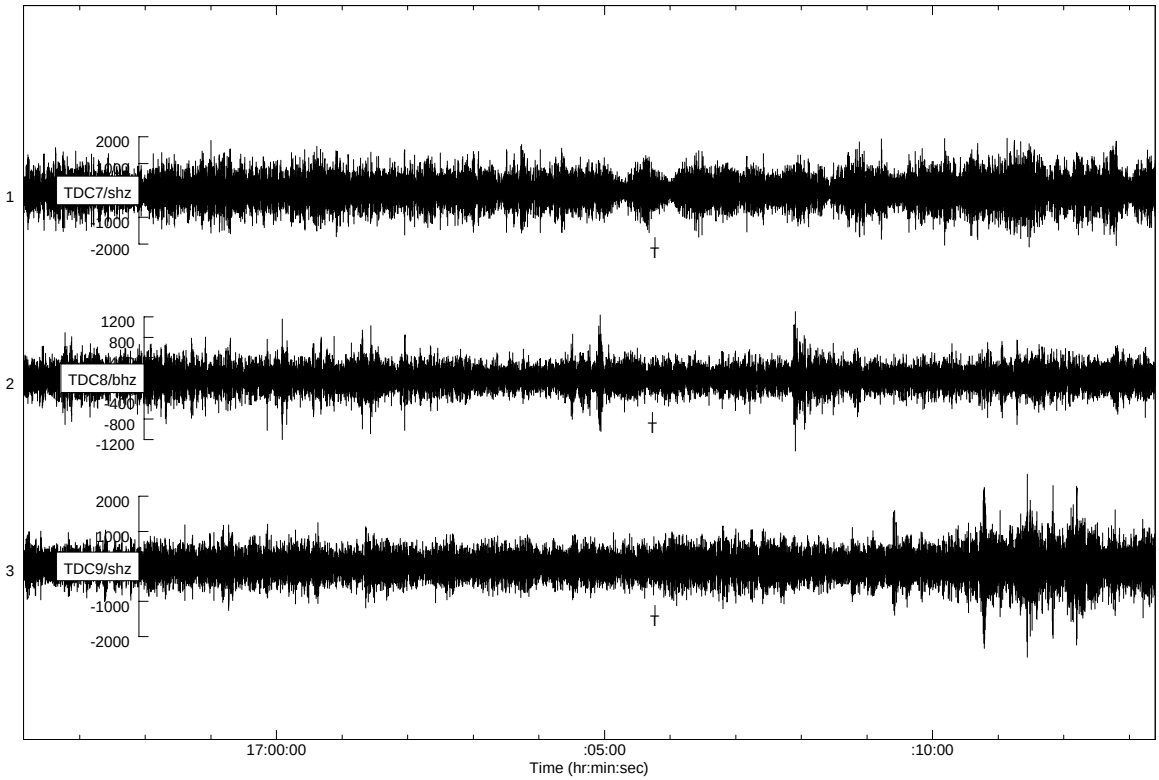

Figure 68. Seismograms shown in Figure 67 filtered with a 4th order Butterworth filter with a pass-band of 3-7 Hz.

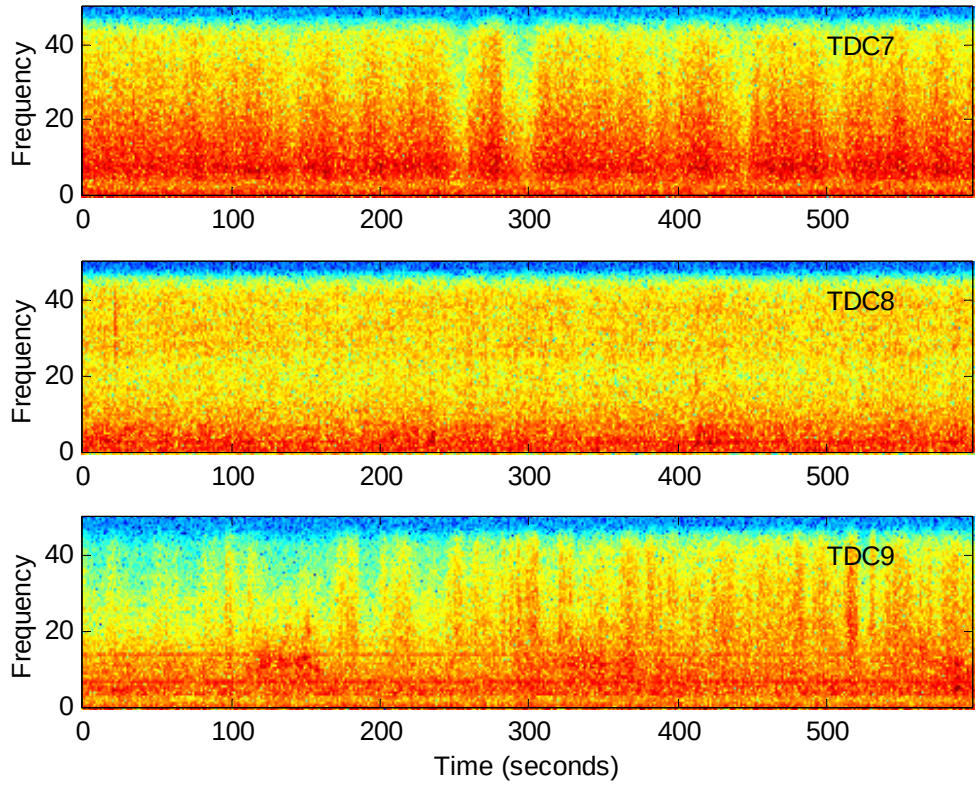

Figure 69. Spectrogram, calculated for the vertical component of ground velocity at stations TDC7, TDC8 and TDC9, of the expected T-phase arrivals from the magnitude 4.0 South Sandwich Islands event on 14 November at 16:38 UTC.

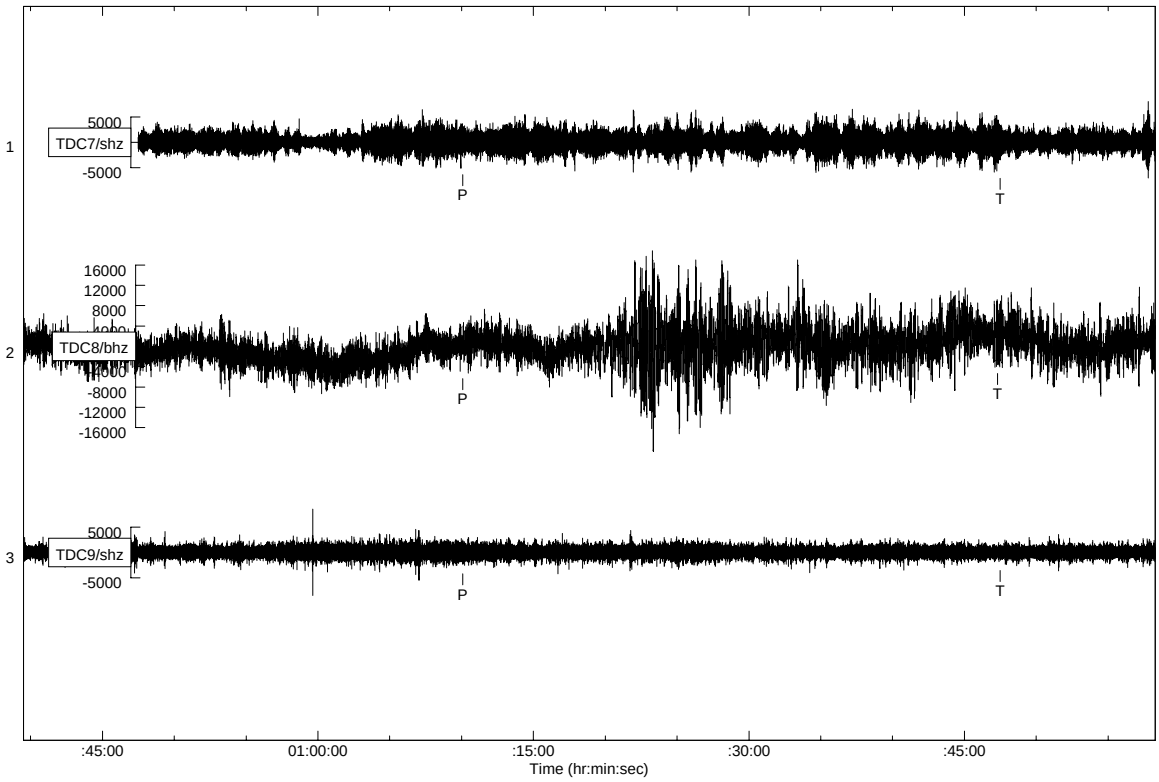

Figure 70. Seismograms of the vertical component of ground velocity recorded at stations TDC7, TDC8 and TDC9 for the magnitude 4.9 Ascension Island event on 15 November at 01:03 UTC.

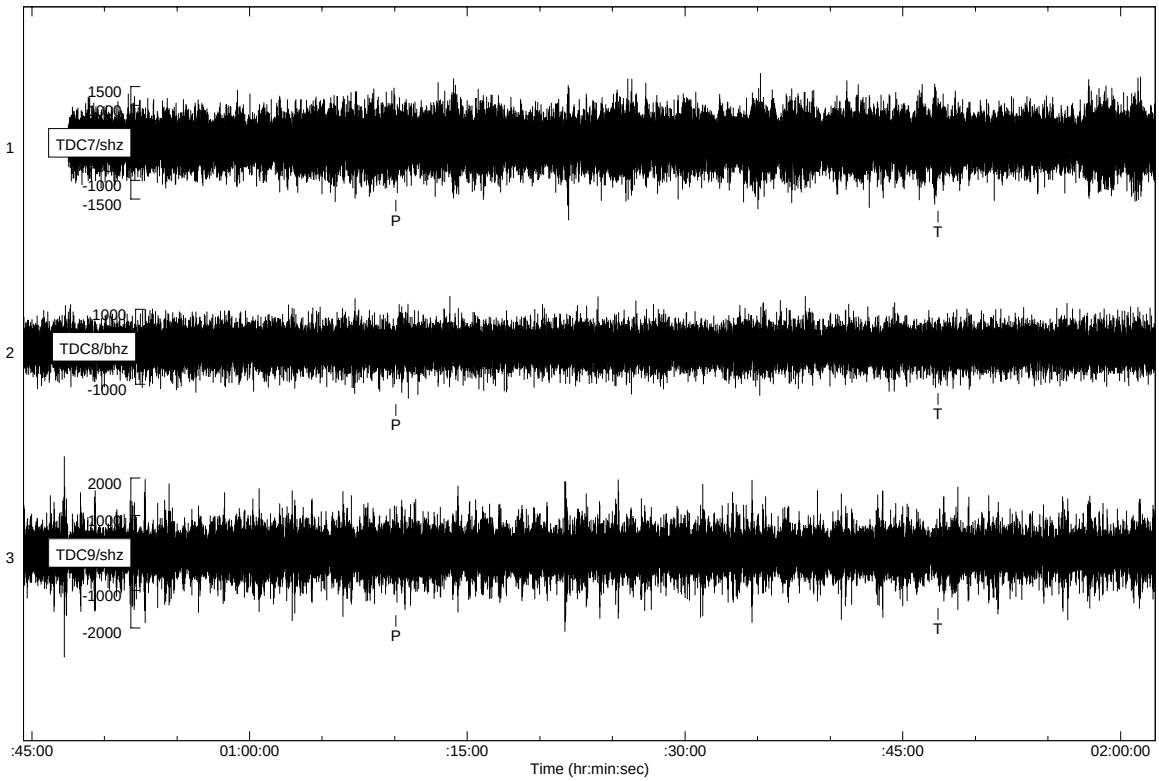

Figure 71. Seismograms shown in Figure 70 filtered with a 4th order Butterworth filter with a pass-band of 3-7 Hz.

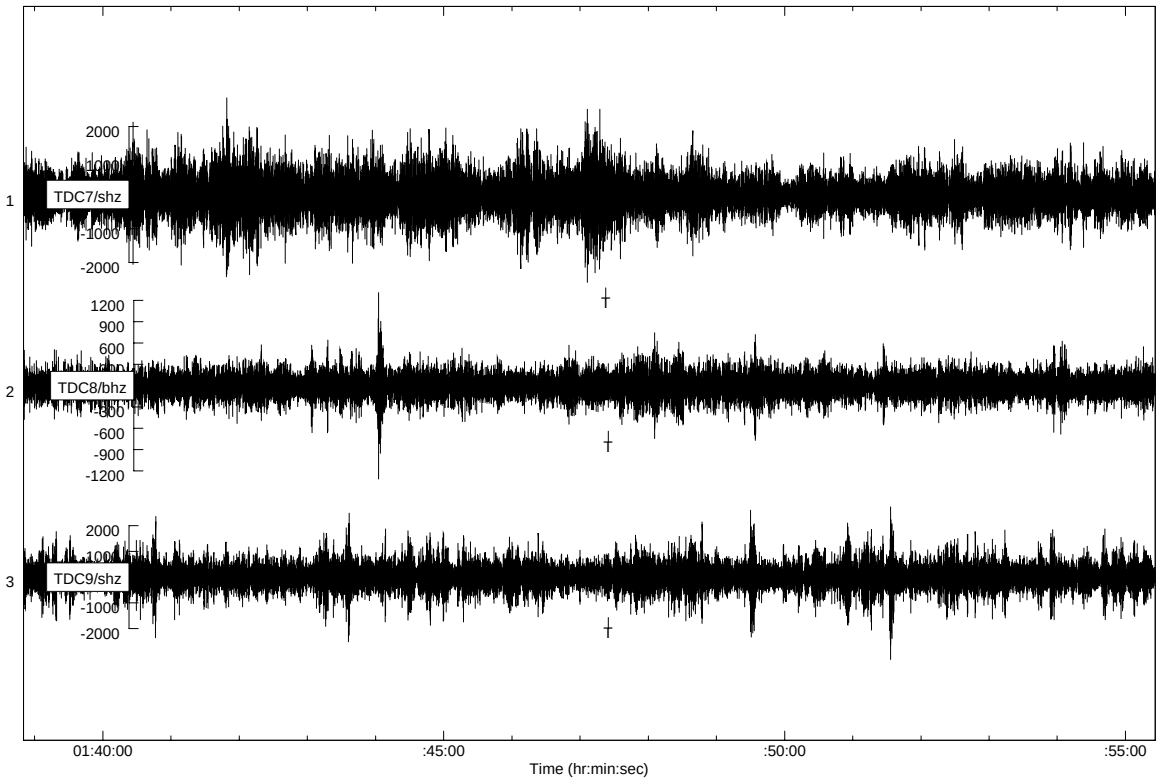

Figure 72. Seismograms of the vertical component of ground velocity recorded at stations TDC7, TDC8 and TDC9 showing the expected T-phase arrival for the magnitude 4.9 Ascension Island event on 15 November at 01:03 UTC.

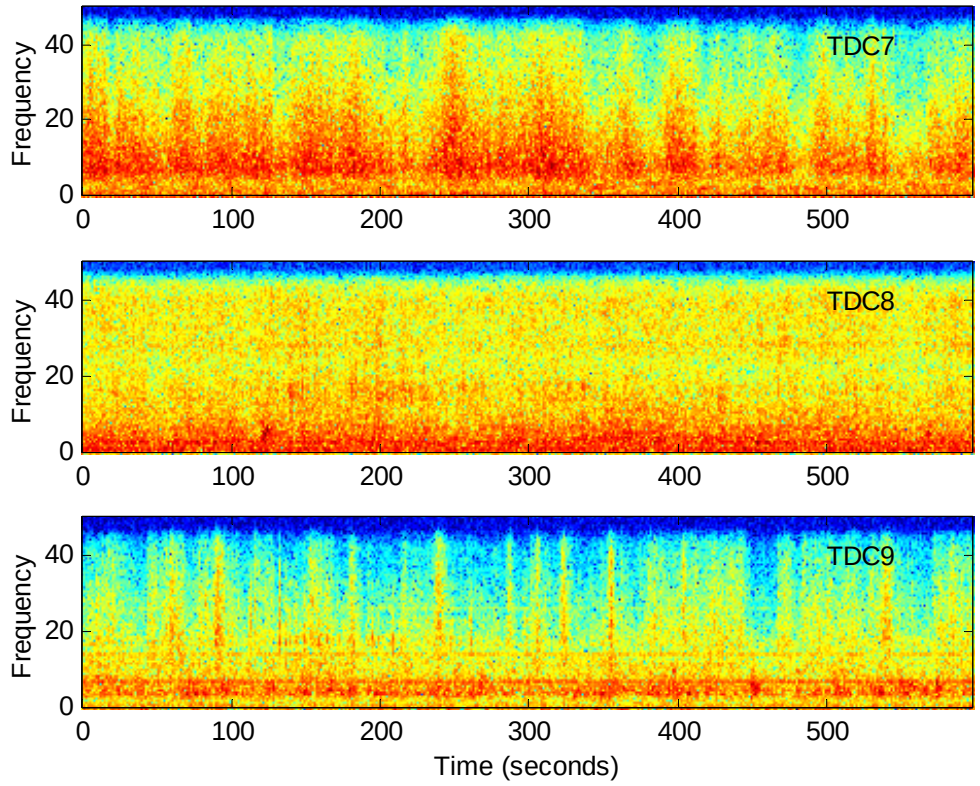

Figure 73. Spectrogram, calculated for the vertical component of ground velocity at stations TDC7, TDC8 and TDC9, of the expected T-phase arrivals from the magnitude 4.9 Ascension Island event on 15 November at 01:03 UTC.

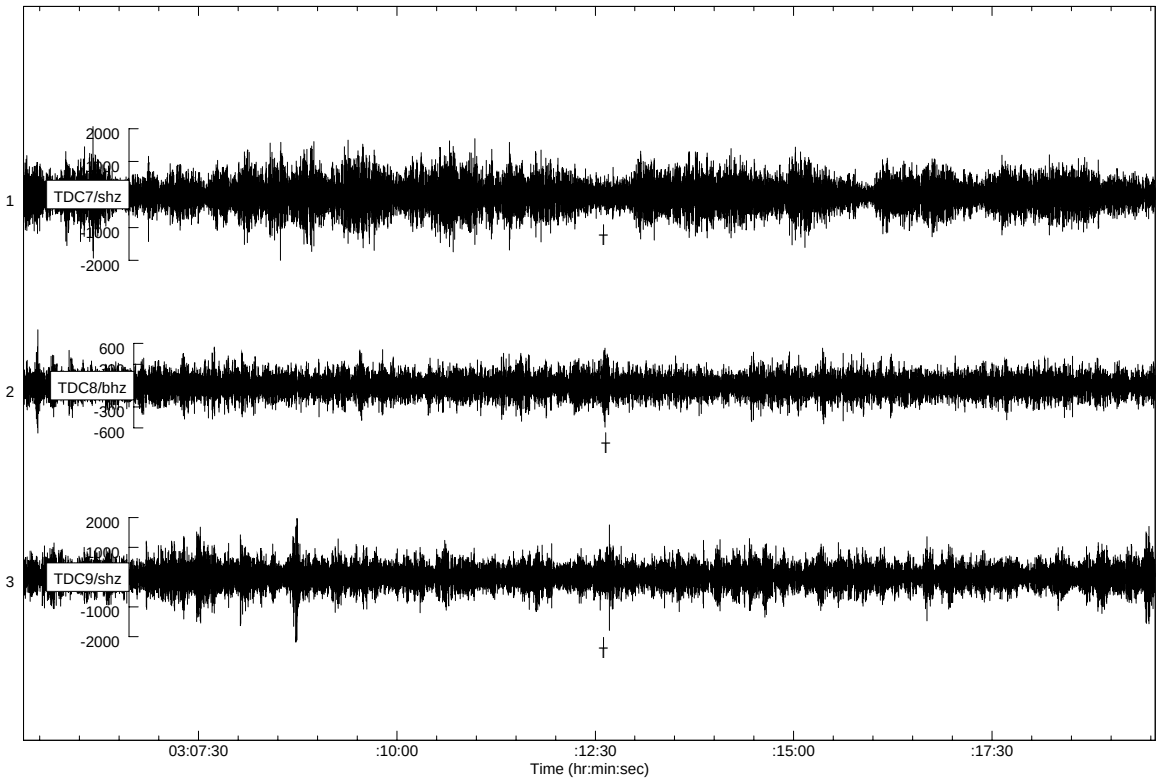

Figure 74. Seismograms of the vertical component of ground velocity recorded at stations TDC7, TDC8 and TDC9 showing the expected T-phase arrival for the magnitude 4.0 Ascension Island event on 15 November at 02:28 UTC.

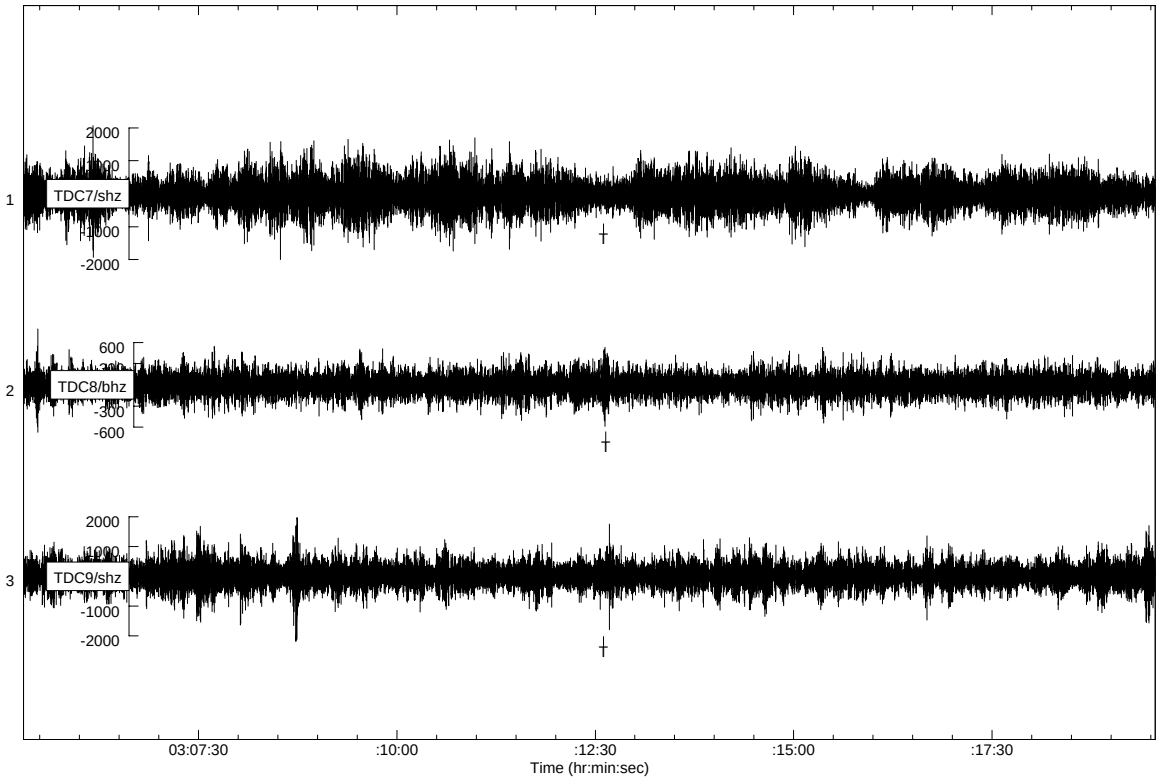

Figure 75. Seismograms shown in Figure 74 filtered with a 4th order Butterworth filter with a pass-band of 3-7 Hz.

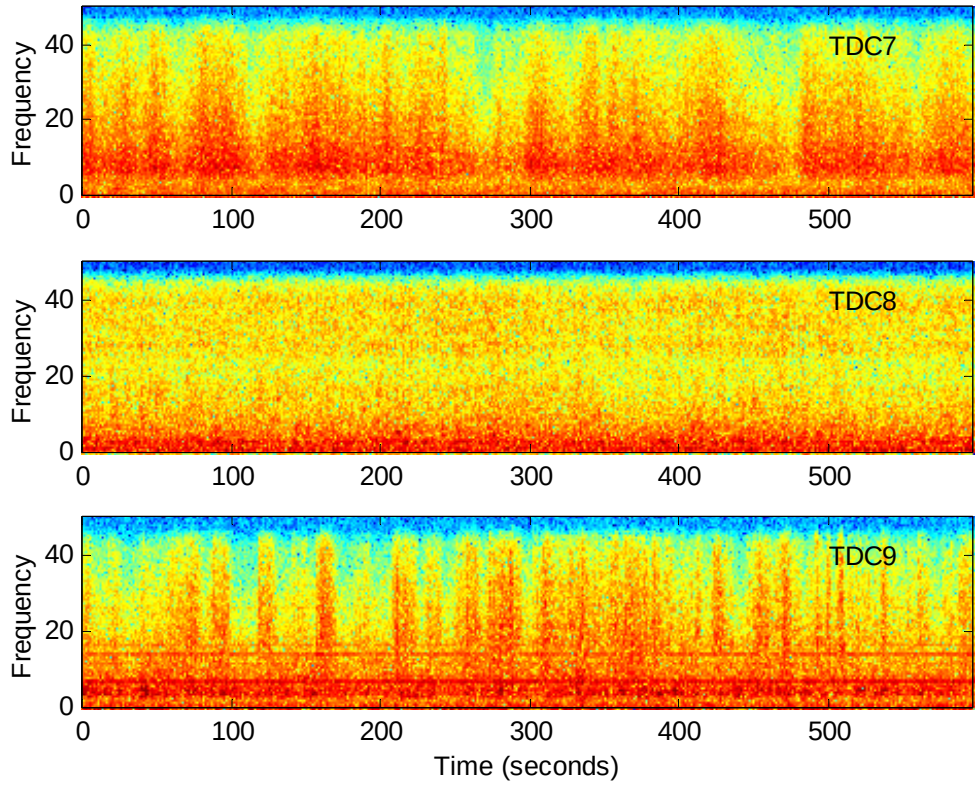

Figure 76. Spectrogram, calculated for the vertical component of ground velocity at stations TDC7, TDC8 and TDC9, of the expected T-phase arrivals from the magnitude 4.0 Ascension Island event on 15 November at 02:28 UTC.